

UNCLASSIFIED

AD NUMBER

AD864013

LIMITATION CHANGES

TO:

Approved for public release; distribution is unlimited. Document partially illegible.

FROM:

Distribution authorized to U.S. Gov't. agencies and their contractors;  
Administrative/Operational Use; NOV 1969. Other requests shall be referred to Air Force Flight Dynamics Lab., Wright-Patterson AFB, OH 45433. Document partially illegible.

AUTHORITY

AFFDL ltr 27 Aug 1973

THIS PAGE IS UNCLASSIFIED

AD 864013

AFFDL-TR-69-76

## AIRCRAFT LANDING GEAR-SOILS INTERACTION AND FLOTATION CRITERIA PHASE II

DAVID C. KRAFT

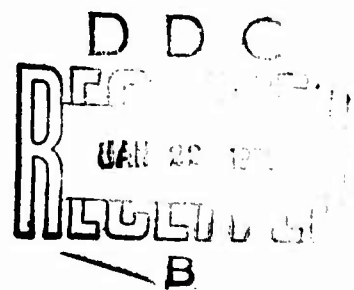
HENRY LUMING

J. RICHARD HOPPENJANS

*University of Dayton  
Research Institute*

TECHNICAL REPORT AFFDL-TR-69-76

NOVEMBER 1969



This document is subject to special export controls and each transmittal to foreign governments or foreign nationals may be made only with prior approval of the Air Force Flight Dynamics Laboratory (FDFM), Wright-Patterson Air Force Base, Ohio 45433.

Reproduced by the  
CLEARINGHOUSE  
for Foreign Distribution  
Information (Springfield, VA 22154)

AIR FORCE FLIGHT DYNAMICS LABORATORY  
AIR FORCE SYSTEMS COMMAND  
WRIGHT-PATTERSON AIR FORCE BASE, OHIO

AFFDL-TR-69-76

**AIRCRAFT LANDING GEAR-SOILS  
INTERACTION AND FLOTATION CRITERIA  
PHASE II**

*DAVID C. KRAFT*

*HENRY LUMING*

*J. RICHARD HOPPENJANS*

*University of Dayton  
Research Institute*

This document is subject to special export controls and each transmittal to foreign governments or foreign nationals may be made only with prior approval of the Air Force Flight Dynamics Laboratory (FDFM), Wright-Patterson Air Force Base, Ohio 45433.

AFFDL-TR-69-76

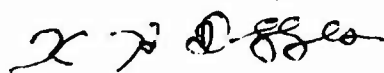
## FOREWORD

This report was prepared by the Aerospace Mechanics Group of the University of Dayton Research Institute under USAF Contract AF 33(615)-3199 and USAF Contract F33615-69-C-1439. This work was conducted under the direction of the Vehicle Equipment Division, Air Force Flight Dynamics Laboratory, Wright-Patterson Air Force Base, Ohio, Mr. George Sperry (FDFM), Project Engineer.

This report covers work conducted from 15 May 1968 to 15 June 1969.

The authors wish to thank Mr. Sperry for his considerable efforts in securing flotation data and information and in integrating the overall effort to meet Air Force flotation research objectives. This report was submitted by the authors in July 1969.

Publication of this technical report does not constitute Air Force approval of the report's findings or conclusions. It is published only for the exchange and stimulation of ideas.



KENNERLY H. DIGGES  
Chief, Mechanical Branch  
Vehicle Equipment Division  
Air Force Flight Dynamics Laboratory

## ABSTRACT

The determination of aircraft flotation performance and operations capability on semi- and unprepared soil runways is a critical factor in developing forward area airfields in limited warfare situations. This investigation, which is a part of a continuing program, was directed at defining landing gear-soil interaction and developing the flotation criteria to permit comparative evaluation of the relative merits of various landing gear configurations.

A basic aircraft tire-soil interaction equation relating the drag ratio ( $R/P$ ) to sinkage ratio ( $Z/D$ ) was developed for the Region II velocity range (5 knots to 40 knots). The influence of high velocity and multiple wheel configurations on flotation performance was determined on a preliminary basis. Empirical sinkage prediction equations were developed for predicting the sinkage of aircraft type tires in cohesive and cohesionless soils with an estimated accuracy of  $\pm 40\%$  within the 90% confidence limits. The results of the Single Wheel Verification Tests are reported and used to verify the developed flotation analysis equations.

An analytical approach to sinkage prediction using finite element techniques was developed to give a more rational approach to sinkage analysis. The soil was assumed to be an elastic-perfectly plastic medium. The results of this analytical approach as given by the computer program and the results of a test case evaluation are described in detail.

A preliminary Single Wheel Relative Merit Index (RMI) was developed for permitting a comparative evaluation of the flotation characteristics of aircraft tires on soil. The RMI was used to rate the flotation capacity of aircraft tires currently used on cargo, bomber, and fighter aircraft.

This document is subject to special export controls and each transmittal to foreign governments or foreign nationals may be made only with prior approval of the Air Force Flight Dynamics Laboratory (FDFM), Wright-Patterson Air Force Base, Ohio 45433.

# TABLE OF CONTENTS

SECTION	PAGE
I INTRODUCTION . . . . .	1
II DRAG-SINKAGE ANALYSIS . . . . .	4
III SINGLE WHEEL VERIFICATION TESTS . . . . .	13
IV SINKAGE PREDICTION EQUATIONS . . . . .	31
V SINGLE WHEEL RELATIVE MERIT INDEX (RMI) . . . . .	71
VI CONCLUSIONS AND RECOMMENDATIONS FOR RESEARCH . . . . .	90
REFERENCES . . . . .	92
APPENDIX I: Single Wheel Verification Tests, Soil Tests and Preparation . . . . .	95
APPENDIX II: Single Wheel Verification Tests, Soil Uniformity Measurement . . . . .	102
APPENDIX III: Flotation Index-Operations Index Computer Program	117
APPENDIX IV: Incremental Strain-Displacement Relations for Stress Points Near the Surface . . . . .	121
APPENDIX V: Derivation of the Stress Correction Equations . . . . .	124
APPENDIX VI: Finite Element Computer Program for Analytical Sinkage Analysis . . . . .	128
APPENDIX VII: Program Listing . . . . .	136

## ILLUSTRATIONS

FIGURE		PAGE
1	Projected Landing Gear-Soils Interaction and Flotation Research Program . . . . .	3
2	Drag Ratio-Sinkage Ratio, Single Wheels on Soil . . . . .	5
3	Multiple Wheel Landing Gear Assemblies . . . . .	7
4	Twin Wheel Drag Effects in Clay Soil . . . . .	9
5	Tandem-Tracking Wheel Drag Effects in Clay Soil . . . . .	9
6	Typical Drag Ratio, Sinkage Ratio vs Horizontal Velocity in Soil . . . . .	10
7	High Velocity (Region III) Drag Ratio Effects in Soil . . . . .	12
8	Test Carriage on Soil Carts . . . . .	16
9	Type III, 7.00-6 Test Tire . . . . .	17
10	Type III, 8.50-10 Test Tire . . . . .	17
11	Cone Index-CBR Soil Correlation . . . . .	21
12	Tire Deflection Effects on Drag and Sinkage, 8.50-10 Tire . . . . .	24
13	Drag Ratio vs Sinkage Ratio, Buckshot Clay . . . . .	25
14	Sinkage Characteristic vs Load-Strength Ratio, Buckshot Clay . . . . .	26
15	Drag Ratio vs Sinkage Ratio, Mortar Sand . . . . .	28
16	Sinkage Characteristic vs Load-Strength Ratio, Mortar Sand . . . . .	30
17	Sinkage Characteristics vs Load-Strength Ratio, Cohesive Soil . . . . .	34
18	Sinkage-Tire Deflection Analysis, Cohesionless Soils . . . . .	36
19	Sinkage-Tire Diameter/Width Ratio Analysis, Cohesionless Soils . . . . .	37
20	Sinkage Characteristics vs Load-Strength Ratio, Cohesionless Soils . . . . .	39
21	Sinkage Range for Soils . . . . .	40
22	Boundary Conditions for Stationary Tire Impulse Loading . . . . .	42
23	Typical Vertical Impulse Pressure Curve . . . . .	43

FIGURE		PAGE
24	Finite Element Model - "Lumped Parameter Method" . . .	46
25	Flow Chart of Computer Program . . . . .	56
26	Development of the Plastic Zone vs Time of Loading . . .	59
27	Vertical Deflection of the Surface vs Radius at Various Times of Loading . . . . .	60
28	Sinkage at $r/a = 0$ for Various Depths . . . . .	61
29	Constant Vertical Stress Contour at Time $\frac{t}{t_d} = 0.35$ . . . .	62
30	Constant Vertical Stress Contour at Time $\frac{t}{t_d} = 0.50$ . . . .	63
31	Sinkage Ratio vs. Vertical Tire Load, 8.50-10 Tire on High Strength Clay, $d = 28\%$ . . . . .	66
32	Sinkage Ratio vs. Vertical Tire Load, 8.50-10 Tire on High Strength Clay, $d = 45\%$ . . . . .	66
33	Sinkage Ratio vs. Vertical Tire Load, 8.50-10 Tire on Low Strength Clay, $d = 28\%$ . . . . .	67
34	Sinkage Ratio vs. Vertical Tire Load, 8.50-10 Tire on Low Strength Clay, $d = 45\%$ . . . . .	67
35	Sinkage Ratio vs. Vertical Tire Load, 7.00-6 Tire on Low Strength Clay, $d = 28\%$ . . . . .	68
36	Sinkage Ratio vs. Vertical Tire Load, 7.00-6 Tire on Low Strength Clay, $d = 45\%$ . . . . .	68
37	Sinkage Ratio vs. Vertical Tire Load, 8.50-10 Tire on Sand, $d = 28\%$ . . . . .	69
38	Sinkage Ratio vs. Vertical Tire Load, 8.50-10 Tire on Sand, $d = 45\%$ . . . . .	69
39	Sinkage Ratio vs. Vertical Tire Load, 7.00-6 Tire on Sand, $d = 28\%$ . . . . .	70
40	Sinkage Ratio vs. Vertical Tire Load, 7.00-6 Tire on Sand, $d = 45\%$ . . . . .	70
41	Flotation Index, Aircraft Cargo Tires on Low Strength Soil . . . . .	74
42	Flotation Index, Aircraft Bomber Tires on Low Strength Soil . . . . .	75



43	Flotation Index, Aircraft Fighter Tires on Low Strength Soil . . . . .	76
44	Flotation Index, Aircraft Cargo Tires on High Strength Soil . . . . .	77
45	Flotation Index, Aircraft Bomber Tires on High Strength Soil . . . . .	78
46	Flotation Index, Aircraft Fighter Tires on High Strength Soil . . . . .	79
47	Operations Index, Aircraft Cargo Tires on Low Strength Soil . . . . .	81
48	Operations Index, Aircraft Bomber Tires on Low Strength Soil . . . . .	82
49	Operations Index, Aircraft Fighter Tires on Low Strength Soil . . . . .	83
50	Operations Index, Aircraft Cargo Tires on High Strength Soil . . . . .	84
51	Operations Index, Aircraft Bomber Tires on High Strength Soil . . . . .	85
52	Operations Index, Aircraft Fighter Tires on High Strength Soil . . . . .	86
53	Flotation Index Nomograph . . . . .	87
54	Grain Size Distribution, Buckshot Clay . . . . .	97
55	Grain Size Distribution, Mortar Sand . . . . .	98
56	Triaxial Test Results, Buckshot Clay . . . . .	100
57	Triaxial Test Results, Mortar Sand . . . . .	101
58	Soil Uniformity Measurements, Buckshot Clay, Tests 6, 7, and 8 . . . . .	104
59	Soil Uniformity Measurements, Buckshot Clay, Tests 9, 10, and 11 . . . . .	105
60	Soil Uniformity Measurements, Buckshot Clay, Tests 12, 13, and 14 . . . . .	106
61	Soil Uniformity Measurements, Buckshot Clay, Tests 15, 16, and 17 . . . . .	107

62	Soil Uniformity Measurements, Buckshot Clay, Tests 18, 19, and 20 . . . . .	108
63	Soil Uniformity Measurements, Buckshot Clay, Tests 21, 22, and 23 . . . . .	109
64	Soil Uniformity Measurements, Buckshot Clay, Tests 24, 25, and 26 . . . . .	110
65	Soil Uniformity Measurements, Buckshot Clay, Test 27 . . . . .	111
66	Soil Uniformity Measurements, Mortar Sand, Tests 4 and 5 . . . . .	112
67	Soil Uniformity Measurements, Mortar Sand, Tests 7, 8, and 9 . . . . .	113
68	Soil Uniformity Measurements, Mortar Sand, Tests 10, 11, and 12 . . . . .	114
69	Soil Uniformity Measurements, Mortar Sand, Tests 14, 15, and 16 . . . . .	115
70	Soil Uniformity Measurements, Mortar Sand, Tests 17 and 18 . . . . .	116

# LIST OF TABLES

TABLE		PAGE
1	Design Test Program . . . . .	14
2	Tire Geometry Data . . . . .	18
3	Moisture-Density Data . . . . .	19
4	Test Bed Soil Conditions . . . . .	19
5	Triaxial Test Results . . . . .	20
6	Drag-Sinkage Data - Clay . . . . .	23
7	Drag-Sinkage Data - Sand . . . . .	27
8	Basic Load Curve . . . . .	129

LIST OF SYMBOLS

$A, A_1, A_2$	Tire contact area (rigid surface)
$A_c$	Cone base area
$a$	Radius of loaded area
$B$	A variable related to the stress invariants
$b$	Tire width
CBR	California bearing ratio
$C_{DI}$	Soil impingement drag coefficient
$CI_{avg}$	Average cone index of soil over 0" to 6" depth
CMN	Clay mobility number
$c$	Cohesion of soil
$c_1$	Dilatational wave propagation velocity
$D$	Tire diameter
$D'$	Additional drag due to high speed effects
$D_c$	Cone diameter
DI	Drag Index
$d$	Tire deflection
$E$	Young's modulus
FI	Flotation Index
$F$	Redefined yield function for stress correction
$f$	Yield function
$G$	Modulus of rigidity
$h$	Space mesh
$I$	First invariant of the stress tensor

$i$	Location identifier (column)
$J$	Second invariant of the deviatoric stress tensor
$j$	Location identifier (row)
$K$	Constant ( $= 1/2 \rho b$ )
$k$	Yield stress in shear
$k_c$	Soil deformation modulus (for cohesion)
$k_\phi$	Soil deformation modulus (for friction)
$l$	Tire footprint in length
$m$	Fraction of tire diameter
$N$	Number of tires
$\bar{N}$	Unit normal vector to the function $F$
$n$	Fraction of tire width and Exponent of sinkage
$OI$	Operations Index
$P$	Single Wheel vertical load (tire)
$P_c$	Cone vertical load
$p$	Tire contact stress
$p_o$	Circular uniform pressure distribution
$Q$	Constant
$R$	Single wheel rolling drag force (tire)
$R_B$	Braking drag force
$r$	Radial coordinate
$S$	Tire slip
$SMN$	Sand mobility number
$t$	Time

$t_d$	Time duration of load pulse
$\Delta t$	Time increment
$u, \dot{u}, \ddot{u}$	Displacement, velocity, and acceleration in the $r$ -direction
$\Delta u$	Incremental radial displacement
$V$	Aircraft horizontal ground velocity
$\Delta W$	Incremental work done on soil medium
$w, \dot{w}, \ddot{w}$	Displacement, velocity, and acceleration in the $z$ -direction
$\Delta w$	Incremental vertical displacement
$Z$	Instantaneous soil sinkage
$Z_c$	Vertical penetration of cone
$z$	Downward space coordinate
$\alpha$	Soil parameter related to the friction angle and Vertical load-contact area ratio
$\beta$	Constant used to define loading and unloading
$\gamma$	Weight density of soil
$\gamma_{rz}$	Shear strain in the $r$ - $z$ direction
$\Delta\gamma_{rz}$	Incremental shear strain in the $r$ - $z$ direction
$\epsilon$	Trace of the strain tensor, $\epsilon_r + \epsilon_\theta + \epsilon_z$
$\epsilon_y$	General strain tensor
$\epsilon_r, \epsilon_\theta, \epsilon_z$	Normal strain in the $r, \theta$ and $z$ directions
$\Delta\epsilon$	Incremental trace of the strain tensor, $\Delta\epsilon_r + \Delta\epsilon_\theta + \Delta\epsilon_z$
$\Delta\epsilon_r, \Delta\epsilon_\theta, \Delta\epsilon_z$	Incremental normal strain in the $r, \theta$ , and $z$ directions
$\eta$	Stress correction factor
$\theta$	Tangential angular coordinate

$\lambda$	Lame's constant
$\Lambda$	Scalar factor in the normality flow rule
$\nu$	Poisson's ratio
$\phi$	Soil friction angle
$\rho$	Mass density of the soil
$\sigma_{ij}$	General stress
$\sigma_r, \sigma_\theta, \sigma_z$	Normal stress in the r, $\theta$ , and z directions
$\sigma_o$	Applied pressure
$\Delta\sigma_r, \Delta\sigma_\theta, \Delta\sigma_z$	Incremental normal stress in the r, $\theta$ , and z directions
$\tau_{rz}$	Shear stress in the r-z direction
$\Delta\tau_{rz}$	Incremental shear stress in the r-z direction

## SECTION I

### INTRODUCTION

The problems associated with the operation of aircraft on forward area soil runways are well documented. These problems include drag resistance due to soil sinkage, dynamic structural loads caused by sinkage and ground roughness leading to structural damage and excessive fatigue accumulations per aircraft mission, multiple pass effects related to continued runway use, and limited runway lengths and widths for landing and takeoff operations.

In order to develop the criteria for the efficient and effective utilization of soil runways while including adequate safety provisions, it is necessary to understand the interaction effects between the tire and soil during rolling and braking modes. In the past, tire-soil interaction studies have been conducted mainly in the area of off-the-road mobility for military vehicles. More recently, significant advances have been made toward defining landing gear-soil interaction and developing the flotation criteria to permit comparative evaluation of the relative merits of various landing gear configurations<sup>(1, 2, 3, 4)</sup>. Flotation in this context is defined as the tire-soil interaction and the ability of the soil to support the tire load system.

The basic objective of this program is to analytically define landing gear-soil interaction and to develop a system for rating the relative flotation capacity of landing gear contact elements and landing gear systems during aircraft operations on semi- and unprepared soil runways. The primary variables associated with evaluating the flotation capacity of a landing gear system include drag, sinkage, multiple wheel effects, and braking effects. Secondary variables which influence flotation capacity include turning, landing impact, and point of rotation effects. The Relative Merit Index (RMI) is the system for incorporating these primary and secondary flotation variables in a suitable manner to permit the comparative evaluation of the flotation capacity of landing gear types and configurations. Phase I<sup>(1)</sup> of this program included a survey of the flotation problem, establishment of the critical flotation parameters, and an investigation of available flotation data leading to the development of a flotation analysis equation.

Phase II, described in this report, included the development of an empirical sinkage prediction equation, a finite element based analytical sinkage prediction equation, conducting the single-rolling wheel verification tests, refinement of the drag ratio-sinkage ratio relationship, and the development of the single wheel Relative Merit Index (RMI) system for



defining comparative flotation capacity. The Phase III portion of the program will include the development and verification of multiple wheel, high velocity, and braking flotation effects and the establishment of the finalized RMI indexing system leading to the development of a final flotation criteria for defining aircraft performance on semi- and unprepared soil airstrips. A flow chart indicating the overall flotation research program is shown in Figure 1.

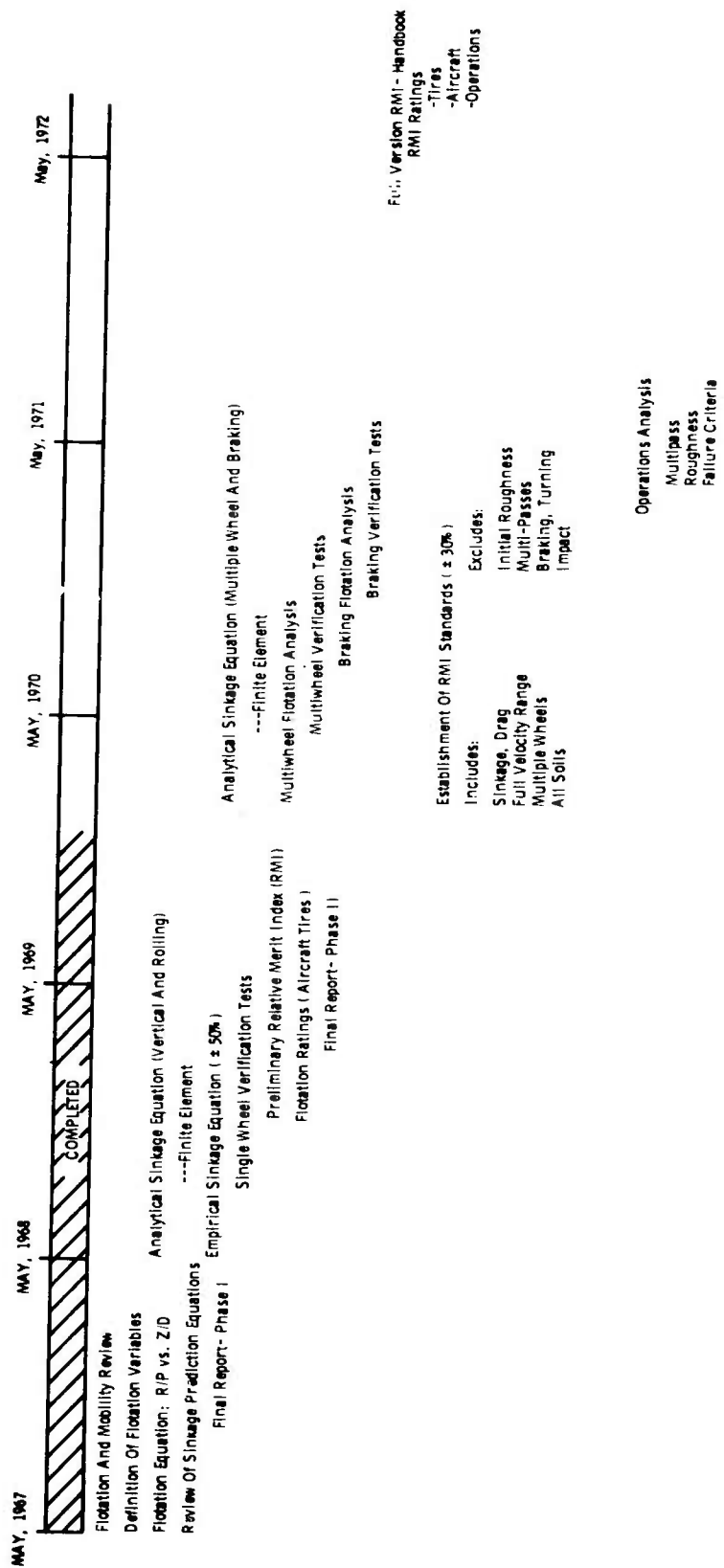


Figure 1 Projected Landing Gear-Soils Interaction and Flotation Research Program

## SECTION II

### DRAG-SINKAGE ANALYSIS

#### 1. Drag Ratio-Sinkage Ratio, Single Wheel

The drag forces exerted by the deformed ground on the aircraft wheel are an important consideration in relation to aircraft thrust for determining the takeoff capability and required runway lengths for aircraft operations on soil surfaces. The results of the Phase I effort indicated that flotation performance of aircraft operating on soil runways is directly related to the sinkage and drag encountered by the aircraft tire.

In the Region II velocity range (5 knots to 40 knots), the drag has been shown to be directly proportional to the sinkage<sup>(1)</sup> as expressed by the functional equation

$$R/P = f(Z/D) \quad (1)$$

where

R = rolling drag force  
P = vertical tire load  
Z = instantaneous soil sinkage  
D = outside tire diameter

Region II has previously been shown to be a velocity range in which the drag ratio (R/P) and sinkage ratio (Z/D) remain relatively constant<sup>(1)</sup>. Subsequent to the development of the initial drag ratio-sinkage ratio relationship, additional flotation data became available from the Single Wheel Verification Test Program and the Lockheed-Langley Test Program<sup>(4)</sup>. Figure 2 presents the drag ratio (R/P) versus sinkage ratio (Z/D) based on all available flotation data<sup>(3, 4, 5, 6, 7, 8)</sup>. The flotation data includes the full range of soil type (cohesive to cohesionless) and tire diameters from 18" to 70", which encompasses the range of tire sizes for military aircraft. The Lockheed-Langley tests measured rut depths rather than sinkage (Z). Measured rut depths in the buckshot clay were converted to instantaneous sinkage for inclusion in Figure 2 using elastic rebound corrections determined from previous aircraft tire tests on buckshot clay<sup>(8)</sup> and the results of the Single Wheel Verification tests for which both permanent rut depth and elastic deformation were measured.

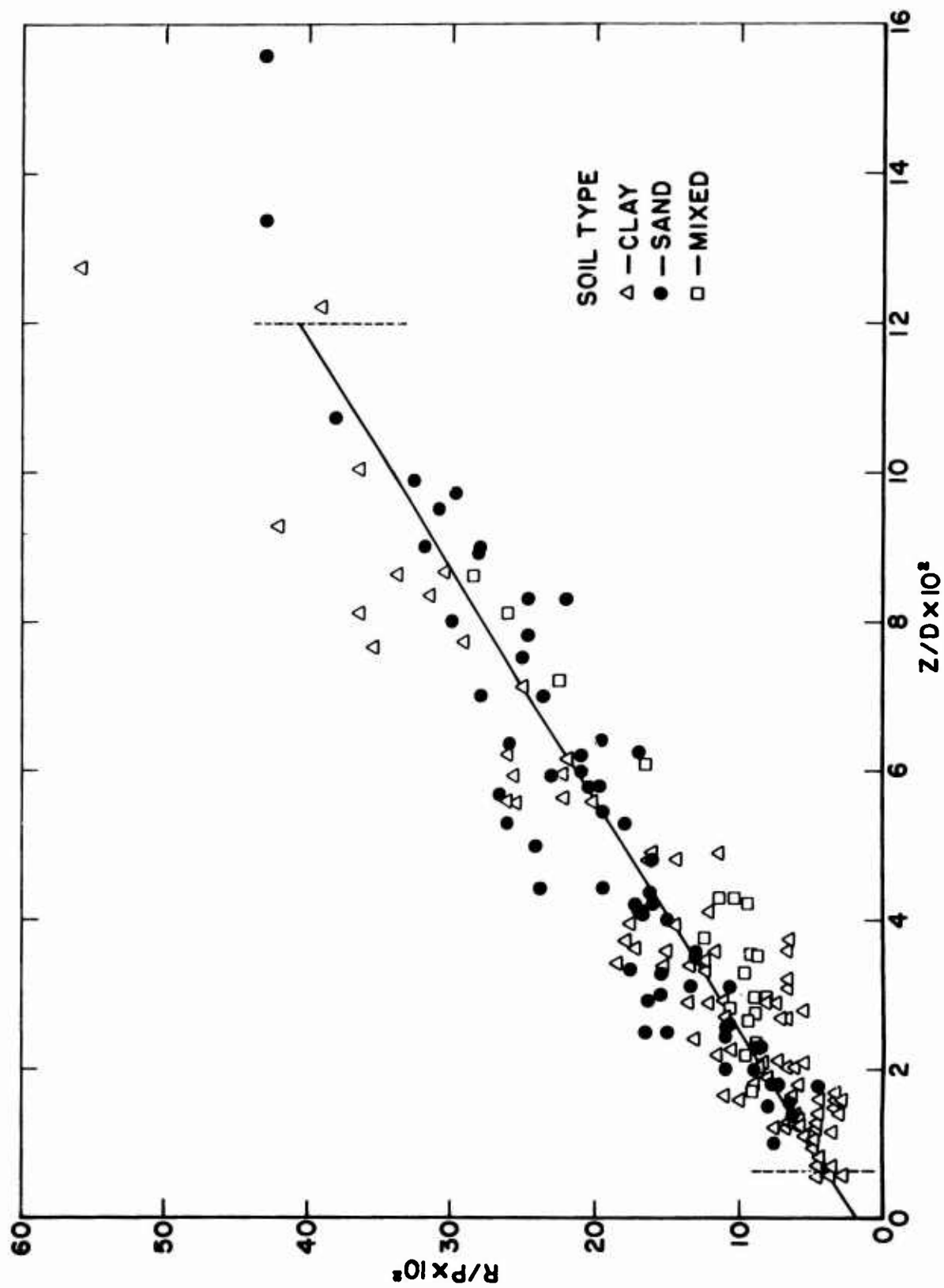


Figure 2 Drag Ratio-Sinkage Ratio, Single Wheels on Soil

A least squares linear fit of the data given in Figure 2, using Equation (1) yields a drag ratio-sinkage ratio as given by

All Soil

$$\frac{R}{P} = 0.018 + 3.23(Z/D) \quad (2)$$

for  $0.01 \leq \frac{Z}{D} \leq 0.12$

The positive R/P intercept at zero sinkage is expected since some rolling resistance (friction) is present at zero sinkage. A closer evaluation of Figure 2 shows a distinct trend of the sand drag ratio relationship in comparison to the clay drag ratio relationship. A least squares linear fit of the data for each soil type gives

Cohesionless Soil

$$\frac{R}{P} = 0.048 + 2.77\left(\frac{Z}{D}\right) \quad (3)$$

Cohesive Soil

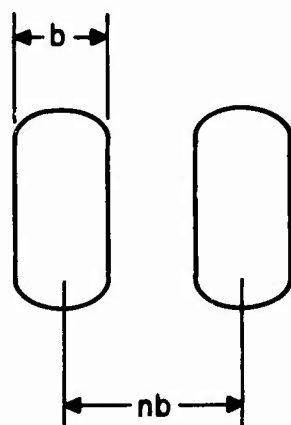
$$\frac{R}{P} = 0.000 + 3.85\left(\frac{Z}{D}\right) \quad (4)$$

which indicates that aircraft tires encounter more drag at low sinkages when operating on sand in comparison to clay but encounter less drag at high sinkages on sand in comparison to clay. Based on an analysis of Figure 2, however, Equation (1) provides a good first approximation for evaluating rolling drag for aircraft tires on any soil type within the restricted range.

## 2. Drag Ratio-Sinkage Ratio, Multiple Wheel

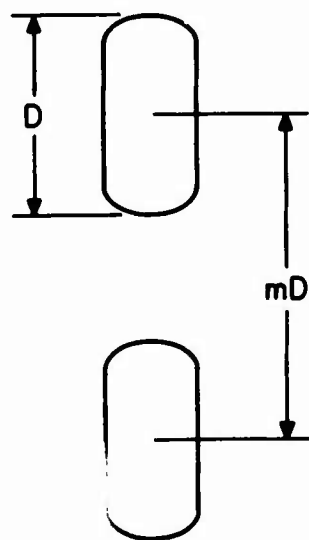
The influence of relative wheel positions in multiple wheel configurations must be considered in evaluating drag and sinkage effects for aircraft tires on soil. Two types of multiple wheel configurations are of interest: dual (twin) and tandem as indicated in Figure 3. An important consideration for tandem tires is the extent to which the rear tire follows in the track of the lead tire.

While dual tires with close spacing are, in many instances, objectionable for off-the-road powered wheel vehicles, close spacing of aircraft tires offer some slight benefits<sup>(1, 5)</sup> in reducing total rolling drag below that which would be encountered if each wheel operated as an isolated wheel. Although very little twin wheel data is available, Figure 4 provides an indication of tire spacing effects on the resulting drag resistance.



TWIN WHEEL

$b$ =TIRE WIDTH  
 $n$ =FRACTION OF TIRE WIDTH



TANDEM WHEEL

$D$ =TIRE DIAMETER  
 $m$ =FRACTION OF TIRE DIAMETER

Figure 3 Multiple Wheel Landing Gear Assemblies

Considerable reduction in drag can be expected in tandem tires operating on soil when the rear tire follows in the forward tire's track since the rear tire will undergo less sinkage. Figure 5 shows this tandem tire effect for clay soil as a function of tandem tire spacing. The higher drag encountered at 123 inch spacing in comparison to the 60 inch spacing is probably related to elastic rebound of the soil after passage of the lead tire.

Figures 4 and 5 show that a "configuration sensitivity" exists for determining drag on multiple aircraft tires and indicates the need for a separate flotation criteria for twin and tandem tire configurations. The results of previous multiple tire studies conducted by WES<sup>(8)</sup> did not recognize any difference between twin and tandem tires when determining a load adjustment for the equivalent single wheel load.

The results, although preliminary, indicate the need for additional research in order to develop the required flotation relationships for multiple tire configurations.

### 3. High Velocity

Aircraft ground speeds range from static conditions up to landing and takeoff speeds of 120 knots. Only recently have these high speed effects been recognized as a separate phenomena from low speed performance in analyzing flotation effects<sup>(1, 3, 4)</sup>. Figure 6 shows the typical trends of the drag ratio and sinkage ratio versus horizontal speed for aircraft tires operating on soil, and indicates at least three distinct zones of velocity response. At low speeds (less than 5 knots), the drag ratio undergoes considerable change with velocity due to the viscous effects in the soil. From 5 knots to approximately 40 knots, the drag ratio remains relatively constant, indicating that the rate of loading effects are no longer significant. In the third velocity region, the drag ratio increases rapidly, peaks at what has been termed the "planing speed", and then decreases. The "planing speed" is apparently a function of the soil type, soil strength, and tire inflation pressure<sup>(3)</sup>.

There are at least two ways to consider the drag ratio response in the Region III velocity range. On the assumption that a tire traversing soil at high velocities responds the same as tires operating on slush,

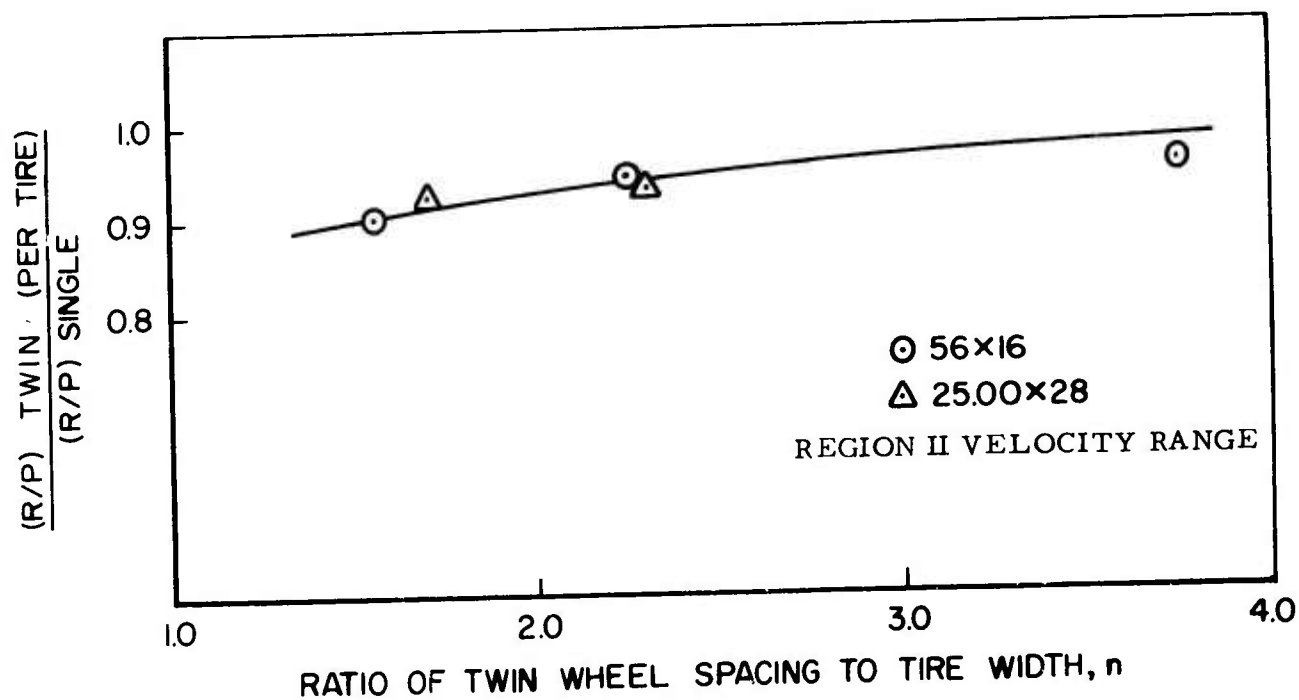


Figure 4 Twin Wheel Drag Effects in Clay Soil

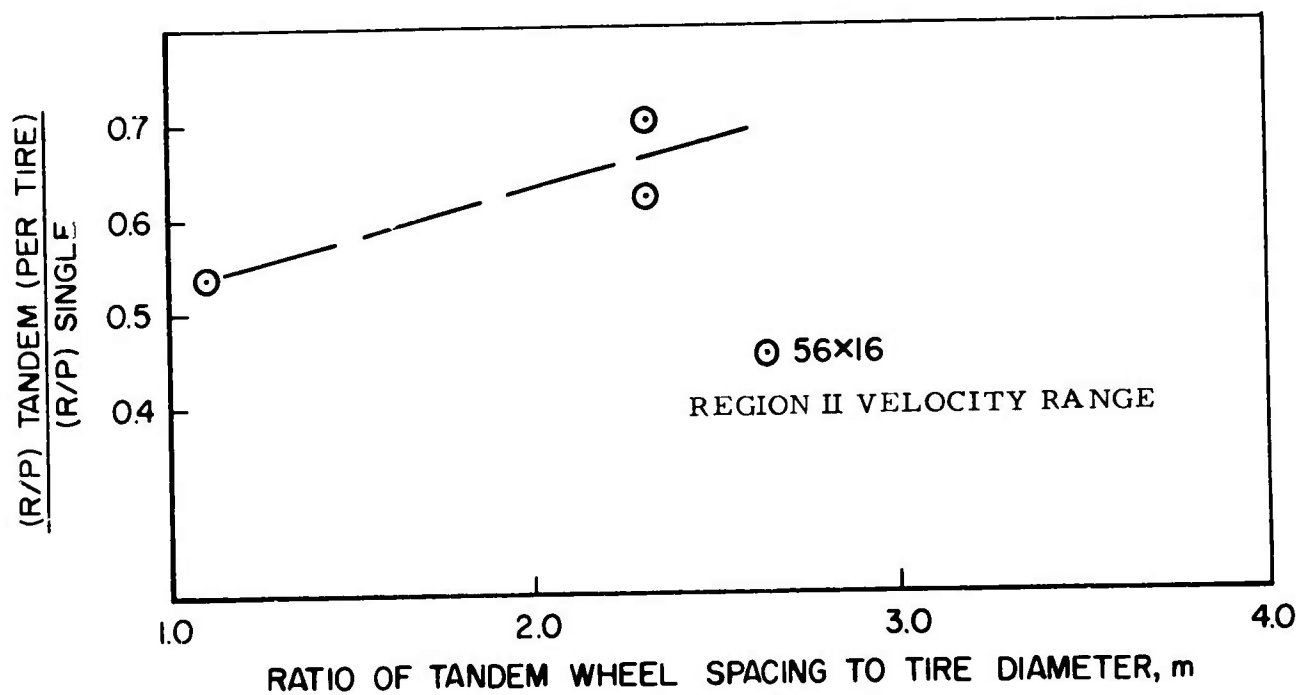


Figure 5 Tandem-Tracking Wheel Drag Effects in Clay Soil



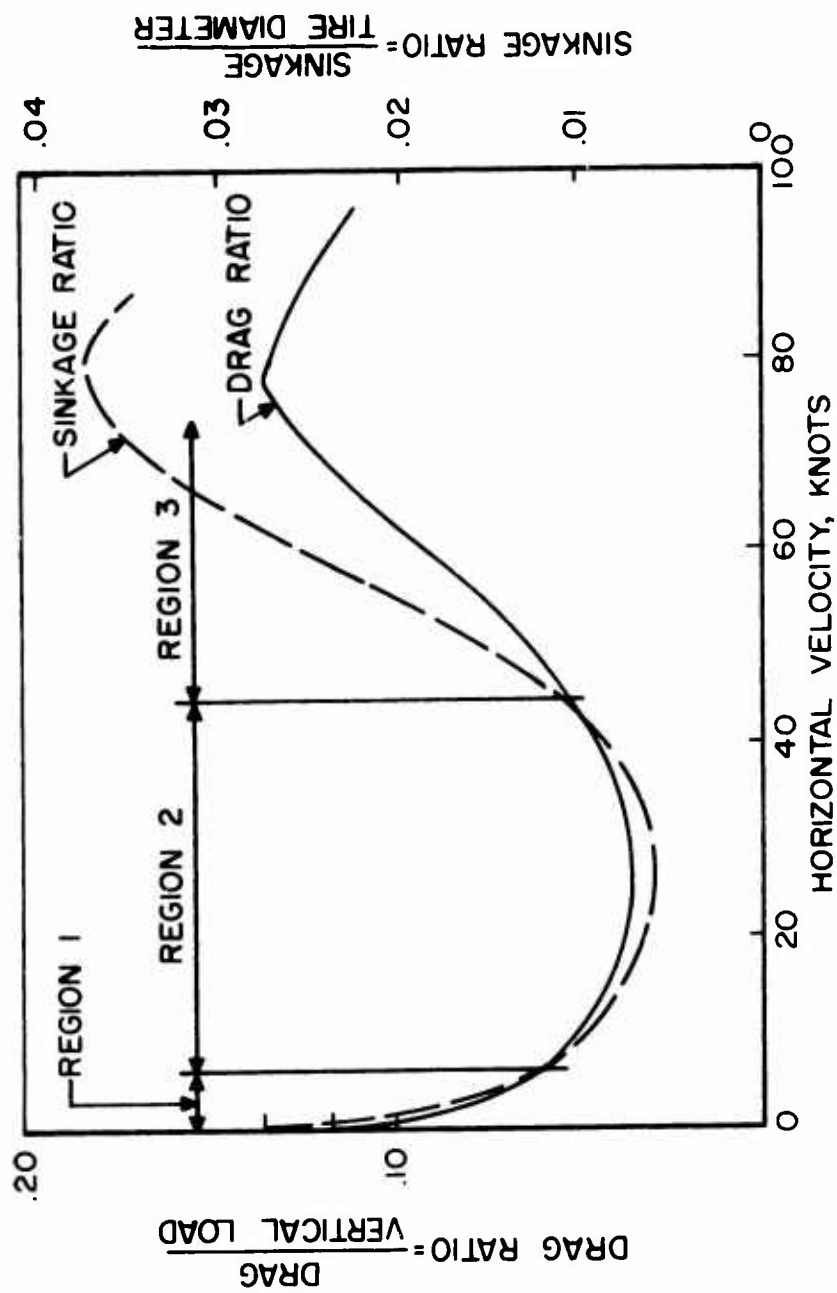


Figure 6 Typical Drag Ratio, Sinkage Ratio vs Horizontal Velocity in Soil

Boeing<sup>(3)</sup> utilized the drag equations developed for slush conditions and interpreted the drag as

$$D' = KC_{DI}ZV^2 \quad (5)$$

where  $D'$  = additional drag due to high speed effects  
 $K$  = constant related to soil density ( $\rho$ ) and tire width ( $b$ ) =  $1/2\rho b$   
 $C_{DI}$  = soil impingement drag coefficient  
 $V$  = horizontal velocity

The soil impingement coefficient, which must be determined experimentally, has not correlated well with the variables of soil strength and tire inflation pressures in a recent experimental effort<sup>(4)</sup>. The drag defined by Equation (5) must be added to the drag developed in Region II (see Equation 2) to determine the total drag acting on the tire in the Region III velocity range.

An alternate approach would be to study the relationship between total drag and instantaneous sinkage in a manner similar to that defined by Equation (1). If a direct correlation exists between the drag and sinkage, then the rapid increase in drag should be attributed more to rate loading effects in soil (i.e., sinkage response related to rate of loading) than to changes in tire contact geometry effects.

While only a limited amount of high speed data is available, Figure 7 shows the results of a recent experimental program<sup>(4)</sup>. For comparison purposes, both the least squares fit of the high velocity test data and the least squares relationship of Equation (2) for the Region II velocity range is shown. The Region III defining equation is given by,

$$\frac{R}{P} = 0.038 + 3.53\left(\frac{Z}{D}\right) \quad (6)$$

for  $0.01 \leq \frac{Z}{D} \leq 0.06$

These results indicate an approximate 15% difference in the drag ratio response. While sufficient experimental evidence is not available at this time to suggest that the drag ratio-sinkage ratio relationship of the form of Equation (1) can be used to interpret drag throughout the entire velocity range, it does indicate that research efforts in studying the effect of rate of loading on soil sinkage may ultimately explain the Region III drag ratio response and "planing speed" effects rather than tire geometry change effects.

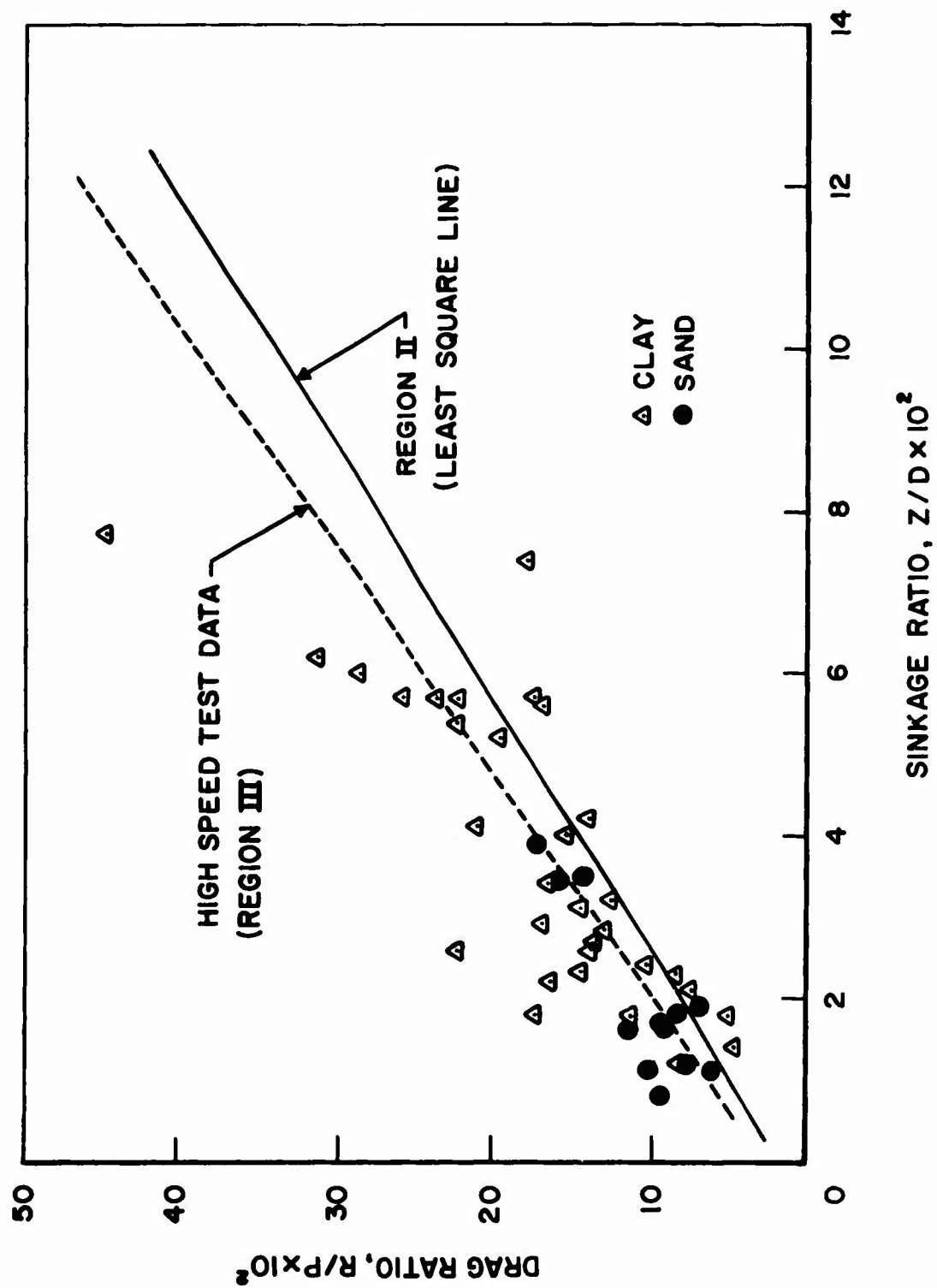


Figure 7 High Velocity (Region III) Drag Ratio Effects in Soil

## SECTION III

### SINGLE WHEEL VERIFICATION TESTS

#### 1. Purpose

The results of the drag ratio/sinkage ratio relationship shown in Figure 2 includes the test results from the Single Wheel Verification Test Program and describes the basic rolling tire-soil interaction phenomena. This test program was conducted to

1. provide additional confirmation of the preliminary drag ratio/sinkage ratio relationship developed in Phase I;
2. provide experimental data for the development of an aircraft tire-soil interaction empirical sinkage equation; and
3. provide experimental data for the preliminary verification of the finite element based-analytical sinkage prediction equation currently under development.

All tests conducted were single pass only.

#### 2. Test Program

To accomplish these objectives a test program was formulated as outlined in Table I. The tires, loads, and soil parameters were selected to provide a range in sinkage of from 1/2 inch to 3 inches in the sand and clay. The following parameters were measured and evaluated in the program:

- wheel vertical load
- wheel drag load
- tire deflection
- tire contact geometry (rigid)
- soil properties (type, strength, and modulus)
- instantaneous soil sinkage
- permanent rut depth
- horizontal wheel velocity

#### 3. Test Facility

All tire-soil interaction tests were conducted at the U.S. Army Engineers Waterways Experiment Station (WES) Mobility and Environmental Divisions Test Facility. The basic facility consists of a row of soil carts joined end to end in which processed soil is placed at predetermined conditions prior to conducting a tire test. The test carriage dynamometer is suspended from an overhead rail system which guides the carriage over the row of

Table 1  
Design Test Program

Tire Type	Diameter (in)	Width (in)	Defl. (%)	Vertical Load (lbs)	Soil Strength (CI)	Velocity (ft/sec)	Soil Type
7.00-6-6PR	18.5	6.8	28	300	25	20	Mortar Sand
"	"	"	"	500	"	"	"
"	"	"	"	700	"	"	"
"	"	"	45	500	"	"	"
"	"	"	"	1000	"	"	"
"	"	"	"	1300	"	"	"
8.50-10-8PR	25.1	8.5	28	500	25	20	Mortar Sand
"	"	"	"	1000	"	"	"
"	"	"	"	1300	"	"	"
"	"	"	45	1000	"	"	"
"	"	"	"	1500	"	"	"
"	"	"	"	2000	"	"	"
7.00-6-6PR	18.5	6.8	28	500	25	20	Buckshot Clay
"	"	"	"	625	"	"	"
"	"	"	"	700	"	"	"
"	"	"	45	500	"	"	"
"	"	"	"	800	"	"	"
"	"	"	"	1000	"	"	"
8.50-10-8PR	25.1	8.5	28	1000	50	20	Buckshot Clay
"	"	"	"	1500	"	"	"
"	"	"	"	2000	"	"	"
"	"	"	"	500	25	"	"
"	"	"	"	800	"	"	"
"	"	"	"	1000	"	"	"
"	"	"	"	1300	"	"	"
"	"	"	45	1000	50	"	"
"	"	"	"	1500	"	"	"
"	"	"	"	2000	"	"	"
"	"	"	"	1000	25	"	"
"	"	"	"	1300	"	"	"
"	"	"	"	1500	"	"	"

soil carts. The test carriage is towed by a steel cable attached to the carriage. Vertical and drag loads are measured using strain gage type load cells mounted within the dynamometer system. Figure 8 shows a view of the overall test system and Figure 9 shows a 7.00-6 Type III aircraft tire mounted in the carriage dynamometer. A complete description of the Test Facility is available in a previous WES report<sup>(9)</sup>.

#### 4. Test Tires

Two test tires were selected for the program which provided an 18 inch to 25 inch range in tire diameters. Figures 9 and 10 show the 7.00-6 and 8.50-10 Type III tires, respectively, and Table 2 gives the pertinent tire geometry data. Each tire was subjected to a series of cyclic loadings before the tire-soil interaction tests to eliminate any prestress effects.

#### 5. Soil Tests and Preparation

The two test soils selected for the program were buckshot clay and mortar sand. The main intent of the soil tests was to provide an accurate description of the test bed soil and its uniformity of placement. Soil tests conducted included moisture and density determinations, mobility cone penetration resistance (CI), California Bearing Ratio (CBR), and plate bearing resistance. A complete description of each soil test is given in Appendix I.

The results of the moisture-density determinations are summarized in Table 3.

In order to establish a relationship between the cone index, CBR, and plate bearing modulus values for use in the sinkage comparison study, controlled cone penetrometer, CBR, and plate bearing tests were conducted for each soil condition. These results as given by the average cone index over 0 to 6 inches, the average surface CBR at 0.1 inch penetration, and Bekker modulus values are summarized in Table 4.

Some difficulties were encountered in determining the Bekker parameters, since the semi-logarithmic plot of the penetration resistance versus sinkage for each plate size did not yield parallel lines as required



Figure 8 Test Carriage on Soil Carts



Figure 9 Type III, 7.00-6 Test Tire



Figure 10 Type III, 8.50-10 Test Tire



Table 2

TIRE DATA

Tire Type	Percent Defl.	Wheel Load P [lbs]	Carcass Diameter [in]	Contact Area [sq in]	Tire Print		Deflection		Inflation Pressure		Section Height		Section Width	
					Length [in]	Width [in]	[in]	[in]	Unloaded psi	Loaded psi	Unloaded [in]	Loaded [in]	Unloaded [in]	Loaded [in]
7.00-6-6PR	28	300	17.74	33.95	7.70	5.50	1.46	3.60	3.60	4.60	5.12	3.69	6.72	7.52
"	"	500	17.94	35.23	7.92	5.50	1.46	10.00	10.00	10.30	5.22	3.76	6.75	7.47
"	"	625	17.96	31.22	7.53	5.30	1.46	14.8	15.7	15.7	5.23	3.77	6.76	7.51
"	"	700	17.98	34.90	7.90	5.50	1.47	16.5	17.20	17.20	5.24	3.77	6.76	7.51
"	"	765	18.00	32.09	7.65	5.25	1.47	18.7	19.6	19.6	5.25	3.78	6.76	7.50
"	"	1000	18.04	35.54	8.07	5.40	1.47	26.60	27.00	27.00	5.27	3.80	6.78	7.52
"	"	1500	18.16	37.65	8.32	5.49	1.49	41.85	42.30	42.30	5.33	3.84	6.80	7.57
"	45	500	17.74	52.30	10.35	5.45	2.31	3.05	4.15	4.15	5.12	2.81	6.72	8.28
"	"	800	17.82	48.13	9.70	5.45	2.32	7.7	9.10	9.10	5.22	2.88	6.74	8.25
"	"	1000	17.94	53.09	10.38	5.50	2.34	11.7	13.0	13.0	5.23	2.88	6.75	8.23
"	"	1300	17.69	53.90	10.40	5.60	2.35	16.0	18.3	18.3	5.24	2.89	6.76	8.26
"	"	1500	17.98	54.76	10.46	5.57	2.35	21.0	22.30	22.30	5.16	2.84	6.77	8.22
8.50-10-8PR	28	500	24.56	53.40	9.90	6.60	1.77	3.5	3.7	3.7	6.28	4.52	8.00	8.80
"	"	1000	24.72	55.78	10.42	6.74	1.78	12.3	12.7	12.7	6.36	4.58	8.01	8.88
"	"	1300	24.66	56.30	10.43	6.60	1.77	16.7	17.9	17.9	6.33	4.56	8.01	8.81
"	"	1500	24.68	59.53	10.58	6.76	1.78	19.6	20.0	20.0	6.34	4.56	8.02	8.82
"	"	2000	24.80	57.88	10.52	6.70	1.79	29.6	30.0	30.0	6.40	4.61	8.01	8.83
"	45	1000	24.50	95.03	13.78	6.93	2.81	4.00	5.00	5.00	6.25	3.44	8.04	9.87
"	"	1250	24.56	87.42	12.10	7.00	2.83	6.40	8.10	8.10	6.28	3.45	8.02	9.85
"	"	1500	24.60	91.50	13.53	6.95	2.83	8.40	9.60	9.60	6.30	3.47	8.02	9.81
"	"	2000	24.68	94.81	13.72	7.00	2.85	13.60	15.20	15.20	6.34	3.49	8.01	9.80

Table 3

## Moisture-Density Data

Test Section	Soil Type	Design Soil Strength $CI_{avg}$ (0 to 6")	Average Conditions	
			Dry Density (pcf)	Moisture Content (%)
1	Buckshot Clay	50	79.9	36.9
2	Buckshot Clay	25	75.1	42.2
3	Mortar Sand	25	99.5	2.5

Table 4

## Test Bed Soil Conditions

Test Section	Soil Type	Design Soil Strength $CI_{avg}$ (0 to 6")	$CI_{avg}$ 0 to 6"	CBR	Bekker Parameters		
					$k_c$	$k_\phi$	n
1	Buckshot Clay	25	25.6	0.8	4.4	10.6	0.05
2	Buckshot Clay	50	48.2	1.4	4.0	22.2	0.09
3	Mortar Sand	25	27.0	0.7	0	4.0	0.4

by the Bekker sinkage equation. Figure 11 shows the results of a comparison between the average cone index and the CBR based on the data used in developing Table 4. An approximate relationship between  $CI_{avg}$  and CBR as shown by the dashed line in Figure 11 is given by

$$CI_{avg}(\text{psi}) = 32 \text{ CBR} \quad (7)$$

which is similar to the results found from previous studies<sup>(4)</sup>.

Undrained triaxial tests were also run on undisturbed samples of the sand and clay taken from the soil carts to determine the cohesion and friction components of the soil strength. These test results, which are described in detail in Appendix I, are summarized below in Table 5.

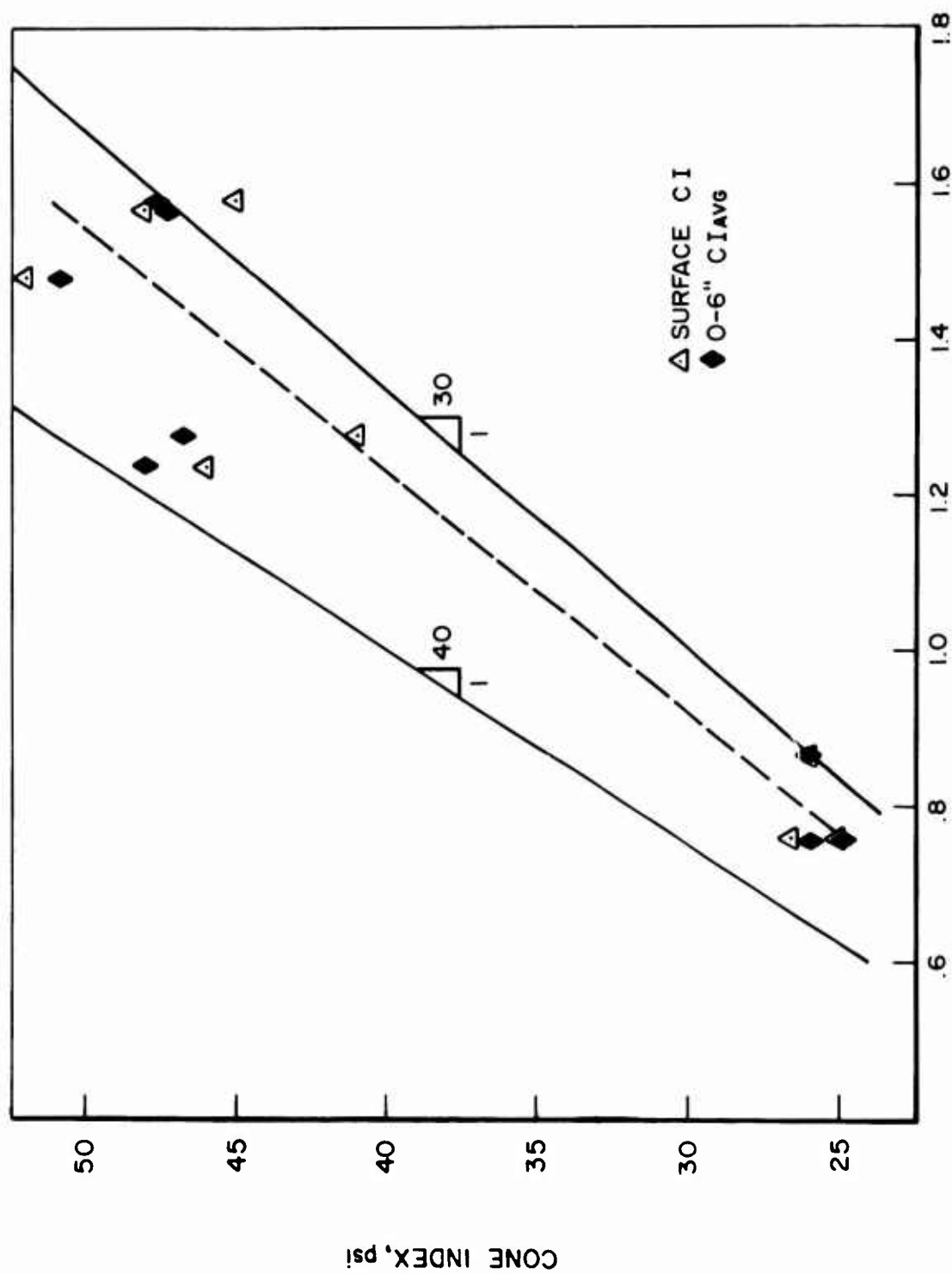
Table 5  
Triaxial Test Results

Test Section	Soil Type	Design Soil Strength	Triaxial Results		Moisture Content
		$CI_{avg}$ (0" to 6")	c	$\phi$	w, %
1	Buckshot Clay	25	202	1°	41.5
2	Buckshot Clay	50	382	1°	38.0
3	Mortar Sand	25	0	36°	0.5

These results are used in defining the yield and plastic deformation conditions in the finite element sinkage prediction equation.

#### 6. Test Results - Buckshot Clay

A total of 14 tire-soil interaction tests were conducted on the clay soil with the 8.50-10 tire and 6 tests with the 7.00-6 tire. Before each test run, cone penetrometer tests were run at two meter intervals to verify the uniformity of soil conditions. The results of these soil uniformity tests for each test condition (by test number) are given in Appendix II. The test parameters previously detailed were measured for each test run. Drag and vertical loads were measured continuously along the test track by the dynamometer load cells and recorded in oscillographic traces which are permanent records. Axle height was also recorded continuously along the test run and was used for calculating the instantaneous tire sinkage<sup>(10)</sup>. Instantaneous soil sinkage gages previously used by WES<sup>(8)</sup> were inserted in a number of test runs to verify the sinkage determinations. Rut depths were determined by the difference between the original soil surface and the



CBR at 0.1" PENETRATION

Figure 11 Cone Index-CBR Soil Correlation

final soil surface after passage of the tire. The difference between the instantaneous sinkage and permanent rut depth is the elastic rebound. All tests were conducted at an approximate horizontal velocity of 20 feet per second. The complete results for the tire-soil interaction tests are summarized in Table 6.

One way in which increased flotation can be obtained is to increase the tire deflection. Figure 12 shows this influence in terms of the reduced sinkage and drag. Although applicable only to these tires and soil conditions, a change in tire deflection from 28% to 45% caused an approximated one-third reduction in drag. Figure 13 shows the variation of the drag ratio ( $R/P$ ) with sinkage ratio ( $Z/D$ ) for each tire and percent deflection. No clear separation of the data exists by tire deflection. Equation (2) is also shown on Figure 13 and shows again the tendency toward higher drags at higher sinkages for aircraft tires on clay soil than for the average of sand and clay (all soil line).

As indicated by Figure 13, it is necessary to predict sinkage in order to estimate drag. Previous efforts <sup>(2)</sup> and the analysis in Section IV of this report have shown an empirical relationship between the sinkage characteristic ( $Z/l$ ) and the load-strength ratio ( $\alpha/CI_{avg}$ ) where

- $l$  = contact footprint length (rigid surface)
- $\alpha$  = ratio of vertical load ( $P$ ) to rigid surface contact area ( $A$ )
- $CI_{avg}$  = average cone index over 0" to 6" depth

Figure 14 shows the results of the tire-soil interaction data plotted in this manner. It is evident from these results that as the  $\alpha/CI_{avg}$  ratio exceeds approximately 0.6, the sinkage characteristic increases more rapidly than in the 0.2 to 0.6 range. Since drag is directly related to sinkage, the drag will increase in a corresponding manner.

## 7. Test Results - Mortar Sand

A total of 6 tire-soil interaction tests were conducted on the sand soil with the 8.50-10 tire and 6 tests with the 7.00-6 tire. Prior to each test run, the uniformity of soil placement was investigated by running cone penetrometer tests at two meter intervals along the test section. The results of these tests are given in Appendix II. As in the clay tests, the basic parameters measured were vertical load, drag, sinkage, and rut depth in addition to the tire and soil parameters. The complete results for the tire-soil interaction tests on mortar sand are given in Table 7. All tests were run at a horizontal velocity of 20 feet per second.

The drag ratio-sinkage ratio results for the sand are shown in Figure 15, together with the least squares fit line for all available data as defined by Equation (2). Reference to Figures 13 and 15 shows that rolling

Table 6

## Drag-Sinkage Data - Clay

Test No.	Tire Type	Percent Defl.	CI <sub>avg</sub>	Sinkage Z [in]	Permanent Rut Depth [in]	Wheel Load P [lbs]	Drag R [lbs]	Sinkage Ratio Z/D in 10 <sup>-2</sup>	Drag Ratio R/P in 10 <sup>-2</sup>
6	8.50-10-8PR	45	48.9	0.3	0.1	1000	75	1.22	7.5
7	"	45	48.3	0.3	0.03	1507	100	1.22	6.64
8	"	45	49.2	0.39	0.12	2019	151	1.58	7.48
9	"	28	50.5	0.3	0.16	1000	45	1.21	4.5
10	"	28	49.1	0.52	0.16	1494	107	2.11	7.16
11	"	28	50.6	0.86	0.59	2016	250	3.47	12.4
12	"	45	22.1	0.91	0.30	995	179	3.71	17.99
13	"	45	24.3	2.12	0.95	1475	499	8.62	33.83
14	"	45	24.0	1.24	0.65	1226	293	5.05	24.31
15	"	28	23.9	2.01	1.38	980	358	8.13	36.53
16	"	28	26.1	2.01	1.54	1260	448	8.15	35.56
17	"	28	22.6	0.56	0.16	495	52	2.28	10.51
18	7.00-6-6PR	45	25.1	1.90	1.25	982	360	10.59	36.66
19	"	45	23.4	0.60	0.12	503	76	3.38	15.11
21	"	45	24.0	1.10	0.38	775	170	6.17	21.94
22	"	28	25.1	1.39	0.75	595	173	7.74	29.08
23	"	28	26.6	0.74	0.16	484	58	4.12	11.98
24	"	28	28.0	1.56	0.89	711	217	8.67	30.52
26	8.50-10-8PR	28	23.7	0.84	0.67	808	149	3.41	18.44
27	"	28	24.7	1.38	0.99	975	245	5.58	25.13

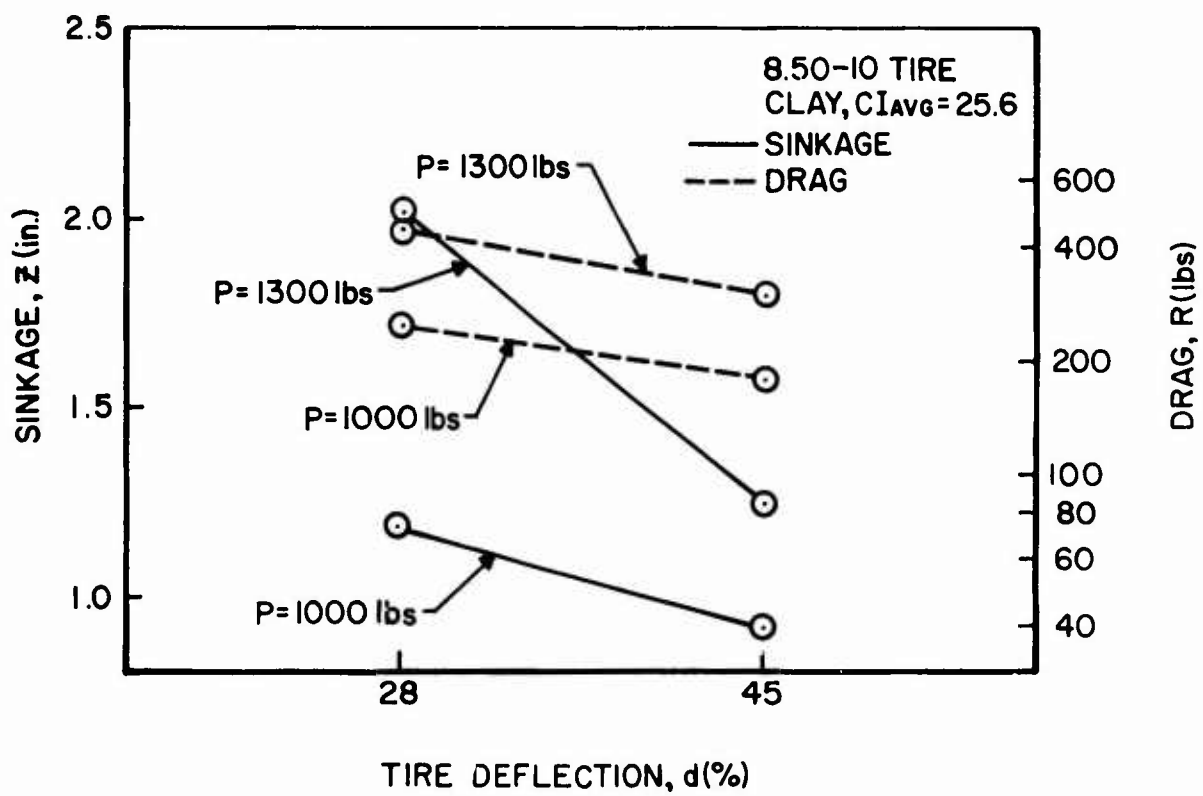


Figure 12 Tire Deflection Effects on Drag and Sinkage,  
8.50-10 Tire

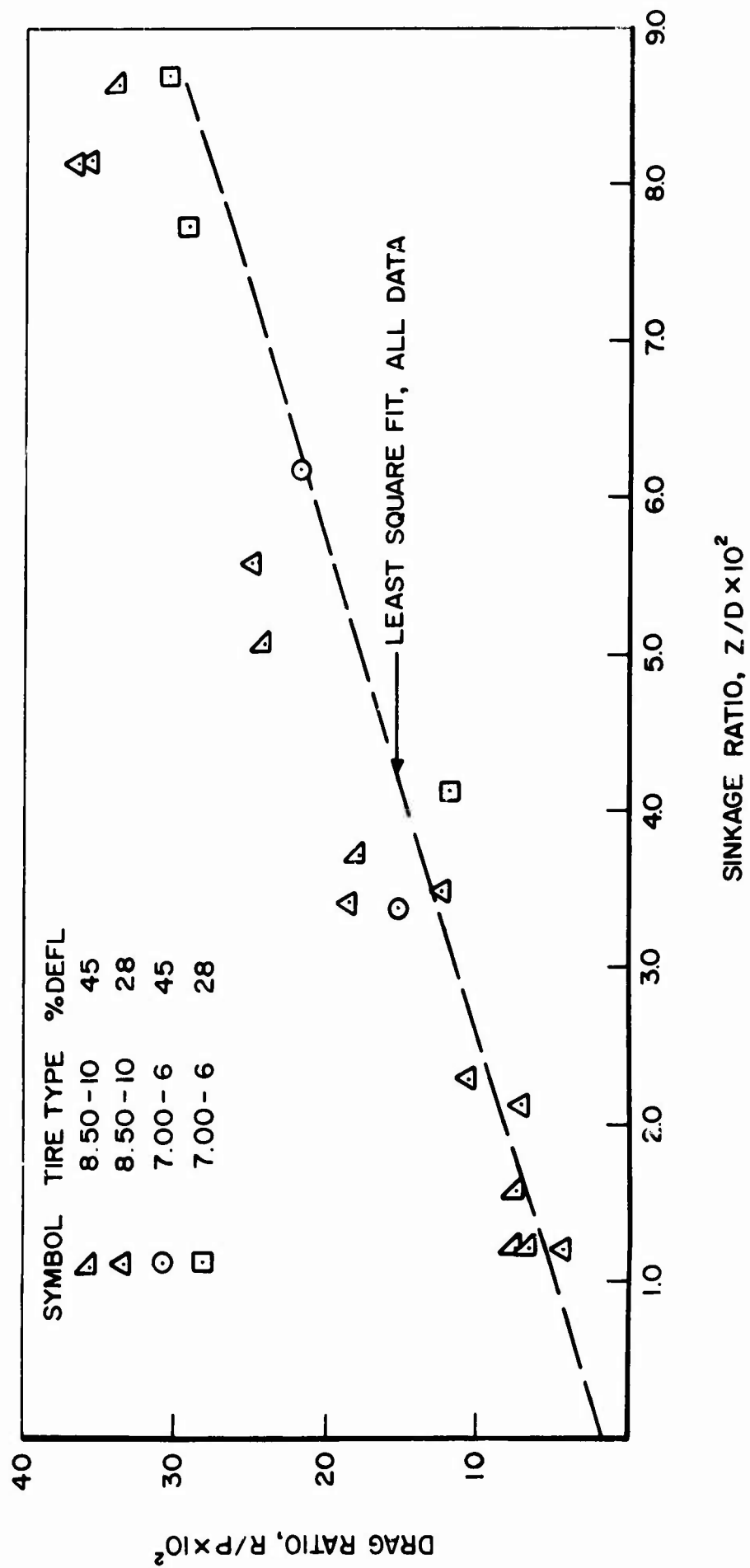


Figure 13 Drag Ratio vs Sinkage Ratio, Buckshot Clay



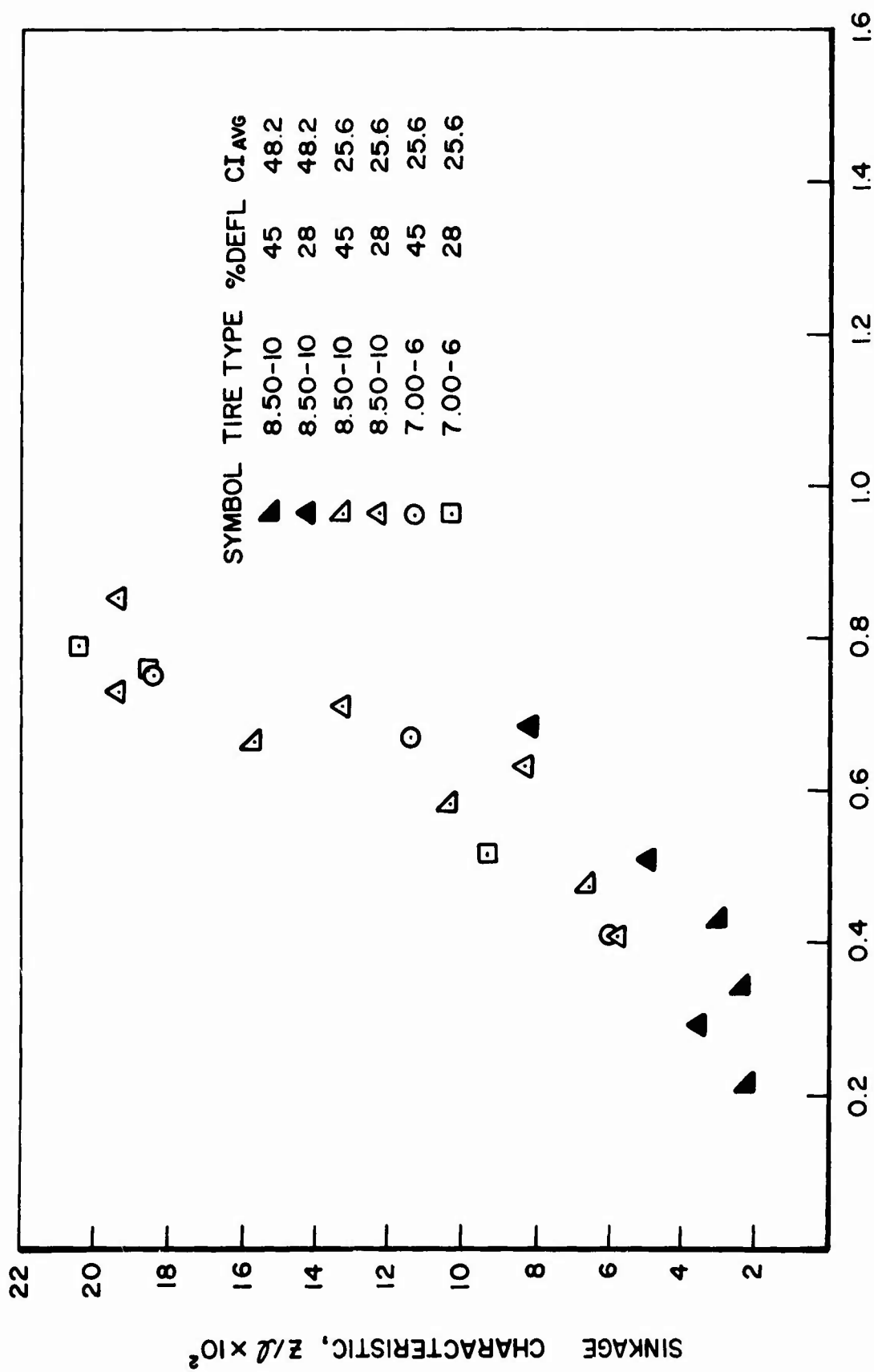


Figure 14 Sinkage Characteristic vs Load-Strength Ratio, Buckshot Clay

Table 7

## Drag-Sinkage Data - Sand

Test No.	Tire Type	Percent Defl.	CI <sub>avg</sub>	Sinkage Z [in]	Permanent Rut Depth [in]	Wheel Load		Drag R [lbs]	Sinkage Ratio		Drag Ratio R/P in 10 <sup>-2</sup>
						P [lbs]	Z/D in 10 <sup>-2</sup>		Z/D in 10 <sup>-2</sup>	R/P in 10 <sup>-2</sup>	
4	7.00-6-6PR	45	26.4	0.78	0.78	486		95	4.4		19.55
5	"	28	26.1	1.02	1.02	488		125	5.69		26.62
7	"	45	25.5	1.77	1.77	984		322	9.87		32.72
9	"	45	27.3	2.75	1.93*	1271		548	15.55		43.12
10	"	28	28.0	0.59	0.59	297		52	3.33		17.51
11	"	28	27.0	2.40	1.54*	700		301	13.35		43.0
12	8.50-10-8PR	45	25.4	1.08	1.01	991		236	4.41		23.81
14	"	28	27.0	1.57	1.42*	987		256	6.37		25.94
15	"	45	27.2	1.46	1.40*	1473		335	5.93		22.74
16	"	45	27.5	2.40	2.13*	2003		600	9.72		29.96
17	"	28	27.5	2.64	1.93*	1267		484	10.71		38.2
18	"	28	26.9	0.72	0.69	493		81	2.91		16.43

\* Sand flowed back into rut

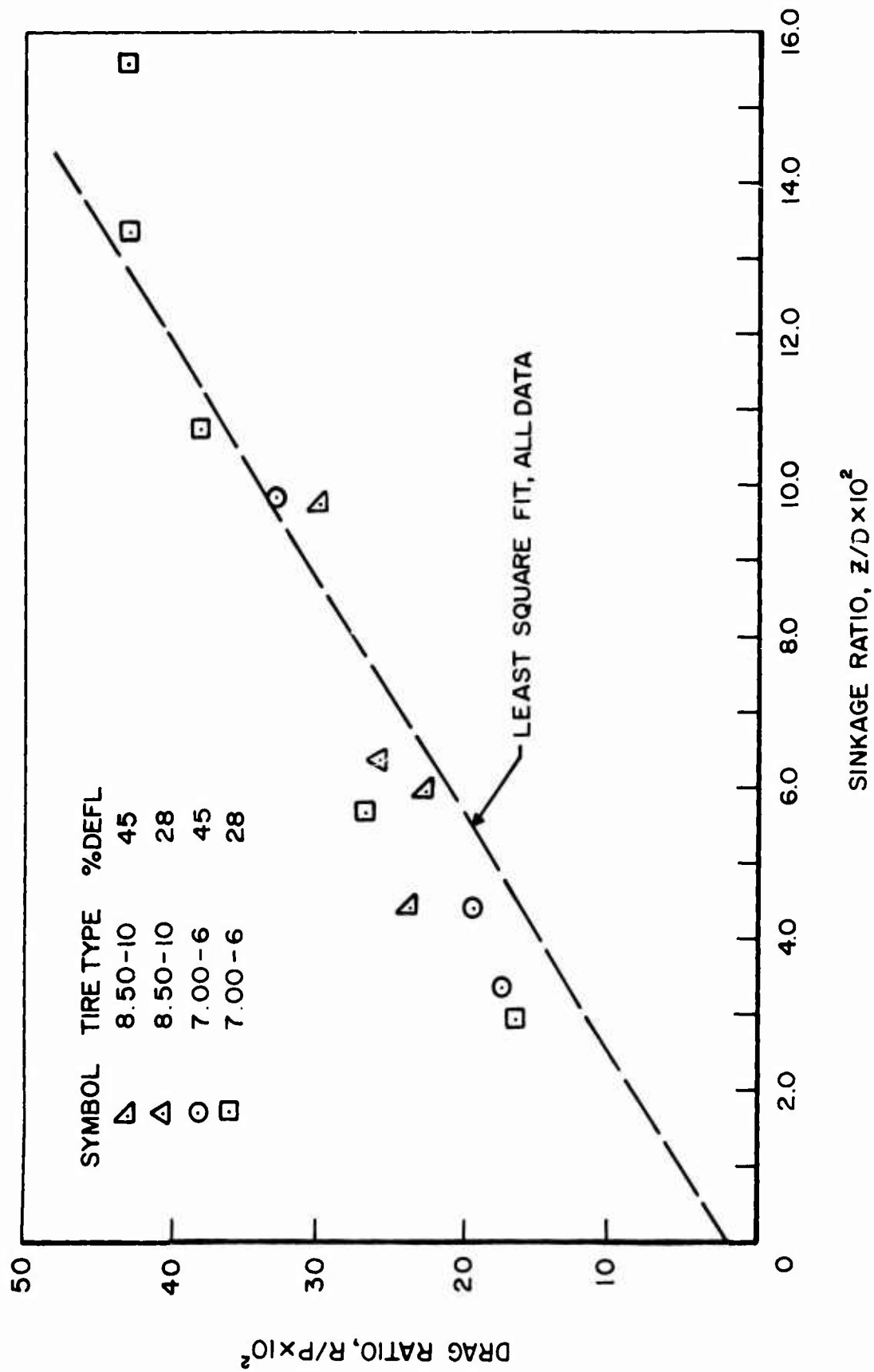


Figure 15 Drag Ratio vs Sinkage Ratio, Mortar Sand

aircraft tires perform differently on clay and sand soil in terms of the drag ratio response although these differences may at most be only  $\pm 25\%$  through the range of  $0.02 \leq \frac{Z}{D} \leq 0.12$ .

Figure 16 shows the results of the sinkage characteristic versus load-strength comparison for sand and it also illustrates the rapid increase in sinkage (and drag) for  $\alpha/CI_{avg}$  ratios in excess of approximately 0.6. Similar reductions in drag for increasing tire deflections as shown for clay in Figure 12 also occur for aircraft tires on sand.

## 8. Summary

While the Single Wheel Verification Tests were limited in the range of test parameters, these results, as well as other available flotation data, substantiate the basic tire-soil interaction equation previously developed<sup>(1)</sup> and subsequently refined in Equation (2). These results have also shown that different drag ratio/sinkage ratio relationships exist for aircraft tires on sand and clay soil, although Equation (2) provides a good approximation for defining drag for all soils. The R/P versus Z/D relationship shows that if sinkage can be predicted, then drag can be determined for aircraft tires operating on soil. Interpretation of these test results leading to sinkage prediction equations are given in Sections IV and V.

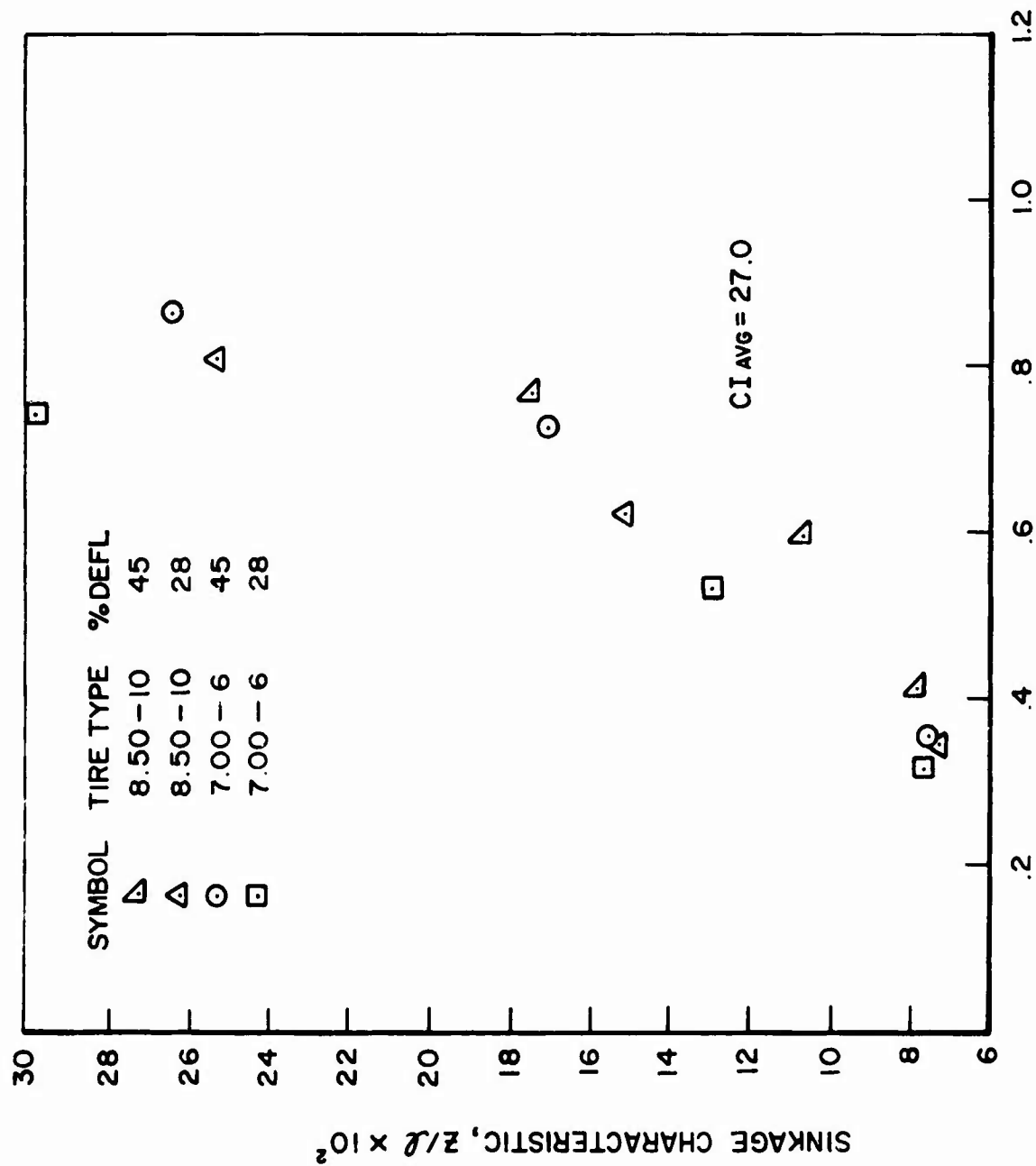


Figure 16 Sinkage Characteristic vs Load-Strength Ratio, Mortar Sand

## SECTION IV

### SINKAGE PREDICTION EQUATIONS

#### 1. General Considerations

The results of the Phase I and Phase II research effort have shown that flotation performance of aircraft operating on soil runways is directly related to sinkage and drag encountered by the aircraft tire. In the Region II velocity range as defined by Equation (2), and perhaps in the Region III velocity range as shown by Figure 7, the drag has been shown to be directly proportional to the sinkage for rolling tires. Based on this relationship, the critical parameter in determining drag on an aircraft wheel is sinkage. If a prediction can be made of the anticipated sinkage, then the developed drag forces can be determined within suitable limits for calculating flotation performance of aircraft tires on soil runways. A previous review<sup>(1)</sup> of presently used empirical sinkage prediction equations, such as Bekker<sup>(11)</sup> and Boeing<sup>(3)</sup> which were developed primarily for mobility analysis, indicated that these equations were not sufficiently accurate to provide the required confidence in the prediction of flotation performance. In order to develop more accurate sinkage prediction techniques and to develop the required flotation performance criteria, an empirical and an analytical (finite element) sinkage prediction analysis were developed for incorporating those variables and conditions specifically related to aircraft operations on soil runways.

#### 2. Sinkage Prediction - Empirical

Numerous experimental and analytical efforts<sup>(3, 11, 12)</sup> have been undertaken to develop load-sinkage equations which adequately interpret soil properties as related to soil deformation characteristics under loading. For rolling wheels on soil, the complex soil response involves elastic, viscous, and plastic deformations. Previously developed empirical sinkage prediction equations have mainly been directed at analyzing off-the-road mobility of transport trucks and vehicles and armored vehicles. While the aircraft on soil problem shares many common variables with the off-the-road mobility problem, sufficient simplifications exist to permit the development of an empirically based sinkage prediction equation related primarily to aircraft type tire interaction with unprepared soil airstrips.

The soil property measurement selected for referencing the soil is the average cone index over the 0" to 6" depth. While most of the tire-sinkage experimental data available used the cone index as the soil strength

measurement, the primary reason for selecting the cone index as a reference is based on an analysis of the variables associated with the cone penetrometer. These variables include  $P_c$ ,  $A_c$ ,  $D_c$ ,  $\gamma$ ,  $c$ ,  $\phi$ , and  $Z_c$  where:

$P_c$  = cone vertical load (lbs)

$A_c$  = cone base area (in<sup>2</sup>)

$D_c$  = cone diameter (in)

$\gamma$  = unit weight of soil (lb/in<sup>3</sup>)

$c$  = soil cohesion (lb/in<sup>2</sup>)

$\phi$  = soil angle of internal friction

$Z_c$  = vertical penetration of cone (in)

For clay type soils ( $\phi=0$ ), arranging these variables in a dimensionless array leads to

$$f \left( \frac{Z_c}{D_c}, \frac{P/A_c}{\gamma D_c}, \frac{c}{\gamma D_c} \right) = 0 \quad (8)$$

Since the cone index is normally defined at  $Z_c = 6''$  or as an average over a 6 inch depth,  $Z_c/D_c$  will be constant and Equation (8) can be arranged as

$$\frac{P/A_c}{\gamma D_c} = f \left( \frac{c}{\gamma D_c} \right) \quad (9)$$

For cohesionless soils ( $c=0$ ), a similar analysis of variables leads to

$$f \left( \frac{Z_c}{D_c}, \frac{P/A_c}{\gamma D_c}, \phi \right) \quad (10)$$

Again, for  $Z_c/D_c$  being constant, the above equation can be written as

$$\frac{P/A_c}{\gamma D_c} = f(\phi) \quad (11)$$

Since the cone penetrometer has a constant diameter and the cone index is defined as the ratio  $P_c/A_c$ , Equations (9) and (11) indicate that cone penetration readings taken in cohesive and cohesionless soils will provide a comparative evaluation of the soil ( $\gamma, c$ ; or  $\gamma, \phi$ ).

Some of the drag-sinkage data included in the sinkage analysis used different soil parameters (e.g., CBR) for soil reference. Conversion of these soil parameters to equivalent cone index were made using techniques previously developed<sup>(1)</sup> for specific soils to provide a common reference basis.

The primary concept behind the development of the sinkage prediction equations was simplicity in the application of the equations developed while still maintaining reliability in the sinkage prediction commensurate with the known response of soil. Previous studies<sup>(3, 6, 13, 14)</sup> have indicated that in the Region II velocity range, the effects of tire tread, tire ply, soil viscosity, and soil inertia are not significant variables in determining sinkage. The variables selected for inclusion in the analysis are

$$Z, \ell, A, P, \text{ and } CI_{\text{avg}}$$

where  $\ell$  = tire contact footprint length (rigid surface) at applicable tire deflection

$CI_{\text{avg}}$  = average cone index over 0" to 6" depth.

The basic dimensionless equation format selected was

$$\frac{Z}{\ell} = f\left(\frac{P/A}{CI_{\text{avg}}}\right) = f\left(\frac{\alpha}{CI_{\text{avg}}}\right) \quad (12)$$

where  $\frac{Z}{\ell}$  = sinkage characteristic (as distinguished from the sinkage ratio,  $Z/D$ )

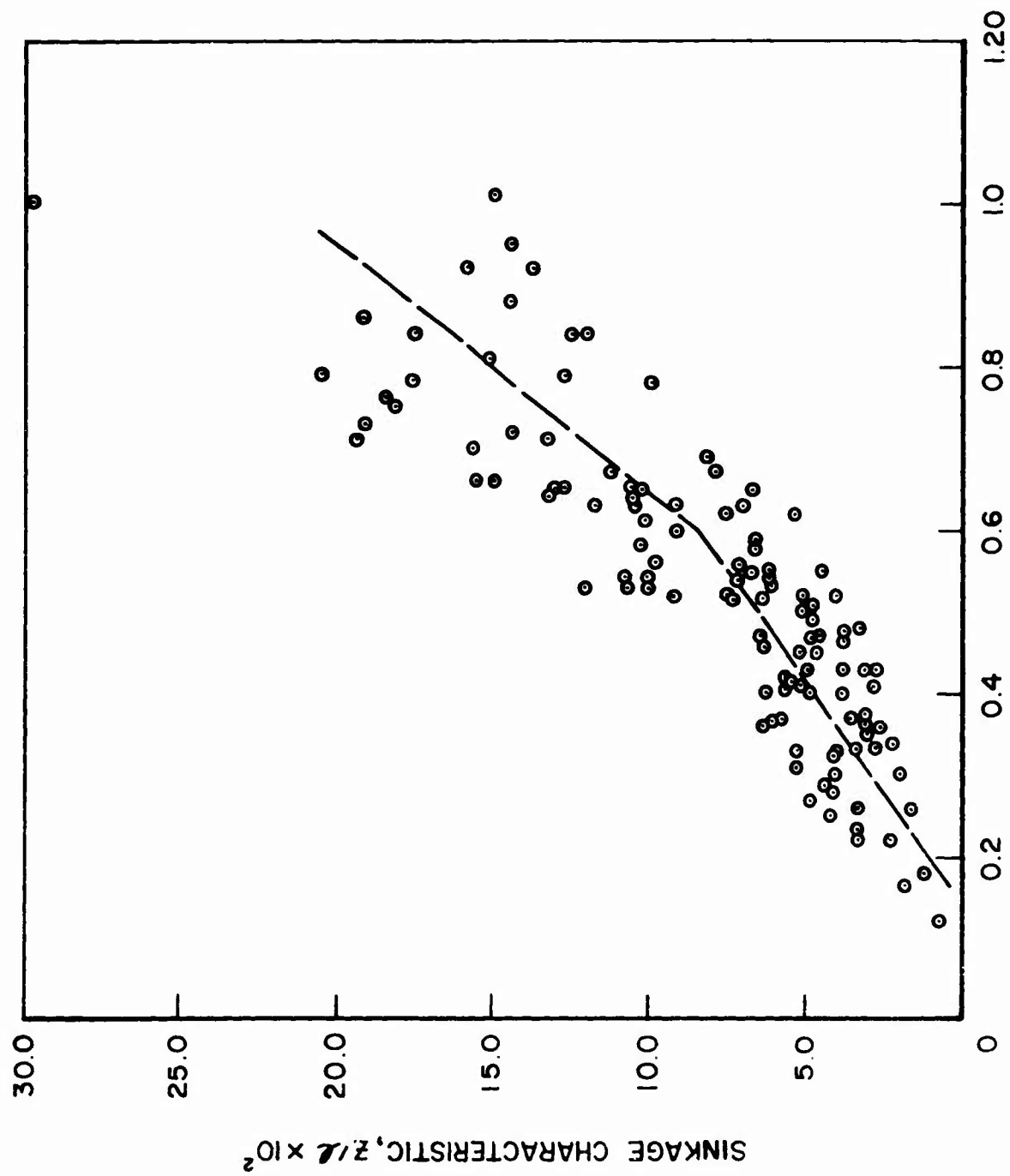
$\frac{\alpha}{CI_{\text{avg}}}$  = load-strength ratio.

The effect of drag on sinkage due to interaction effects was not included in the basic sinkage equation since the range of interest for the drag ratio is normally less than 0.30 for effective aircraft operation on soil surfaces.

#### Cohesive Soils

A limited amount of sinkage data was available for aircraft operations on clay soil. The results of the analysis<sup>(3, 4, 8, 14, 15, 16)</sup> which include the more recent Lockheed-Langley and Single Wheel Verification Tests are shown in Figure 17. The data shown in Figure 17 includes two different clays (Harpers Lake and buckshot), tire diameters ranging from 18 inches to 70 inches, tire deflections from 15% to 60%, and equivalent average cone indices (CBR converted to CI) ranging from 16 psi to 600 psi with sinkages from 0.25 to 4.0 inches.





LOAD-STRENGTH RATIO,  $a/cI_{avg}$

Figure 17 Sinkage Characteristics vs Load-Strength Ratio, Cohesive Soil

Based on an examination of the data shown in Figure 17, the sinkage can be defined in two different ranges as given by

$$\frac{Z}{l} = -0.03 + 0.19 \frac{\alpha}{CI_{avg}} \quad (13)$$

$$\text{for } 0.20 \leq \frac{\alpha}{CI_{avg}} \leq 0.60$$

$$\text{and } \frac{Z}{l} = -0.11 + 0.33 \frac{\alpha}{CI_{avg}} \quad (14)$$

$$\text{for } 0.60 \leq \frac{\alpha}{CI_{avg}} \leq 0.90$$

The negative constant coefficient in Equations 13 and 14 results from the limited load-strength ratio range used in the analysis. Reference to Figure 17 indicates that if the available data is representative of clay type soil response under aircraft tires, sinkage predictions within the 90% confidence limits would be within a  $\pm 40\%$  accuracy based on the use of Equations 13 and 14 within its restricted region of application.

#### Cohesionless Soils

Considerably more sinkage data (4, 14, 17) was available for tire operations on cohesionless soils. Unlike the clay data, however, much of the data from the experimental studies in sand did not use aircraft type tires. Sufficient data was available, however, to examine the effects of such additional variables as percent tire deflection ( $d$ ) and tire diameter to width ratio ( $D/b$ ) to show that extensions of the existing analysis could be made to include interpretation of sinkage performance of aircraft type tires operating on cohesionless soils.

To examine the influence of tire deflection, linear least squares fits were made for tire deflections of 15%, 25%, and 35% for the 4.00-18 and 9.00-14 tires. These results as shown in Figure 18 indicate no consistent trend in the sinkage-footprint length ratio for varying tire deflections. An examination was also made of the influence of the tire diameter-to-width ratio on the sinkage characteristic ( $Z/l$ ). Aircraft tires have a tire diameter-to-width ratio ranging from approximately 2.8 to 3.6. Figure 19 was developed to show the effect of the  $D/b$  ratio on the operating level of each tire as determined by the variation of the sinkage characteristic ( $Z/l$ ) with the load-strength ratio. The line

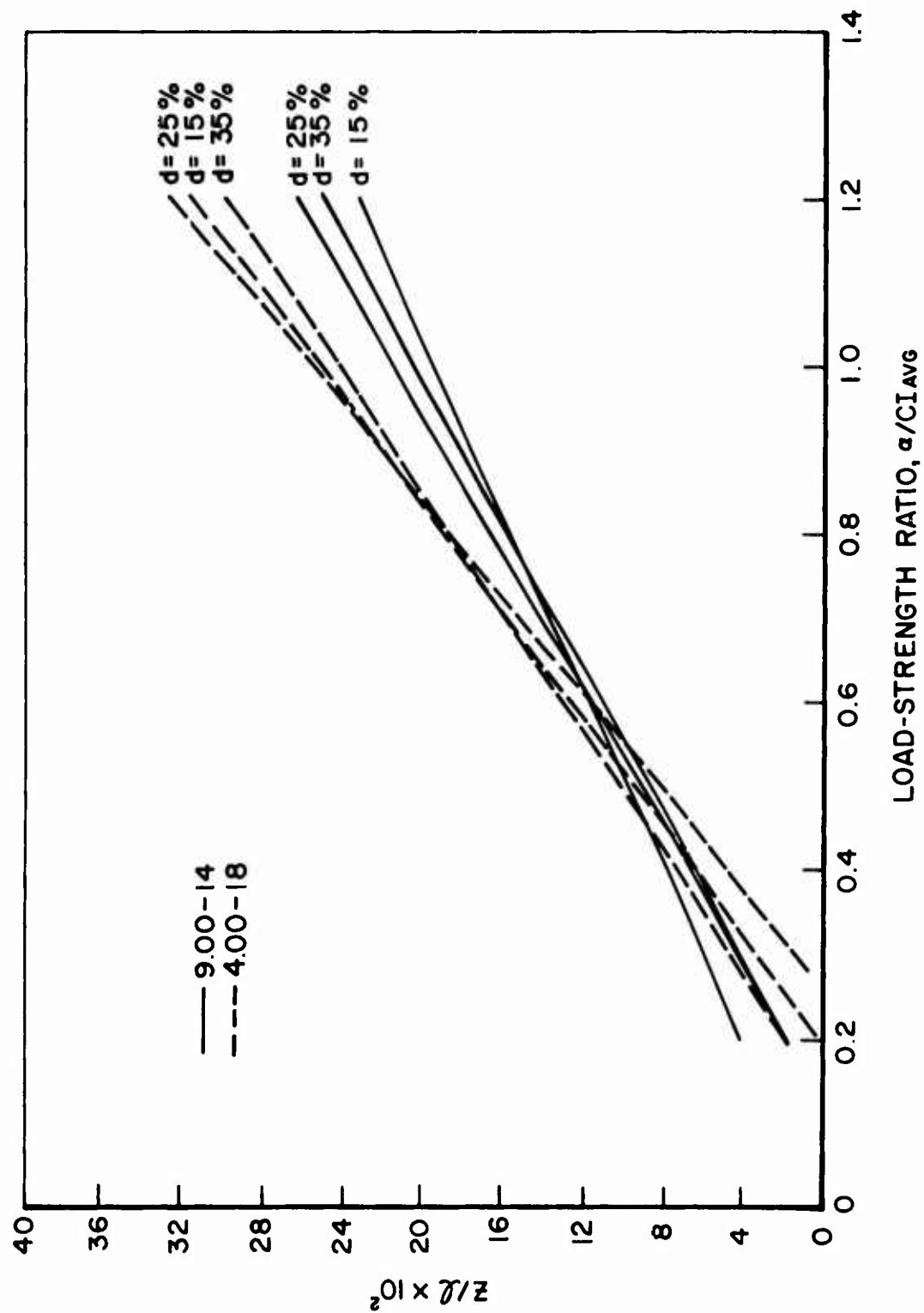


Figure 18 Sinkage-Tire Deflection Analysis, Cohesionless Soils

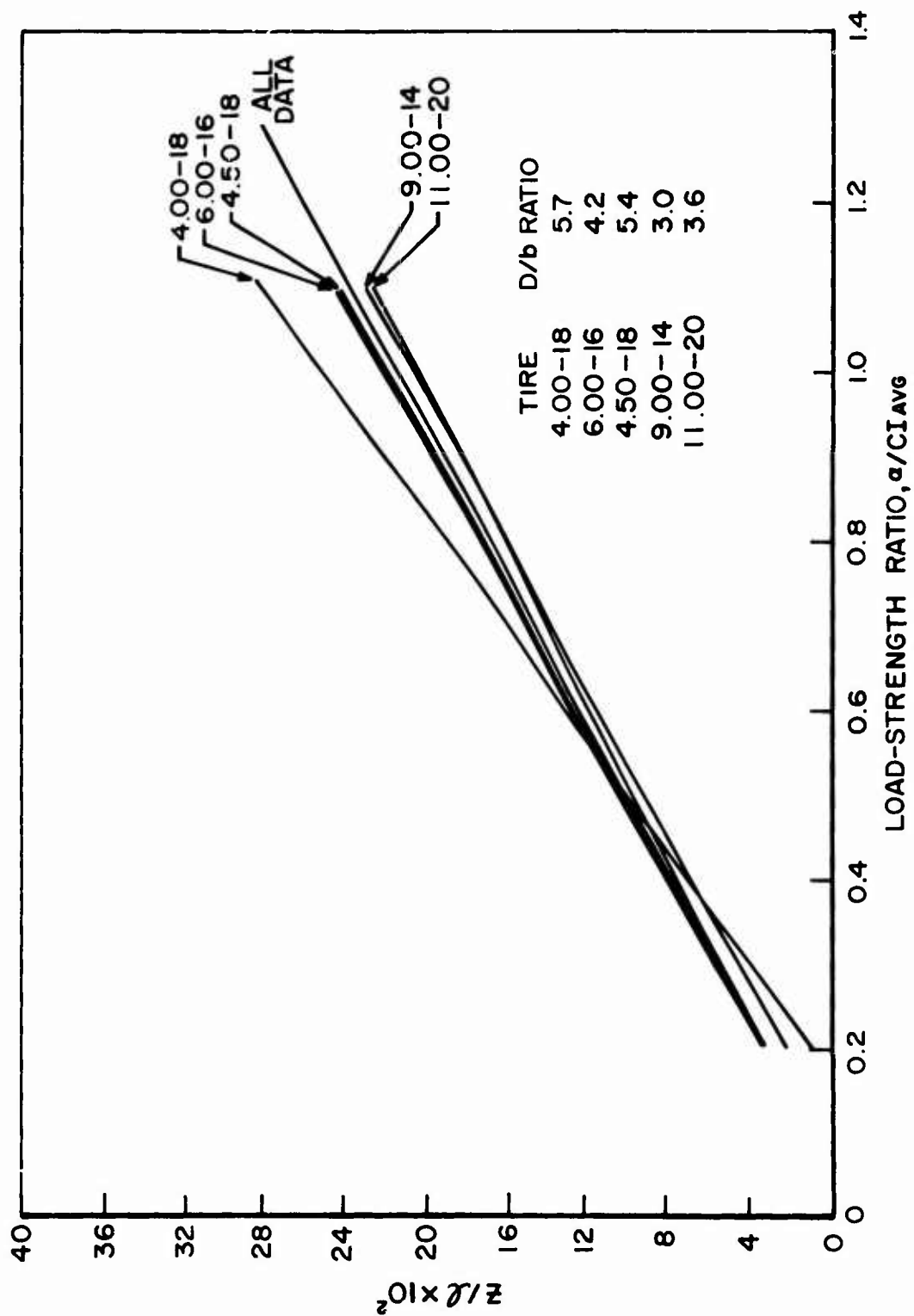


Figure 19 Sinkage-Tire Diameter/Width Ratio Analysis, Cohesionless Soils

representing the operating level of each tire is the linear least squares fit line for all available data for that tire. Analysis of Figure 19 shows no consistent relationship of the sinkage characteristic ( $Z/l$ ) with tire diameter-to-width ratio.

Based on the results of these comparisons, available sinkage data (4, 14, 17) in cohesionless soil, which includes the Lockheed-Langley and Single Wheel Verification tests presented herein were examined based on Equation 12. The results of this analysis, as shown in Figure 20, includes three different soils, tire diameters ranging from 18 inches to 42 inches, tire deflection from 15% to 45%, and average cone indices ranging from 15 psi to 325 psi with corresponding sinkages from 0.25 to 3.0 inches. The sinkage response is defined by two ranges as

$$\frac{Z}{l} = -0.015 + 0.24 \frac{\alpha}{CI_{avg}} \quad (15)$$

$$\text{for } 0.15 \leq \frac{\alpha}{CI_{avg}} \leq 0.70$$

$$\text{and } \frac{Z}{l} = -0.020 + 0.50 \frac{\alpha}{CI_{avg}}$$

$$\text{for } 0.70 \leq \frac{\alpha}{CI_{avg}} \leq 1.00$$

Analysis of Figure 20 indicates that sinkages can be predicted based on the 90% confidence limits within an approximate accuracy of  $\pm 40\%$  for the indicated region of application.

In order to provide an indication of the range of performance for aircraft tires operating on cohesive and cohesionless soils, Figure 21 was prepared illustrating this range. It is evident from reference to Figure 21 that for all other conditions being constant, sinkages in cohesionless soils are larger than in cohesive soils.

### 3. Sinkage Prediction - Analytical (Finite Element)

The empirical sinkage prediction equations, as indicated in the preceding section, can at best predict sinkage to within an approximate accuracy of  $\pm 40\%$  based on 90% confidence limits for the restricted range of soil properties used. Since using an empirical approach alone to develop adequate sinkage prediction equations for all soil types and loading conditions is

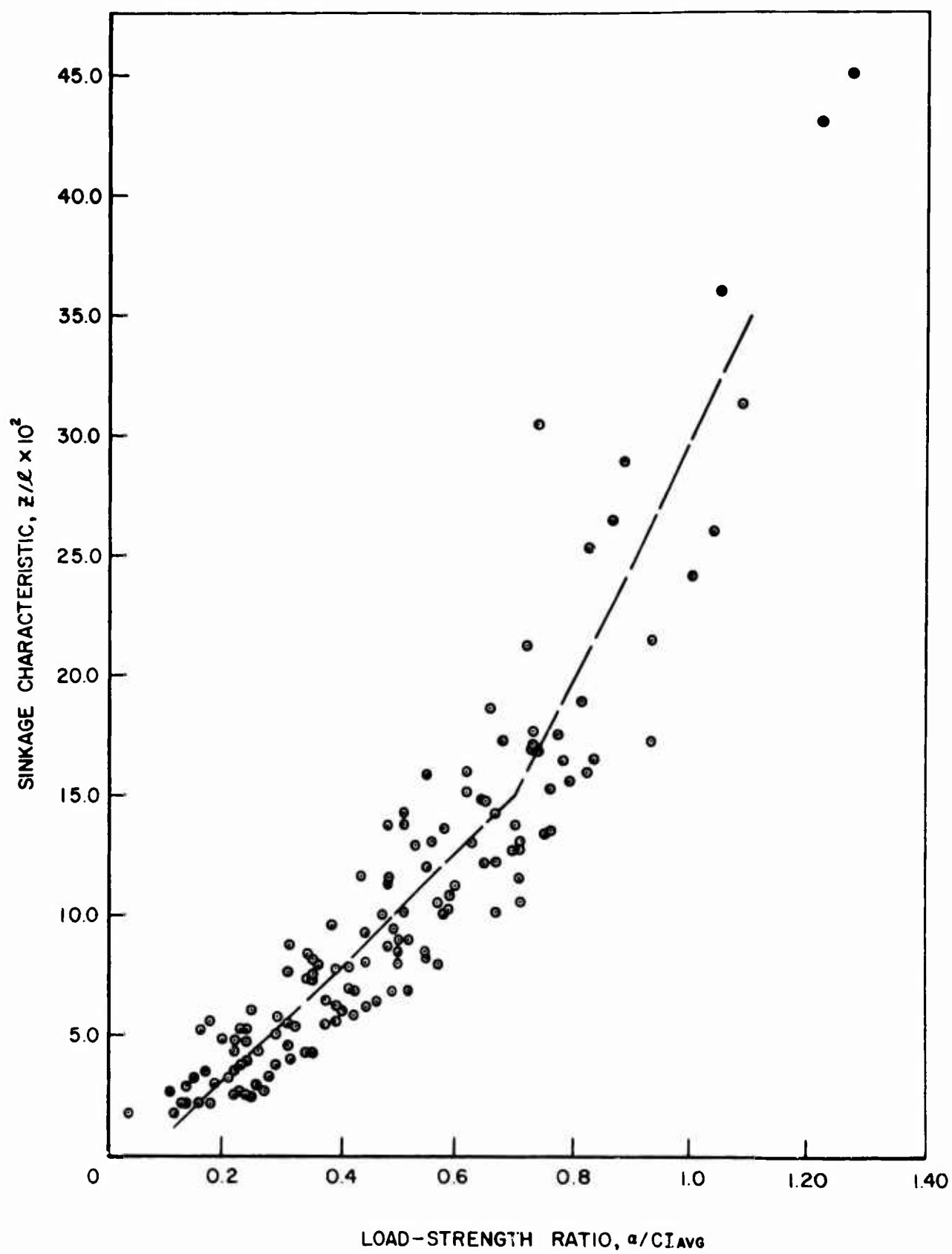


Figure 20 Sinkage Characteristics vs Load-Strength Ratio, Cohesionless Soils

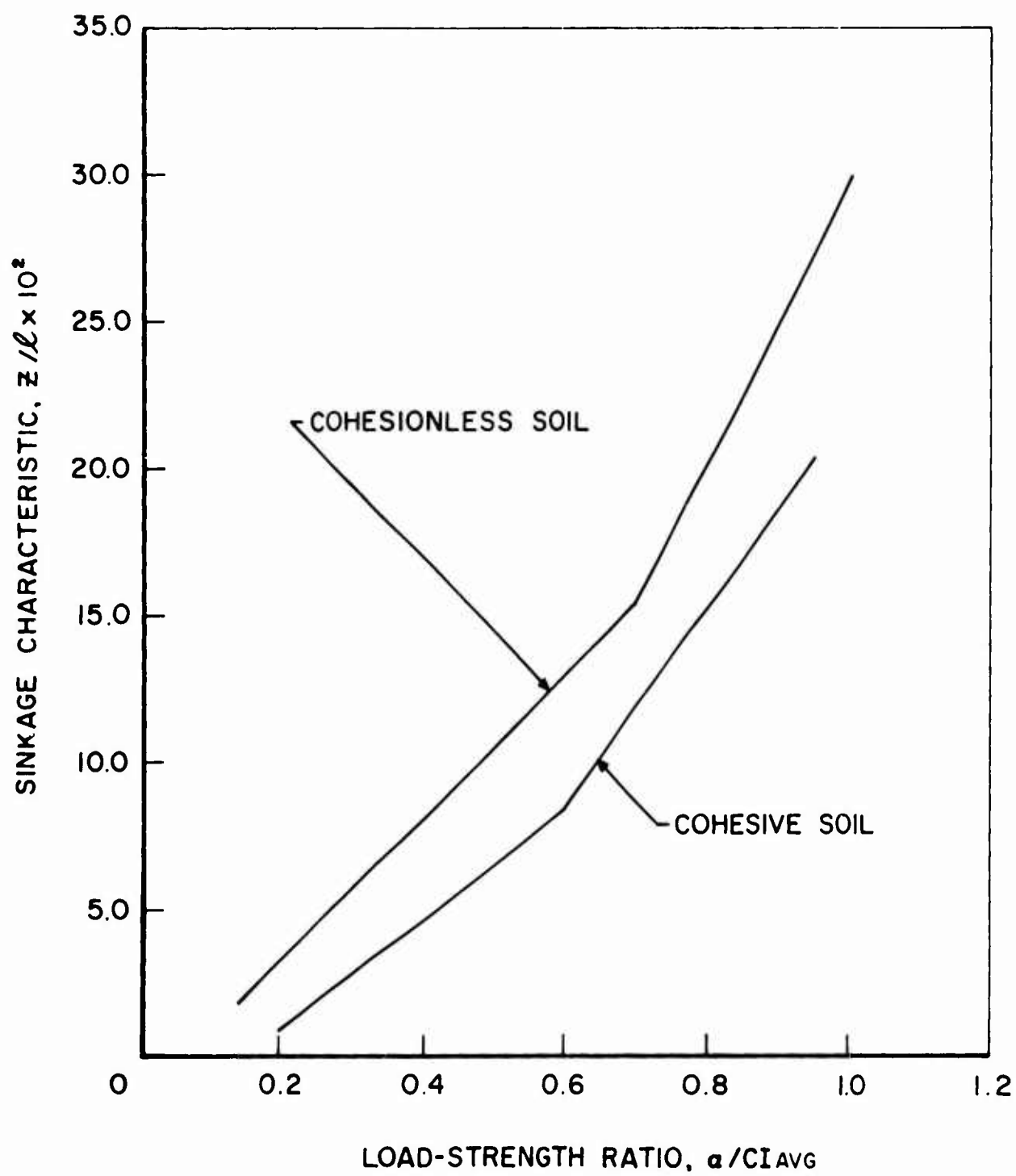


Figure 21 Sinkage Range for Soils

prohibitively costly and time consuming, an analytical approach using the finite element technique was developed to give a more rational approach to sinkage prediction and to provide a long term solution to sinkage prediction for any contact element in soil. The results of this analytical approach, when correlated with presently available experimental data, should lead to more dependable sinkage prediction for a broader range of soil properties and loading conditions.

The analysis developed considers the soil as an elastic-plastic medium described by the best currently available plastic flow stress-strain relations and yield criterion, and the action of the tire is considered as a pressure distribution applied on the surface of the medium. The sinkage is then equivalent to the surface displacement due to the applied pressure distribution. To obtain the surface displacement, then, requires the development of the complete stress and displacement solutions of the elastic-plastic problem.

#### The Vertical Pulse Loading Problem

Initial efforts were directed at determining the sinkage caused by a rolling aircraft wheel where the loading condition was approximated, according to a dynamic analogy<sup>(1)</sup>, by the action of a stationary wheel subjected to a time dependent vertical pulse load. The interface tire-soil contact stress distribution was approximated by a uniform pressure distribution applied on the surface of the soil medium over a circular area equivalent to the tire footprint area (see Figure 22). The magnitude of the pressure was taken to be equal to the average pressure experienced by a point near the surface of the soil when a rolling tire moves across the point. The dependence of the pressure at a point in time has been experimentally measured for land vehicles<sup>(18)</sup> and has the form of a load pulse as shown in Figure 23. The peak pressure of the pulse is related to the vertical load on the aircraft tire, while the time duration of the pulse is related to the aircraft ground velocity.

This vertical pulse is axisymmetric and is essentially a two dimensional problem. The conversion of the actual problem to the vertical case in using the finite element method leads to a simplification in the solution over that of the more complicated three dimensional rolling wheel problem. The three dimensional rolling wheel problem will be considered in the subsequent phase of this research effort.



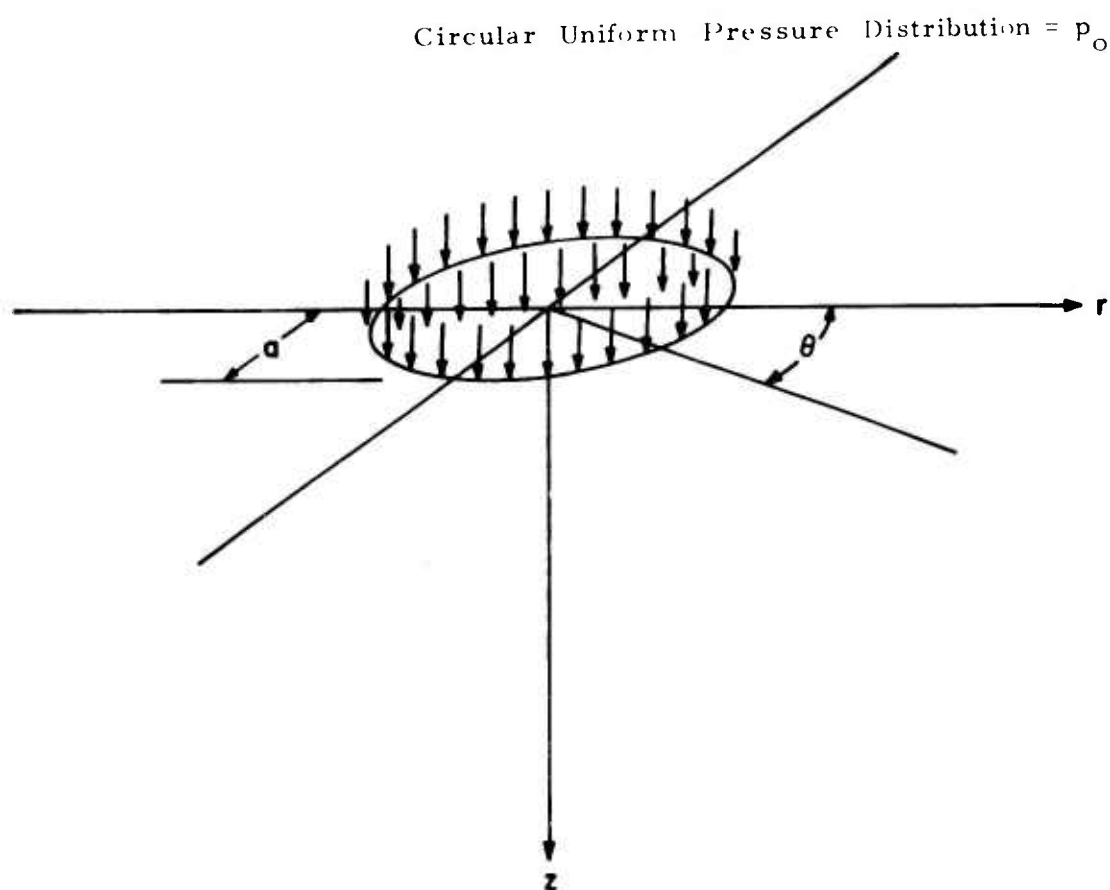


Figure 22 Boundary Conditions for Stationary Tire Impulse Loading

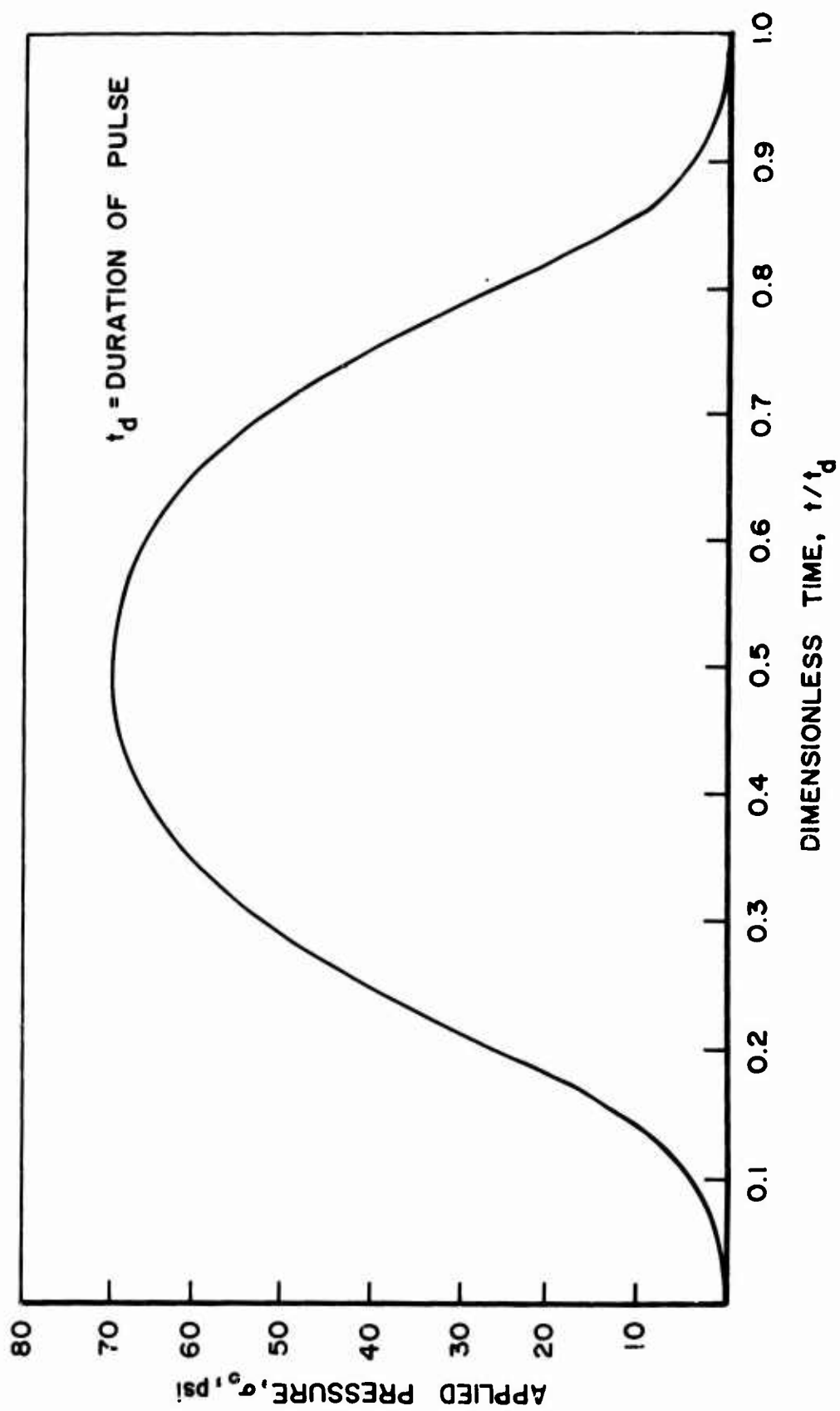


Figure 23 Typical Vertical Impulse Pressure Curve

### The Elastic-Plastic Soil Medium

Recent works (19,20,21) indicate that soil media can be simulated as an elastic-plastic material. In the present problem, the soil medium was assumed to be a homogeneous, isotropic, time-independent, temperature independent, and elastic-perfectly-plastic material. The elastic deformation was assumed to obey Hooke's law, and plastic flow was assumed to be described by an incremental stress-strain relation which is based on the normality flow rule.

The yielding of soil is a complicated phenomenon and at present there is no satisfactory theory to account completely for all the variables in the yielding behavior of soil. The best currently available criterion is the Prager-Drucker Yield Criterion (19,22) which describes the yielding in terms of two parameters, the cohesion and the friction angle of the soil. These two parameters, which are universally recognized soil parameters, can be determined from triaxial shear tests. While there are other indicators of soil strength and deformation such as the California Bearing Ratio (CBR) and the Cone Index (CI), these parameters, which are normally used for empirical flotation and mobility studies, cannot be interpreted in relation to yield functions and plastic deformation in analytical studies.

### Analytical Finite Element Approach - The Lumped Parameter Iteration Method

A survey of past and current literature indicates that both the vertical loading and rolling wheel problem can be solved using the finite element approach. Finite element analysis has been used quite effectively in the solutions of problems in nuclear blast effects (25) and dynamic soil response of strip footings (23). These problems are quite similar to the present vertical pulse loading problem. The primary advantages of a finite element type of approach are:

1. It permits the inclusion of the plastic response of the soil.
2. It provides complete flexibility in applying surface geometry and pressure boundary conditions (this is an important feature for extending the work to other contact elements).

There are two finite element techniques that are applicable to the vertical pulse loading problem. They are the direct-stiffness matrix method (24,27) and the lumped parameter iteration method (26). The latter method was chosen for the present problem because the computer program would be easier to develop and fewer problems would be encountered with computer capacity, although it would require longer computing time.

In the lumped parameter iteration method, the continuous soil medium is divided into lumped mass elements called mass points, and spring elements called stress points which can transmit both normal and shear stresses between the lumped masses. These mass and stress points are interwoven alternately as shown in Figure 24. In this model, the variables are indicated only at discrete points. Consequently, displacements, velocities, and accelerations may be prescribed and solved for only at the mass points, while stresses and strains may be prescribed and solved for only at the stress points.

The pressure boundary conditions are applied on the surface,  $z = 0$ , through a row of fictitious stress points (see Figure 24). Outside the limits of the loaded area, the vertical and shear stresses of the fictitious stress points are zero. Within the loaded area, the vertical stress of the fictitious stress points are equal to the prescribed pressure, and for the present problem the shear stresses are such that the radial displacement on the surface is zero. A shear stress distribution can be prescribed in future research efforts to take into account effects such as braking and turning.

Using the finite element model and the method of applying the boundary conditions described above, the lumped parameter iteration method obtains the solution of the problem by applying the prescribed pressure according to the load pulse (see Figure 23) through small increments of time, and finding the stresses and displacements at the discrete points of the model for each increment of time by a point-by-point calculation and iteration procedure.

#### Governing Equations

The equations of continuum elasticity and plasticity, which include the equations of motion, quadrature equations, yield and plastic equations, strain displacement relations, and the constitutive equations, are given in this section in the form applicable to the finite element model. These equations form the basis for the development of the computer program. (Refer to the List of Symbols for detailed nomenclature.)

(a) Dynamic Equations of Motion - It was shown by Ang<sup>(26)</sup> that the equations of motion for the lumped parameter finite element model described earlier are the same as the differential equations of motion for the corresponding continuum model expressed in terms of central finite difference. The differential equations of motion for the continuum model in the polar coordinates are:

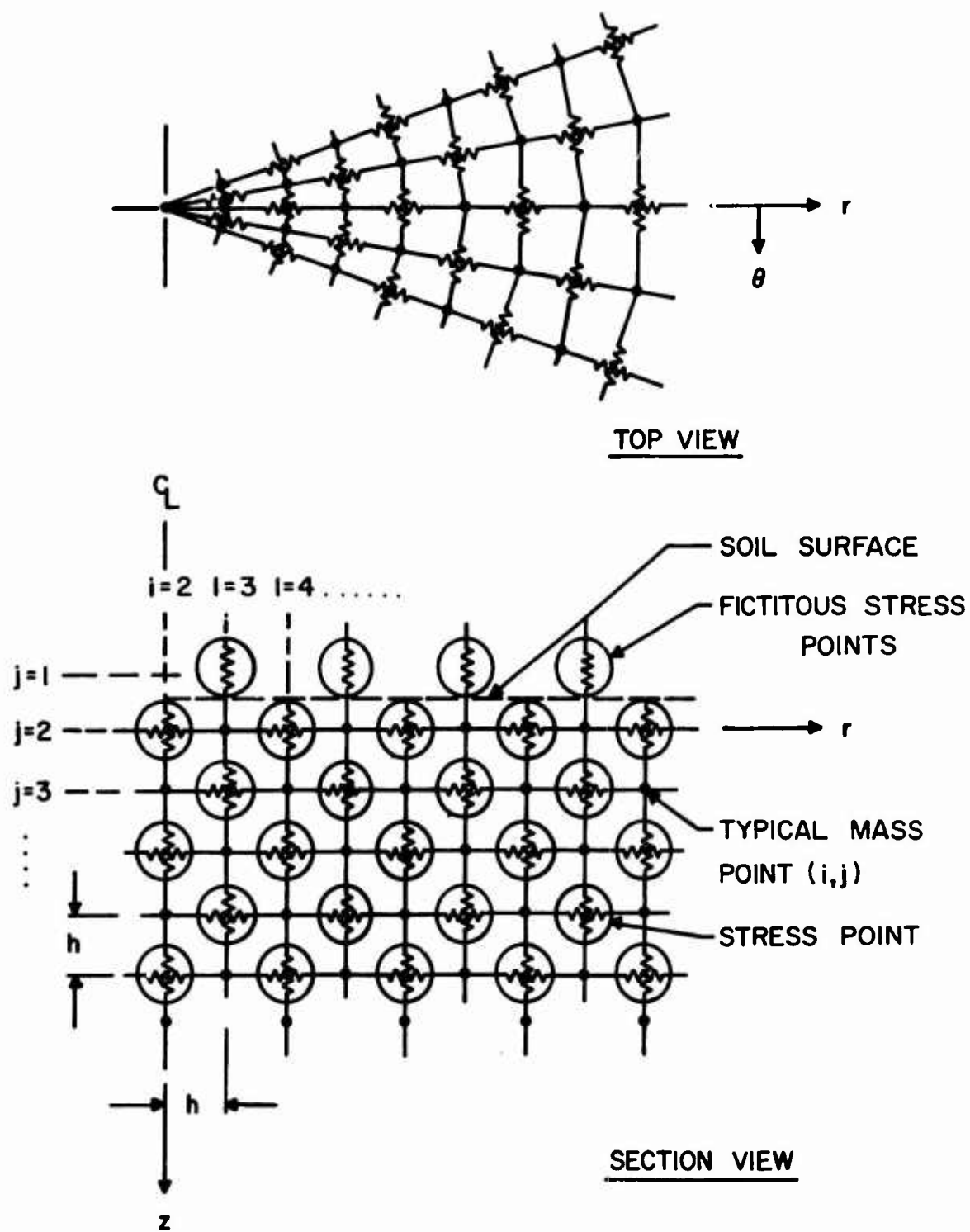


Figure 24 Finite Element Model - "Lumped Parameter Iteration Method"

$$\rho \frac{\partial^2 u}{\partial t^2} = \frac{\partial \sigma_r}{\partial r} + \frac{\partial \tau_{rz}}{\partial z} + \frac{\sigma_r - \sigma_\theta}{r} \quad (17)$$

$$\rho \frac{\partial^2 w}{\partial t^2} = \frac{\partial \sigma_z}{\partial z} + \frac{\partial \tau_{rz}}{\partial r} + \frac{\tau_{rz}}{r} \quad (18)$$

These equations written in central finite difference form for a typical mass point (i, j) of the finite element model are: (The superscripts indicate the time of the variables, and the indices enclosed in parenthesis indicate the spatial location of the variables according to the indices shown on Figure 24.)

$$\ddot{u}^t(i, j) = \frac{1}{\rho} \left[ \frac{\sigma_r^t(i+1, j) - \sigma_r^t(i-1, j)}{2h} + \frac{\tau_{rz}^t(i, j+1) - \tau_{rz}^t(i, j-1)}{2h} + \frac{\sigma_r^t(i-1, j) + \sigma_r^t(i+1, j) - \sigma_\theta^t(i-1, j) - \sigma_\theta^t(i+1, j)}{2r(i, j)} \right] \quad (19)$$

$$\ddot{w}^t(i, j) = \frac{1}{\rho} \left[ \frac{\sigma_z^t(i, j+1) - \sigma_z^t(i, j-1)}{2h} + \frac{\tau_{rz}^t(i+1, j) - \tau_{rz}^t(i-1, j)}{2h} + \frac{\tau_{rz}^t(i+1, j) + \tau_{rz}^t(i-1, j)}{2r(i, j)} \right] \quad (20)$$

For the mass points that lie on the axis of symmetry, these equations of motion reduce to:

$$\ddot{u}^t(i, j) = 0 \quad (21)$$

$$\ddot{w}^t(i, j) = \frac{\sigma_z^t(i, j+1) - \sigma_z^t(i, j-1)}{2h} + \frac{2\tau_{rz}^t(i+1, j)}{h} \quad (22)$$

(b) Quadrature Equations - The velocities and displacements at a typical mass point at time t are approximately determined from the velocities at time t-Δt, displacements at time t-Δt, and the accelerations at time t-Δt and t by the quadrature equations which are derived as follows.

By Taylor's series expansion,

$$\dot{u}^t = \dot{u}^{t-\Delta t} + (\Delta t)\ddot{u}^{t-\Delta t} + \frac{(\Delta t)^2}{2}\ddot{\dot{u}}^{t-\Delta t} + \dots \quad (23)$$

$$\dot{w}^t = \dot{w}^{t-\Delta t} + (\Delta t)\ddot{w}^{t-\Delta t} + \frac{(\Delta t)^2}{2}\ddot{\dot{w}}^{t-\Delta t} + \dots \quad (24)$$

$$u^t = u^{t-\Delta t} + (\Delta t)\dot{u}^{t-\Delta t} + \frac{(\Delta t)^2}{2}\ddot{u}^{t-\Delta t} + \frac{(\Delta t)^3}{6}\ddot{\dot{u}}^{t-\Delta t} + \dots \quad (25)$$

$$w^t = w^{t-\Delta t} + (\Delta t)\dot{w}^{t-\Delta t} + \frac{(\Delta t)^2}{2}\ddot{w}^{t-\Delta t} + \frac{(\Delta t)^3}{6}\ddot{\dot{w}}^{t-\Delta t} + \dots \quad (26)$$

Since  $\ddot{\dot{u}}^{t-\Delta t} \approx \frac{\ddot{u} - \ddot{u}^{t-\Delta t}}{\Delta t}$  and

$$\ddot{\dot{w}}^{t-\Delta t} \approx \frac{\ddot{w} - \ddot{w}^{t-\Delta t}}{\Delta t},$$

Equations (23) through (26) can be written as

$$\dot{u}^t = \dot{u}^{t-\Delta t} + \frac{\Delta t}{2}(\ddot{u}^{t-\Delta t} + \ddot{u}^t) \quad (27)$$

$$\dot{w}^t = \dot{w}^{t-\Delta t} + \frac{\Delta t}{2}(\ddot{w}^{t-\Delta t} + \ddot{w}^t) \quad (28)$$

$$u^t = u^{t-\Delta t} + (\Delta t)\dot{u}^{t-\Delta t} + \frac{(\Delta t)^2}{3}\ddot{u}^{t-\Delta t} + \frac{(\Delta t)^2}{6}\ddot{u}^t \quad (29)$$

$$w^t = w^{t-\Delta t} + (\Delta t)\dot{w}^{t-\Delta t} + \frac{(\Delta t)^2}{3}\ddot{w}^{t-\Delta t} + \frac{(\Delta t)^2}{6}\ddot{w}^t \quad (30)$$

(c) **Prager-Drucker Yield Criterion** - The criterion states that if the yield function,  $f$ , as defined below is less than zero, the stress point is elastic, and if  $f$  is equal to or greater than zero, the stress point has yielded.

$$\text{Yield Function} = f = \alpha I + \sqrt{J} - k \quad (31)$$

where

$$I = \sigma_r + \sigma_\theta + \sigma_z, \quad (32)$$

$$J = \frac{1}{6} [(\sigma_r - \sigma_\theta)^2 + (\sigma_\theta - \sigma_z)^2 + (\sigma_z - \sigma_r)^2 + 6\tau_{rz}^2], \quad (33)$$

$$\alpha = \frac{2 \sin \varphi}{\sqrt{3} (3 - \sin \varphi)} \quad (34)$$

$$k = \frac{6 c \cos \varphi}{\sqrt{3} (3 - \sin \varphi)} = \text{yield stress in shear, and} \quad (35)$$

$c$  = cohesion

$\varphi$  = friction angle

(d) Incremental Strain-Displacement Relations - The usual definition of strains in terms of displacements are shown below in the incremental form for a general stress point of the finite element model.

$$\Delta \epsilon_r^t(i, j) = \frac{\Delta u^t(i+1, j) - \Delta u^t(i-1, j)}{2h} \quad (36)$$

$$\Delta \epsilon_\theta^t(i, j) = \frac{\Delta u^t(i+1, j) + \Delta u^t(i-1, j)}{2r(i, j)} \quad (37)$$

$$\Delta \epsilon_z^t(i, j) = \frac{\Delta w^t(i, j+1) - \Delta w^t(i, j-1)}{2h} \quad (38)$$

$$\Delta \gamma_{rz}^t(i, j) = \frac{1}{2} \left[ \frac{\Delta w^t(i+1, j) - \Delta w^t(i-1, j)}{2h} + \frac{\Delta u^t(i, j+1) - \Delta u^t(i, j-1)}{2h} \right] \quad (39)$$

where

$$\Delta u^t = u^t - u^{t-\Delta t} \quad (40)$$

$$\Delta w^t = w^t - w^{t-\Delta t} \quad (41)$$

For the stress points that lie on the axis of symmetry, the incremental strain-displacement relations become,

$$\Delta \epsilon_r^t(i, j) = \frac{\Delta u^t(i+1, j)}{h} \quad (42)$$

$$\Delta \epsilon_\theta^t(i, j) = \Delta \epsilon_r^t(i, j) \quad (43)$$

$$\Delta \epsilon_z^t(i, j) \text{ is the same as Equation (38)}$$

$$\Delta \gamma_{rz}^t(i, j) = 0 \quad (44)$$



For the stress points that lie on the first row near the surface (that is,  $j=2$ ), relations for  $\Delta\epsilon_r^t(i, j)$  and  $\Delta\epsilon_\theta^t(i, j)$  are the same as Equations 36 and 37 or Equations 42 and 43, whichever apply, but  $\Delta\gamma_{rz}^t(i, j)$  and  $\Delta\epsilon_z^t(i, j)$  are defined differently as follows: (See Appendix IV for detailed derivations.)

**Incremental shear-strain** - For stress points that do not lie on the axis of symmetry,

$$\Delta\gamma_{rz}^t(i, j) = \frac{1}{2} \left[ \frac{\Delta w^t(i+1, j) - \Delta w^t(i-1, j)}{2h} + \frac{2\Delta u^t(i, j+1) - \Delta u^t(i-1, j) - \Delta u^t(i+1, j)}{3h} \right] \quad (45)$$

and for the stress point that lies on the axis of symmetry,

$$\Delta\gamma_{rz}^t(i, j) = 0 \quad (46)$$

**Incremental vertical normal strain** - If the stress point is elastic or unloading from plastic state,

$$\Delta\epsilon_z^t(i, j) = \sigma_z^t(i, j) - \sigma_z^{t-\Delta t}(i, j) - \frac{\lambda}{\lambda + 2G} [\Delta\epsilon_r^t(i, j) + \Delta\epsilon_\theta^t(i, j)] \quad (47)$$

and if the stress point is plastic and loading,

$$\begin{aligned} \Delta\epsilon_z^t(i, j) = & \left\{ \sigma_z^t(i, j) - \sigma_z^{t-\Delta t} - \lambda [\Delta\epsilon_r^t(i, j) + \Delta\epsilon_\theta^t(i, j)] \right. \\ & + Q \left( \frac{\sigma_z^t(i, j)}{2\sqrt{J^t}} + B \right) \left( \frac{\sigma_r^t(i, j) \Delta\epsilon_r^t(i, j) + \sigma_\theta^t(i, j) \Delta\epsilon_\theta^t(i, j) + \tau_{rz}^t(i, j) \Delta\gamma_{rz}^t(i, j)}{2\sqrt{J^t}} \right. \\ & \left. \left. + B [\Delta\epsilon_r^t(i, j) + \Delta\epsilon_\theta^t(i, j)] \right) \right\} / \left[ \lambda + 2G - Q \left( \frac{\sigma_z^t(i, j)}{2\sqrt{J^t}} + B \right)^2 \right] \quad (48) \end{aligned}$$

For the stress points that do not lie on the axis of symmetry,

$$\sigma_z^t(i, j) = \frac{1}{4} [\sigma_z^t(i+1, j-1) + \sigma_z^t(i+1, j+1) + \sigma_z^t(i-1, j-1) + \sigma_z^t(i-1, j+1)] \quad (49)$$

and for the stress point that does lie on the axis of symmetry,

$$\sigma_z^t(i, j) = \frac{1}{2} [\sigma_z^t(i+1, j-1) + \sigma_z^t(i+1, j+1)] \quad (50)$$

and the symbols  $\lambda$ ,  $Q$ ,  $B$ , and  $J$  are defined by Equations 55, 64, 63, and 33, respectively.

(e) **Constitutive Equations** - The incremental stress strain relations applicable to the idealized elastic-plastic material for a typical stress point are shown below with the  $(i, j)$  indexing omitted, since all the variables are referred to the same stress point.

**Elastic Relations** - Hooke's law written in the incremental form:

$$\Delta \sigma_r^t = \lambda \Delta \epsilon^t + 2G \Delta \epsilon_r^t \quad (51)$$

$$\Delta \sigma_\theta^t = \lambda \Delta \epsilon^t + 2G \Delta \epsilon_\theta^t \quad (52)$$

$$\Delta \sigma_z^t = \lambda \Delta \epsilon^t + 2G \Delta \epsilon_z^t \quad (53)$$

$$\Delta \tau_{rz}^t = 2G \gamma_z^t \quad (54)$$

where

$$\lambda = \frac{E\nu}{(1+\nu)(1-2\nu)} = \frac{2\nu G}{1-2\nu} \quad (55)$$

$$\Delta \epsilon^t = \Delta \epsilon_r^t + \Delta \epsilon_\theta^t + \Delta \epsilon_z^t \quad (56)$$

**Plastic relations** - The plastic stress-strain relations are based on the normality flow rule which states that the plastic strain increment tensor is given by

$$\left[ \Delta \epsilon_{ij} \right]_{\text{plastic}} = \Lambda \frac{\partial f}{\partial \sigma_{ij}}, \quad (57)$$

where  $f$  is the yield function defined by Equation 31 and  $\Lambda$  is a scalar factor that depends on the current stresses for perfectly plastic material. The final incremental stress-strain relations for Prager-Drucker yield criterion were derived by Christian<sup>(19)</sup> and are presented below in equivalent forms<sup>(27)</sup>.

$$\Delta \sigma_r^t = \lambda \Delta \epsilon^t + 2G \Delta \epsilon_r^t - \beta Q \left( \frac{\sigma_r^t}{2\sqrt{J^t}} + B \right) \left( \frac{\Delta W^t}{2\sqrt{J^t}} + B \Delta \epsilon^t \right) \quad (58)$$

$$\Delta \sigma_\theta^t = \lambda \Delta \epsilon^t + 2G \Delta \epsilon_\theta^t - \beta Q \left( \frac{\sigma_\theta^t}{2\sqrt{J^t}} + B \right) \left( \frac{\Delta W^t}{2\sqrt{J^t}} + B \Delta \epsilon^t \right) \quad (59)$$

$$\Delta \sigma_z^t = \lambda \Delta \epsilon^t + 2G \Delta \epsilon_z^t - \beta Q \left( \frac{\sigma_z^t}{2\sqrt{J^t}} + B \right) \left( \frac{\Delta W^t}{2\sqrt{J^t}} + B \Delta \epsilon^t \right) \quad (60)$$

$$\Delta \tau_{rz}^t = 2G \Delta \gamma_{rz}^t - \beta Q \left( \frac{\tau_{rz}^t}{2\sqrt{J^t}} + B \right) \left( \frac{\tau_{rz}^t}{2\sqrt{J^t}} + B \Delta \epsilon^t \right) \quad (61)$$

where  $\Delta W = \sigma_r \Delta \epsilon_r + \sigma_\theta \Delta \epsilon_\theta + \sigma_z \Delta \epsilon_z + \tau_{rz} \Delta \gamma_{rz}$  (62)

$$B = \frac{1+\nu}{1-2\nu} \alpha - \frac{I^t}{6\sqrt{J^t}} \quad (63)$$

$$Q = \frac{4G}{1 + \frac{6(1+\nu)\alpha^2}{1-2\nu}} \quad (64)$$

$$\beta = \begin{cases} 1 & \text{if } \Delta W > 0, \text{ loading} \\ 0 & \text{if } \Delta W < 0, \text{ unloading} \end{cases}$$

$\alpha, I, J$  are defined in Equations (32) through (34).

Then, the stresses at time  $t$  are:

$$\sigma_r^t = \sigma_r^{t-\Delta t} + \Delta \sigma_r^t \quad (65)$$

$$\sigma_\theta^t = \sigma_\theta^{t-\Delta t} + \Delta \sigma_\theta^t \quad (66)$$

$$\sigma_z^t = \sigma_z^{t-\Delta t} + \Delta \sigma_z^t \quad \text{and} \quad (67)$$

$$\tau_{rz}^t = \tau_{rz}^{t-\Delta t} + \Delta \tau_{rz}^t \quad (68)$$

Stress Correction for Perfectly Plastic Yielding - The soil medium has been assumed to be a perfectly plastic material, that is, there is no strain hardening. This type of material requires that after yielding occurs, the yield function  $f$  must be near zero and not significantly above zero. Since computational errors usually cause  $f$  to vary significantly from zero, a form of correction on the stresses are usually applied. In the present problem, the corrections were applied such that the correction stress vector is normal to the yield function treating each component of the stress tensor, that is,  $\sigma_r$ ,  $\sigma_\theta$ ,  $\sigma_z$ ,  $\tau_{rz}$ , and  $\tau_{zr}$  as independent variables. The detailed formulation of the correction equations are presented in Appendix V and the resulting equations are shown below.

$$\sigma_r' = (1-\eta) \sigma_r + \eta \left[ (1+6\alpha^2) \frac{I}{3} - 2\alpha k \right] \quad (69)$$

$$\sigma_\theta' = (1-\eta) \sigma_\theta + \eta \left[ (1+6\alpha^2) \frac{I}{3} - 2\alpha k \right] \quad (70)$$

$$\sigma_z' = (1-\eta) \sigma_z + \eta \left[ (1+6\alpha^2) \frac{I}{3} - 2\alpha k \right] \quad (71)$$

$$\tau_{rz}' = (1-\eta) \tau_{rz} \quad (72)$$

$$\text{where } \eta = \frac{J - (k - \alpha I)^2}{2J + 12\alpha^2(k - \alpha I)^2} \quad (\text{Note that the numerator is not zero since } f \neq 0.) \quad (73)$$

and  $\sigma_r'$ ,  $\sigma_\theta'$ ,  $\sigma_z'$ ,  $\tau_{rz}'$  are the corrected stresses.

#### Numerical Procedure for the Development of the Computer Program

For convenience in the numerical calculations, the above governing equations were first expressed in terms of dimensionless variables. The dimensionless variables were formed in the following manner: the variables having a dimension of stress were divided by the yield stress in shear,  $k$ , (see Equation 35); the variables having a dimension of length were divided by the radius,  $a$ , of the applied surface pressure distribution; and time was divided by the time duration of the pulse,  $t_d$ .

The pulse curve of the applied pressure on the surface of the soil was approximated by linear segments. For each segment, the change in pressure through an increment of time was determined. The size of the time

increment was determined from criteria that will be discussed in a subsequent section. For each increment of time the stresses at the fictitious stress points in the plane ( $j = 1$ ) were changed based on the pressure increments of the particular linear segment of the approximate pulse curve. Then the following steps were performed starting with the mass point at  $(i, j) = (3, 2)$ :

(1) The accelerations  $\ddot{u}$  and  $\ddot{w}$  at time  $t$  were obtained by means of the dynamic equations of motion, Equations 19 and 20 or Equations 21 and 22, using the most current stresses that were known at time  $t$  (if not known, those at time  $t - \Delta t$  were used).

(2) The accelerations at time  $t$  and the accelerations, velocities, and displacements at time  $t - \Delta t$  were then substituted into the quadrature equations, Equations 27 through 30, to give  $u$ ,  $w$ ,  $\dot{u}$ , and  $\dot{w}$  at time  $t$ . Then the incremental displacements,  $\Delta u^t$  and  $\Delta w^t$ , were obtained from Equations 40 and 41.

(3) The stresses at the three stress points immediately surrounding the mass point  $(i, j)$ , that is, the stress points  $(i, j+1)$ ,  $(i-1, j)$ , and  $(i+1, j)$ , were recalculated according to the following steps for each stress point:

(i) The yield indicating table was checked to determine if the stress point had yielded. (Initially, the table would indicate all stress points to be elastic.)

(ii) The incremental strains at time  $t$  were calculated using the incremental strain-displacement relations, Equations 36 through 50, whichever set applied.

(iii) The stress increments were then calculated from the incremental stress strain relations. If the stress point were elastic, the elastic relations, Equations 51 through 56, were used. If the stress point were plastic, the plastic relations, Equations 58 through 64, were used. The stresses at time  $t$  were then calculated by Equations 65 through 68.

(iv) The newly obtained stresses were then substituted into the yield criterion, Equation 31, to check if the stress point had yielded. The result was then recorded in the yield indicating table. If the stress point was plastic, and the yield function  $f$  had exceeded zero above the limit at which stress correction is required, the newly calculated stresses were corrected by Equations 69 through 73.

(4) Steps 1 through 3 were repeated for the rest of the mass points, proceeding from the axis outward and then row by row downward.

(5) Using the new stresses obtained for all the stress points, steps 1 through 4 were repeated thus starting the iteration cycle. This was done until the desired accuracy was reached. It was determined that about 5 or 6 iterations produced the desired accuracy.

(6) Steps 1 through 5 were repeated for the subsequent time increments, in which the applied pressure on the boundary was incremented according to the vertical pulse load curve.

A flow diagram for the computer program is shown in Figure 25, and a listing of the computer program is given in Appendix VI.

#### Tolerance for Yielding, Unloading, and Stress Correction

In the Prager-Drucker yield criterion, a stress point is plastic when the yield function,  $f$ , of that point is greater than zero and is elastic if  $f$  is less than zero. This means that the yield surface has zero thickness. In the numerical calculation the yield function of a stress point fluctuates about zero during the process of loading due to computational accuracy. Therefore, a tolerance thickness of the yield surface was used to avoid the fluctuation between elastic and plastic states at a stress point. A tolerance equal to 1.5% of the yield stress in shear was used above and below zero.

A similar phenomena occurs in the unloading from plastic state. The incremental work done,  $\Delta W$ , defined in Equation 62 also fluctuates about zero causing intermittent loading and unloading in the plastic state. To avoid this, a tolerance of 2% of the maximum incremental work done up till that time was used for below zero limit.

Stress correction on the newly calculated stresses was applied only if the yield function is above zero past a certain limit. In the present problem, 2% of the yield stress in shear was considered as the limit. It should be noted that all the tolerances used were chosen somewhat arbitrarily but were considered to be reasonable for this type of problem.

#### Selection of Mesh Size and Time Increment

The vertical pulse loading is a time-dependent dynamic problem and consequently, the selection of the mesh size and the selection of time increment size are interdependent. There are two criteria for selecting the mesh size and the time increment. The first criteria is related to the convergence of the iteration, and the second is related to the stability of the numerical calculation.

The convergence criterion depends on the constant factor that multiplies with the  $\ddot{u}^t$  and  $\ddot{w}^t$  terms in Equation 28 and 29 of the quadrature equations. For the quadrature equation used, the criterion is given by

$$\frac{\text{Space Mesh Size}}{\text{Time Increment}} = \frac{2h}{\Delta t} > \frac{c_1}{6}$$

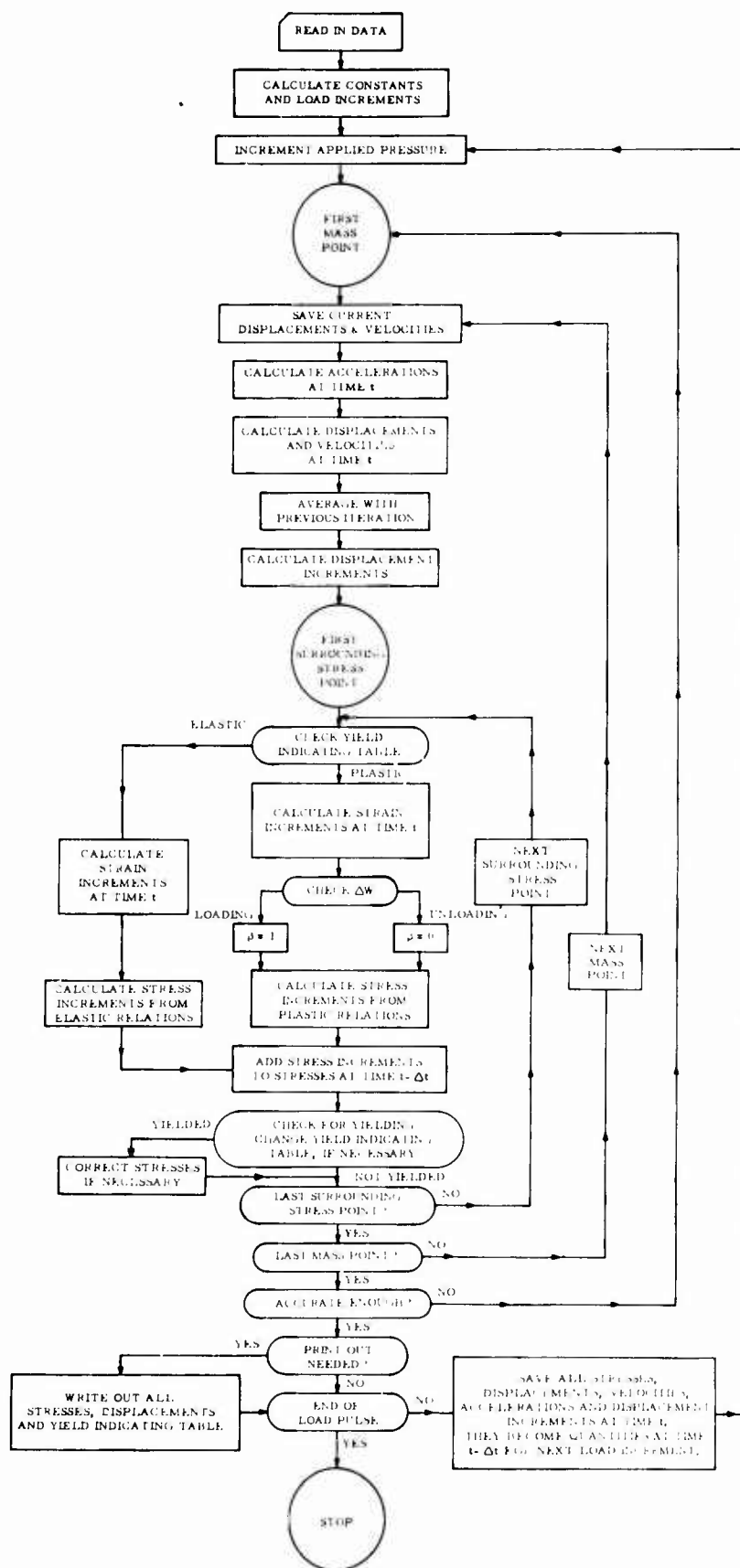


Figure 25 Flow Chart of Computer Program

where  $c_1$  = the velocity of elastic dilatational wave propagation in the soil medium.

The stability criterion requires that

$$\frac{\text{Space Mesh Size}}{\text{Time Increment}} = \frac{2h}{\Delta t} \gg c_1.$$

It was found that, in order to avoid instability (28, 29) this ratio must be at least three times larger than  $c_1$ . In the present problem, the space mesh size was first selected such that there were at least five fictitious stress points within the radius of the loaded area. The time increment was then determined according to the stability criterion given above. Because of this restriction, the time increment used was unavoidably small and consequently for load pulses that have long time durations, the computer time required for the numerical calculations would be quite long.

#### Region of Solution

Although the problem to be analyzed is a loaded semi-infinite half space the use of numerical procedures requires that the extent of the region influenced by the load be restricted to a finite region. If the boundary of the mesh selected is not sufficiently deep, an elastic rebound wave will propagate upward causing inaccuracies in the solution near the region of the loaded area. Although researchers are investigating ways of preventing this type of reflected wave by modification of the lower boundary conditions, no satisfactory procedure has been developed to date. This reflected wave condition was avoided in the numerical solution developed herein by selecting the lower boundary sufficiently deep to prevent any significant influence of this phenomenon on the solution in the region of the loaded area.

#### Test Case Evaluation

A test case having the following typical soil and loading parameters was analyzed using the finite element computer program developed.

##### Soil Parameters:

Density	$\gamma = 110 \text{ lbs/cu ft}$
Shear modulus	$G = 0.546 \times 10^6 \text{ psf}$
Poisson's ratio	$\nu = 0.4$
Cohesion	$c = 500 \text{ psf}$
Friction angle	$\phi = 20 \text{ degrees}$
Yield stress in shear	$k = 612.3 \text{ psf}$



Loading Parameters:

Radius of the loaded area	$a = 5.0$ inches
Peak pressure	$\sigma_0 = 10,000$ p.s.f.
Time duration of pulse	$t_d = 0.05$ sec

Computational Parameters:

Space Mesh Size	$h = 0.5$ inch
Time increment	$\Delta t = 25 \times 10^{-6}$ sec
Boundary size	15.5" radius x 15.5" deep

This test case was run until the applied pressure was at the peak load and a large portion of the soil medium under the loaded area had become plastic. The plastic zone started along a ring just under the boundary between the loaded and unloaded area and developed towards the axis along a 45-degree conical surface as the applied surface pressure increased. The development of the plastic zone with time and loading is shown in Figure 26. This plastic zone development is consistent with other known plastic soil response, for example, the corresponding plane strain static problem obtained by Christian (19).

The vertical deflections at the surface of the soil were plotted against the radius from the axis of the loaded area and is shown in Figure 27. At  $\frac{t}{t_d} = 0.50$ , the applied pressure was sufficiently large to push some portion of the unloaded surface above its original level. At that same applied pressure of 69.5 psi, the sinkage at  $r=0$  was comparable to the estimated sinkage based on empirical equations for sinkage prediction. The vertical deflections at the middle of the applied pressure (i.e., at  $r=0$ ) and at various depths from the soil surface were plotted against the time of loading as shown in Figure 28.

Figures 29 and 30 give the constant vertical stress contours at  $\frac{t}{t_d} = 0.35$  and  $\frac{t}{t_d} = 0.50$ , respectively. The comparison of the two figures indicates the increase of vertical stress within the soil medium as the applied pressure increases.

Currently, the soil and loading parameters of a few selected tests from the Single Wheel Verification Test Program (see Section III) are being used in the computer program. The selected tests were chosen such that

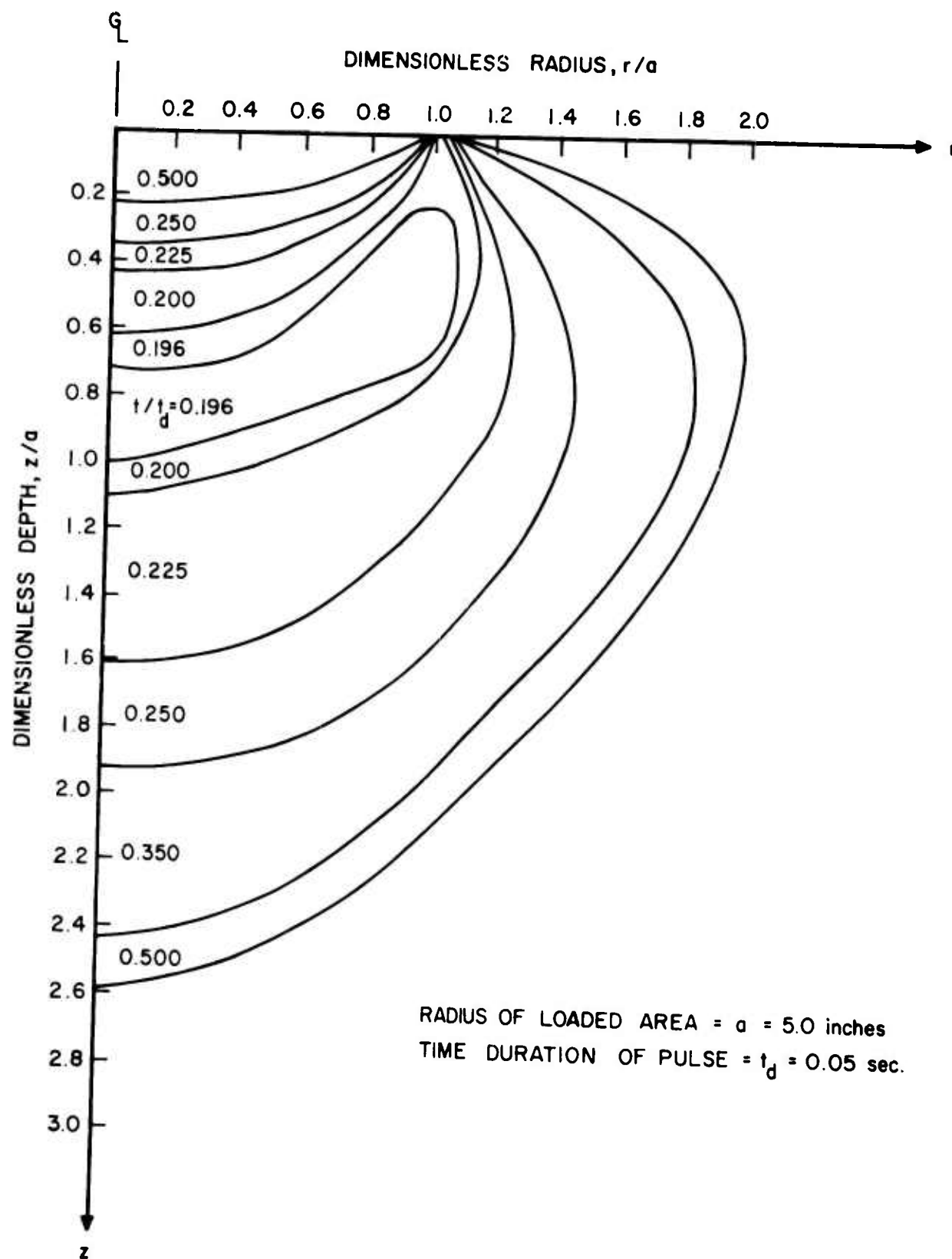


Figure 26 Development of the Plastic Zone vs Time of Loading

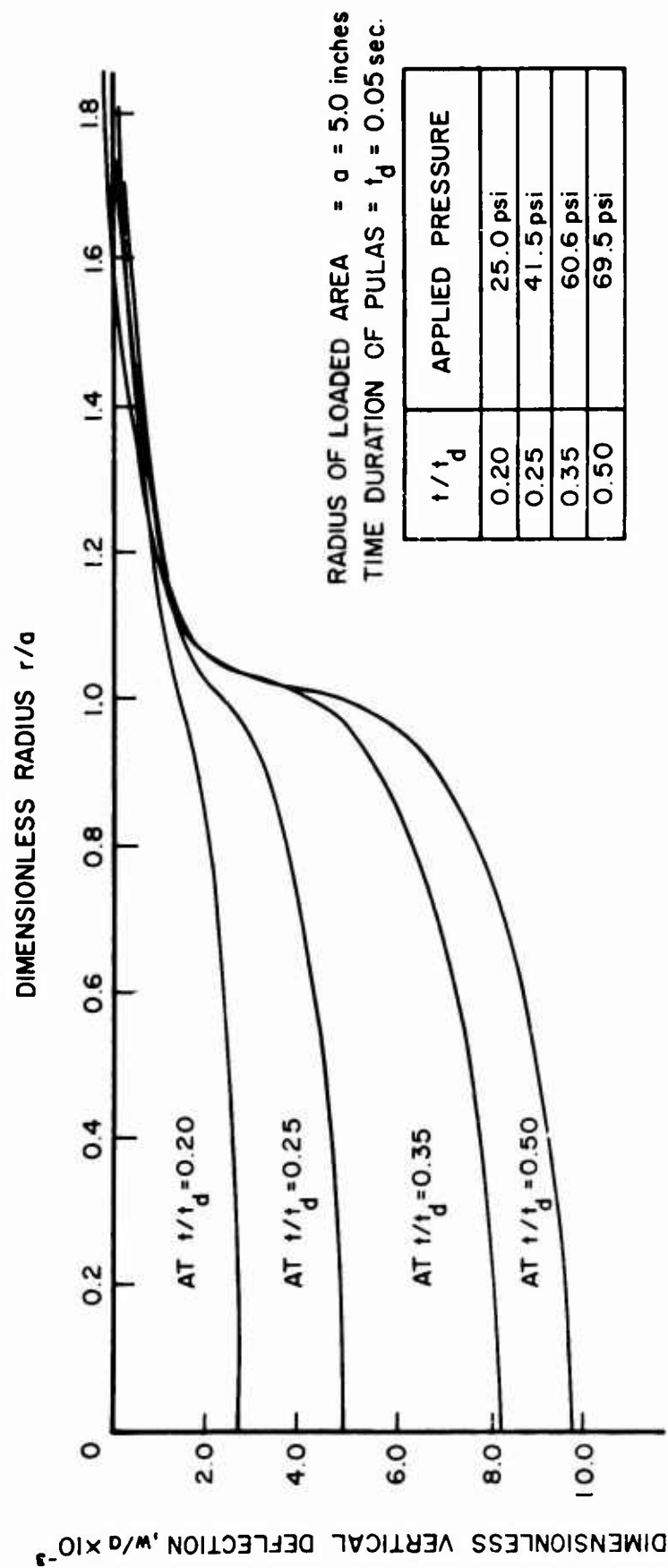


Figure 27 Vertical Deflection of the Surface vs Radius at Various Times of Loading

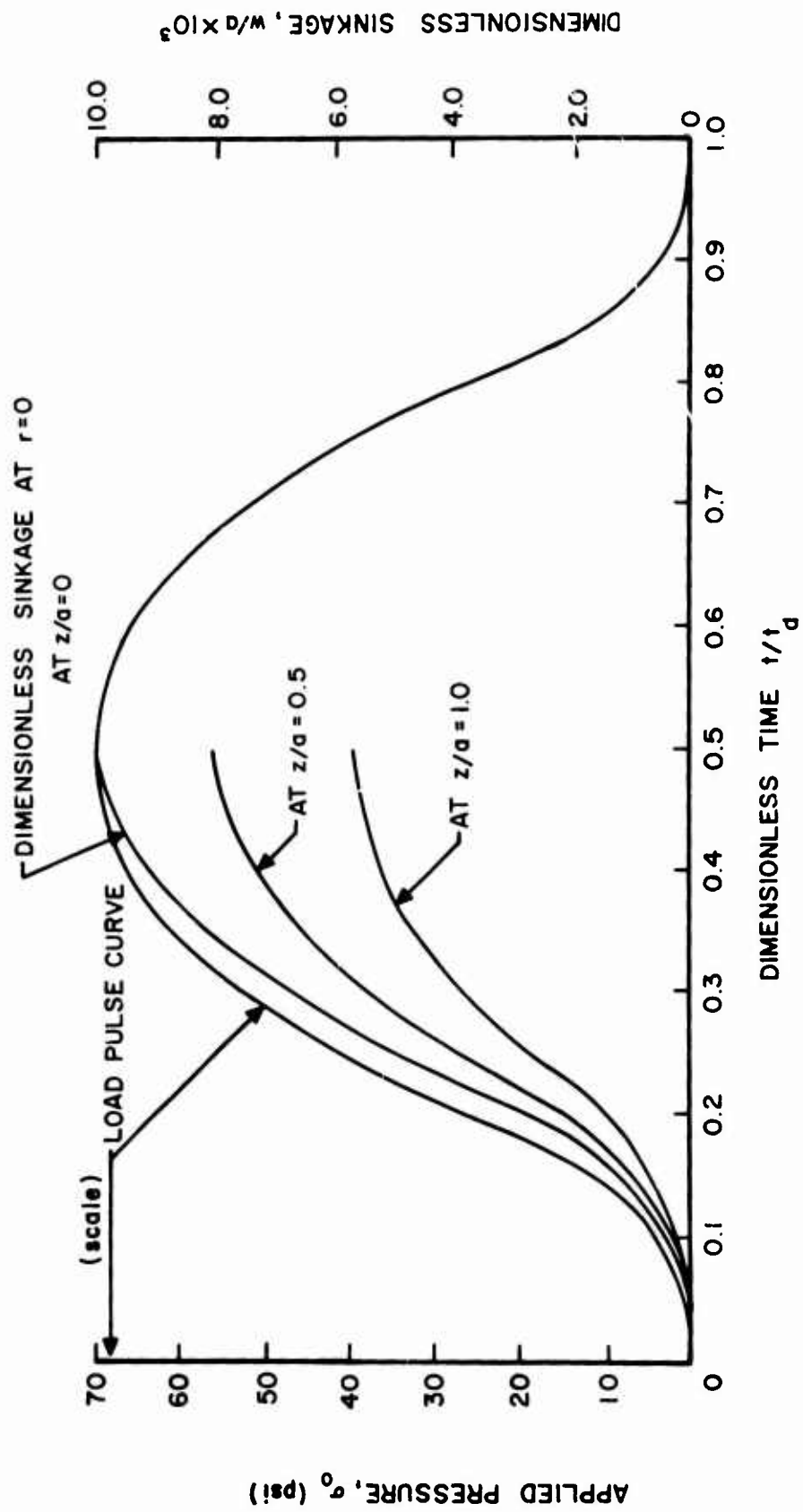


Figure 28 Sinkage at  $r/a = 0$  for Various Depths

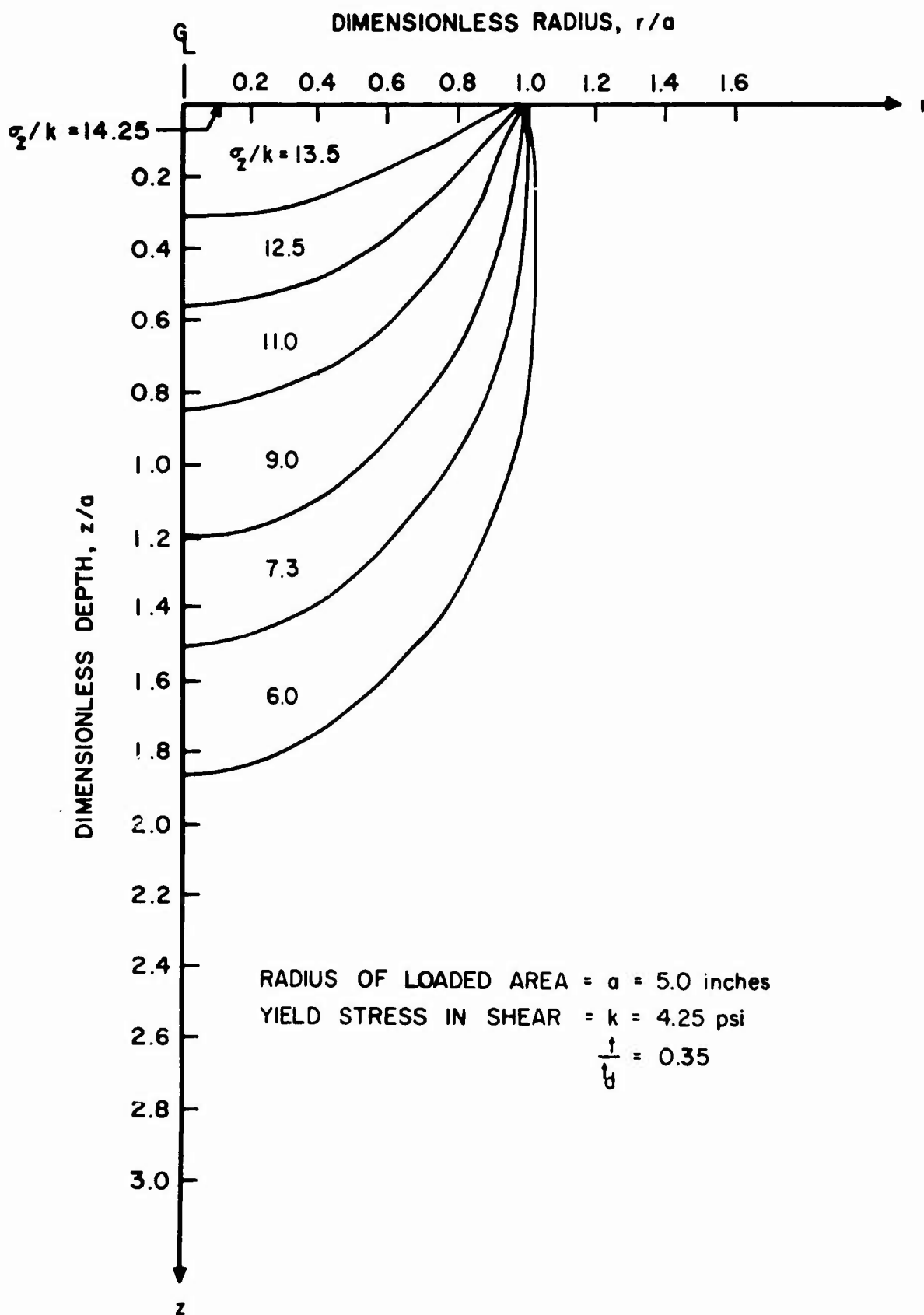


Figure 29 Constant Vertical Stress Contour at Time  $\frac{t}{t_d} = 0.35$

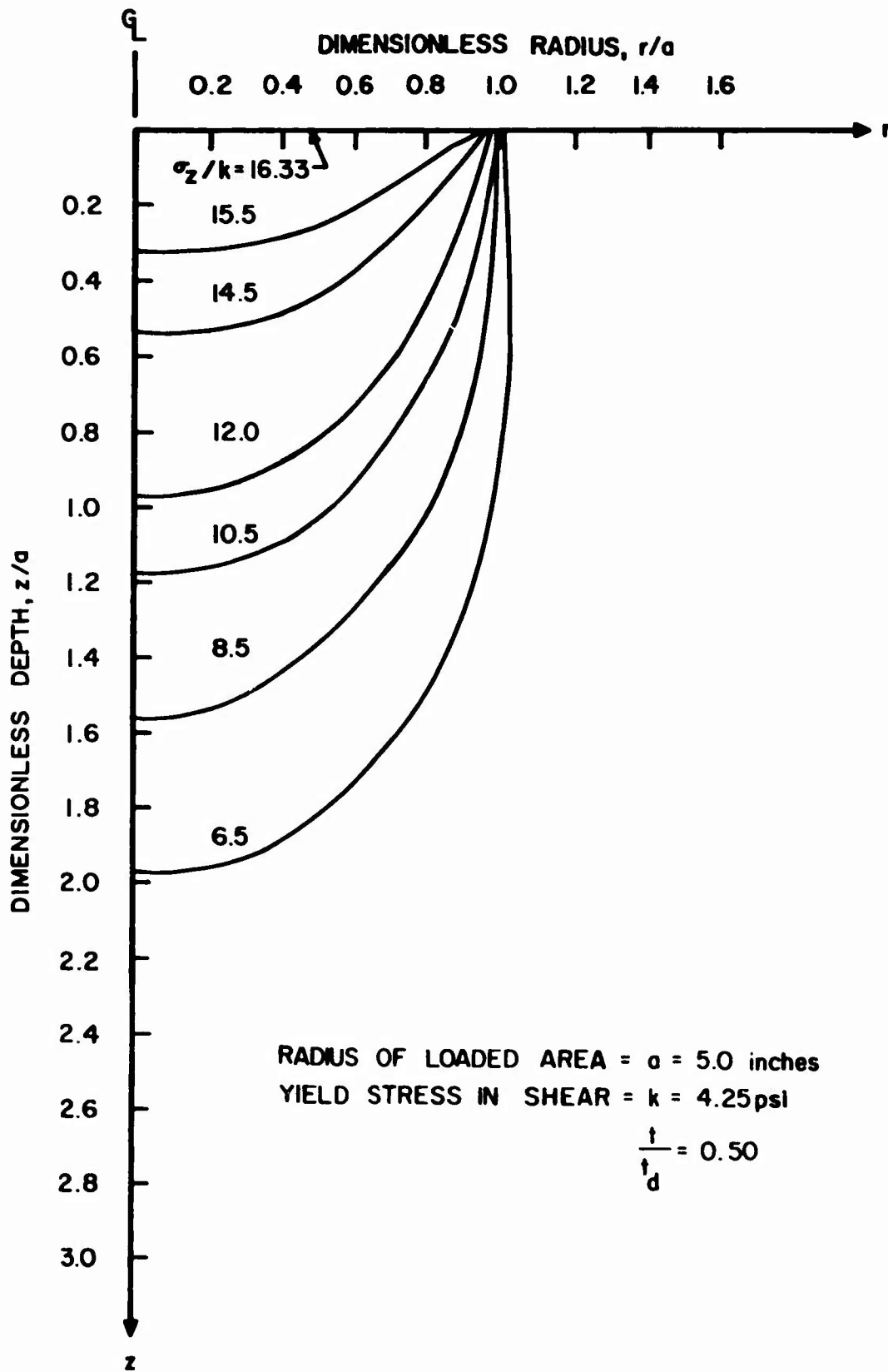


Figure 30 Constant Vertical Stress Contour at Time  $\frac{t}{t_d} = 0.50$

they would be representative of a range of sinkage in both clay and sand. The results of these cases will be available at a later date in the form of an Interim Report.

#### 4. Comparative Sinkage Prediction Study

The results of the Single Wheel Verification Tests were used as a basis on which to compare currently used sinkage prediction equations (Bekker and Boeing-WES) and the revised University of Dayton Research Institute (UDRI) sinkage prediction equation. The UDRI sinkage prediction equation (as developed in Section IV-2) is based on laboratory tire-soil test data developed by WES and UDRI, field tire-soil test data developed by WES and Lockheed-Langley, and aircraft operational tire-soil data developed by Lockheed and Boeing.

The Bekker sinkage equation as given in Equation 74 was used together with the soil properties data from Table 4

$$p = \left( \frac{k_c}{b} + k_\phi \right) Z^n \quad (74)$$

where  $p$  = tire contact stress, psi  
 $k_c, k_\phi$  = soil deformation moduli (Table IV)  
 $n$  = exponent of sinkage (Table IV)  
 $b$  = smallest dimension of contact area, in.  
 $Z$  = vertical sinkage, in.

Previously developed <sup>(1)</sup> curve fits to the Boeing (WES) sinkage relationships gave the sinkage equations as

$$\frac{Z}{D} = 0.003 + (CMN)^{-2.8} \quad \text{for } 3 \leq CMN \leq 10 \quad (75)$$

$$\frac{Z}{D} = 0.003 + (SMN)^{-1.8} \quad \text{for } 5 \leq SMN \leq 40 \quad (76)$$

$$\text{where } CMN = \text{Clay Mobility Number} = \frac{(CI)bD}{P} (d)^{1/2} \quad (77)$$

$$SMN = \text{Sand Mobility Number} = \frac{(G)(bD)^{3/2} d}{P} \quad (78)$$

and           CI = average cone index over 0" to 6", psi  
              G = slope of cone index versus depth averaged over a depth  
                    equal to the tire width, psi per in.  
              b = tire width  
              d = tire deflection, percent

The defining soil properties were developed from the soil data as given in Table IV. The revised UDRI sinkage prediction equations are given in Equations 13 through 16 and used soil property data as given in Table 4.

Figures 31 through 40 show the experimental trend of the sinkage ratio ( $Z/D$ ) versus increasing vertical load ( $P$ ) from the Single Wheel Verification Tests and also the corresponding trends as predicted by the Boeing (WES) and UDRI equations. The use of the Bekker equation, even when accounting for the increased tire contact area with sinkage, resulted in sinkages which in most cases were an order of magnitude higher than the measured sinkage, and consequently, these results are not shown on Figures 31 through 40. The dashed line used in the figures indicates the predictions are outside the restricted range of use of the prediction equations. Analysis of Figures 31 through 40 indicates that the UDRI prediction equations which are based on a broader range of tire variables and soil conditions would be more reliable for predicting the sinkage of aircraft type tires in clay and sand types of soil.

## 5. Summary

The results of the sinkage study have shown that the UDRI sinkage prediction equations are presently the most reliable method of predicting the sinkage of aircraft type tires in sand and clay soil for the Region II velocity range (5 knots to 40 knots). These empirically developed equations can be used to predict sinkages with an approximate accuracy of  $\pm 40\%$  with 90% confidence within the restricted range of analysis (see Equations 13 through 16). This restricted range of application would, however, cover most conditions encountered by aircraft operating on soil. The effects of high velocity (Region III) on sinkage are not adequately defined at this time and considerable emphasis in research efforts should be placed in studying high velocity effects on tire-soil interaction.

The finite element approach to sinkage analysis using elastic-plastic soil response should ultimately provide a reliable method for extending tire-soil interaction studies to other soil types and other contact elements without undertaking extensive experimental efforts. The results of the comparisons between analytical (finite element) sinkages and those determined in the Single Wheel Verification Tests which will be available in a subsequent report should provide considerable insight into tire-soil interaction phenomena.



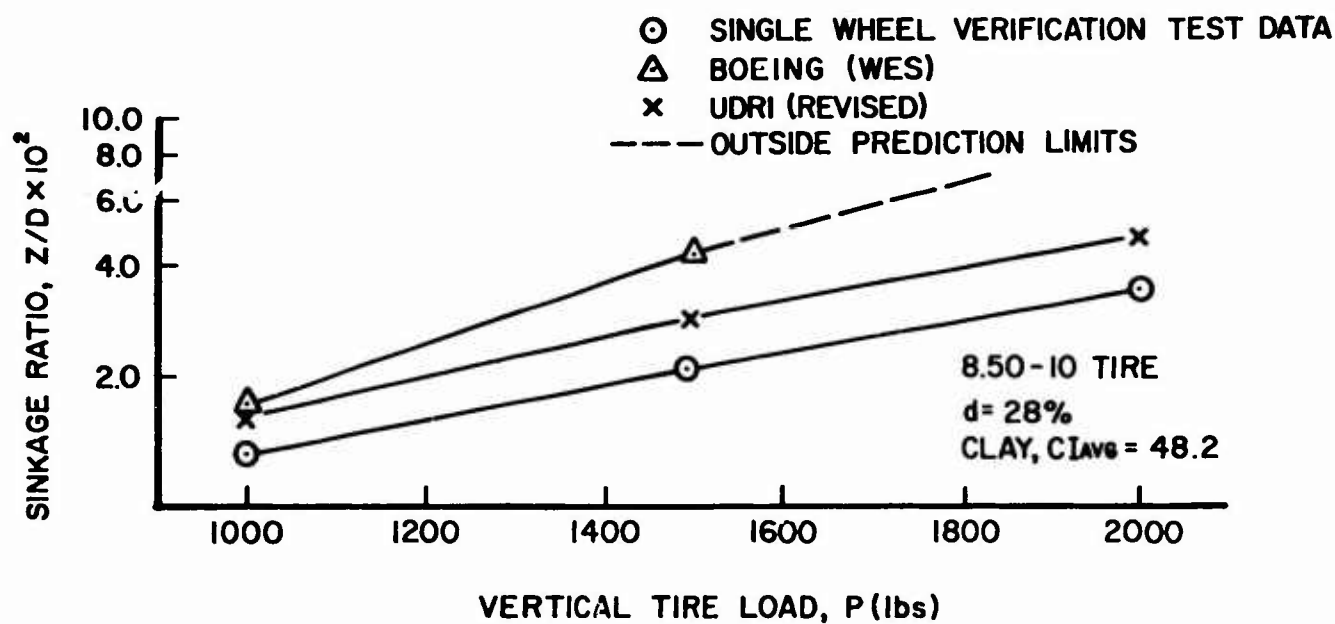


Figure 31 Sinkage Ratio vs. Vertical Tire Load, 8.50-10 Tire on High Strength Clay,  $d = 28\%$

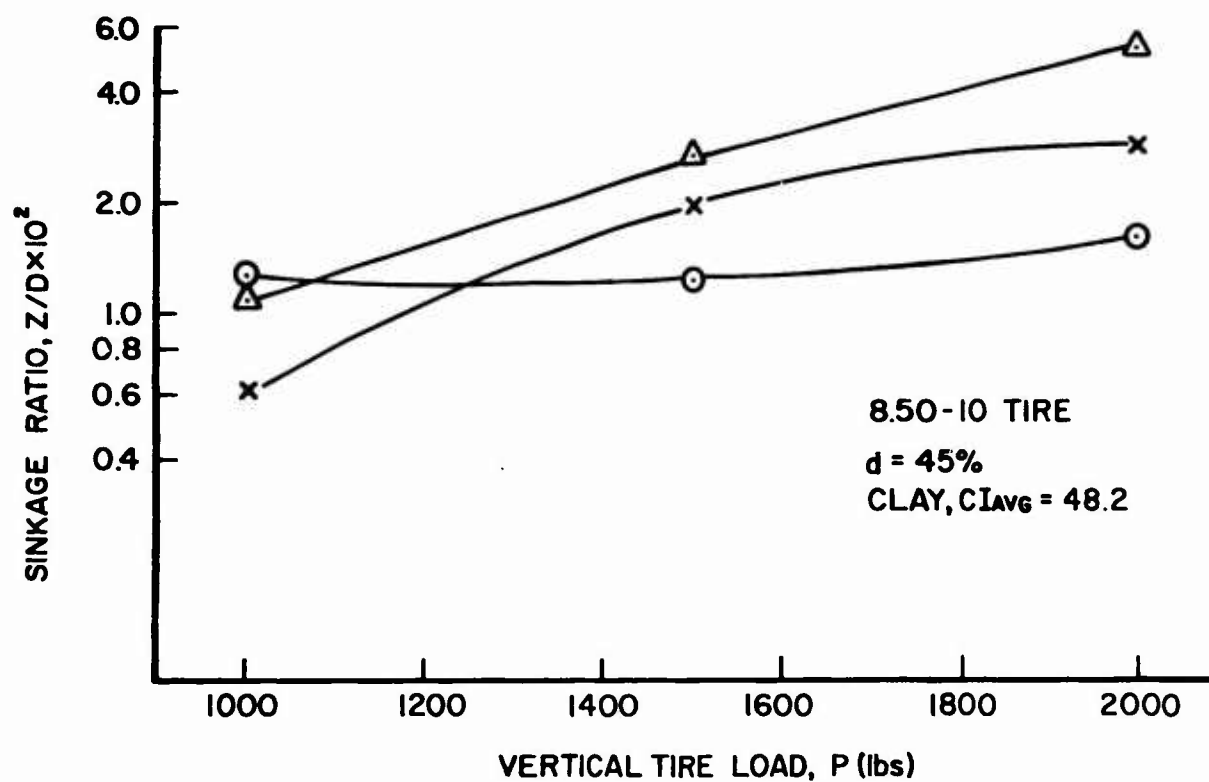


Figure 32 Sinkage Ratio vs. Vertical Tire Load, 8.50-10 Tire on High Strength Clay,  $d = 45\%$

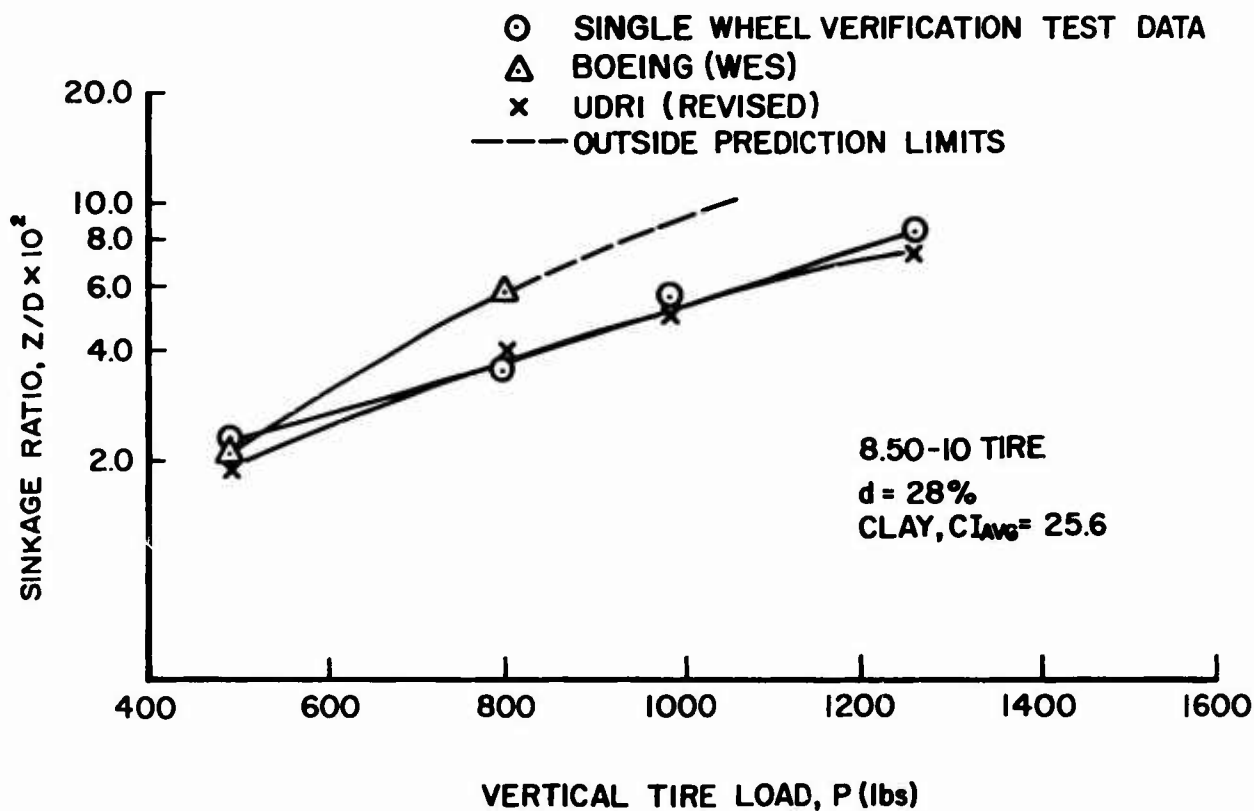


Figure 33 Sinkage Ratio vs. Vertical Tire Load, 8.50-10 Tire on Low Strength Clay,  $d = 28\%$

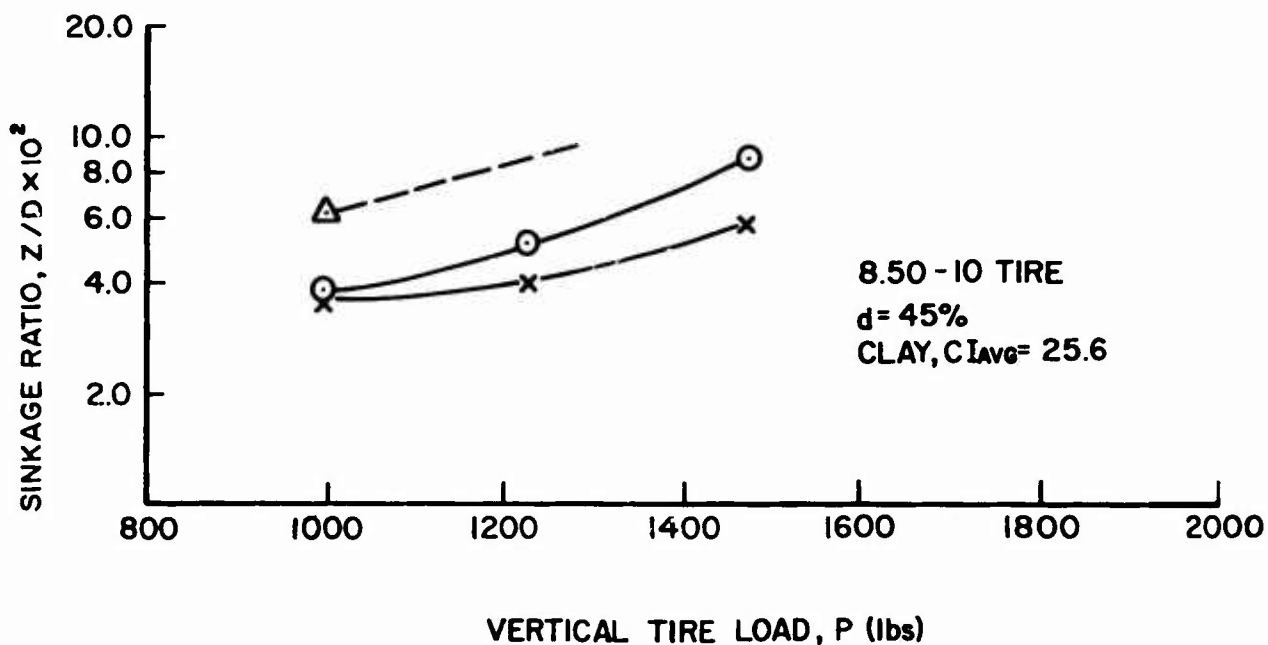


Figure 34 Sinkage Ratio vs. Vertical Tire Load, 8.50-10 Tire on Low Strength Clay,  $d = 45\%$

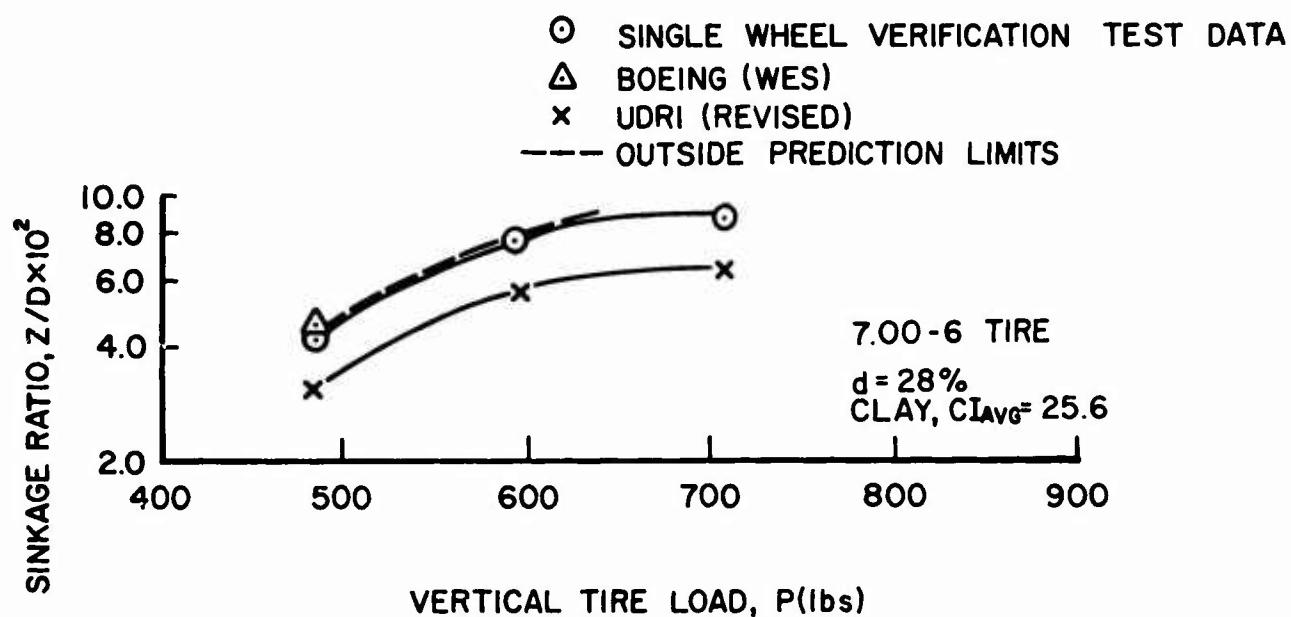


Figure 35 Sinkage Ratio vs. Vertical Tire Load, 7.00-6 Tire on Low Strength Clay,  $d = 28\%$

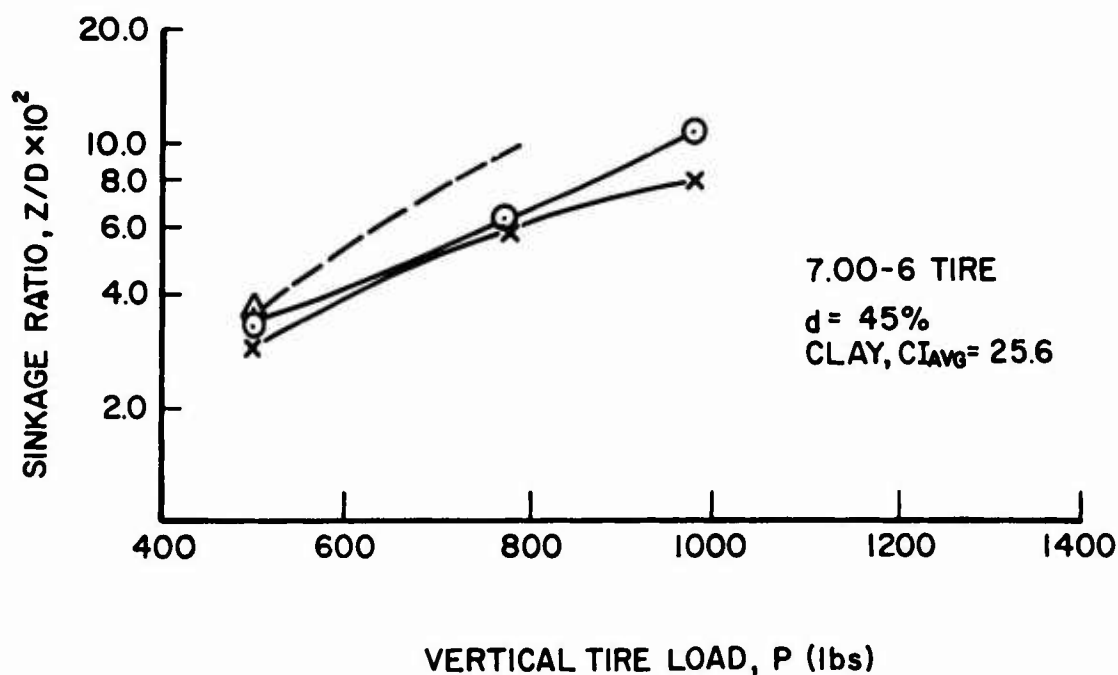


Figure 36 Sinkage Ratio vs. Vertical Tire Load, 7.00-6 Tire on Low Strength Clay,  $d = 45\%$

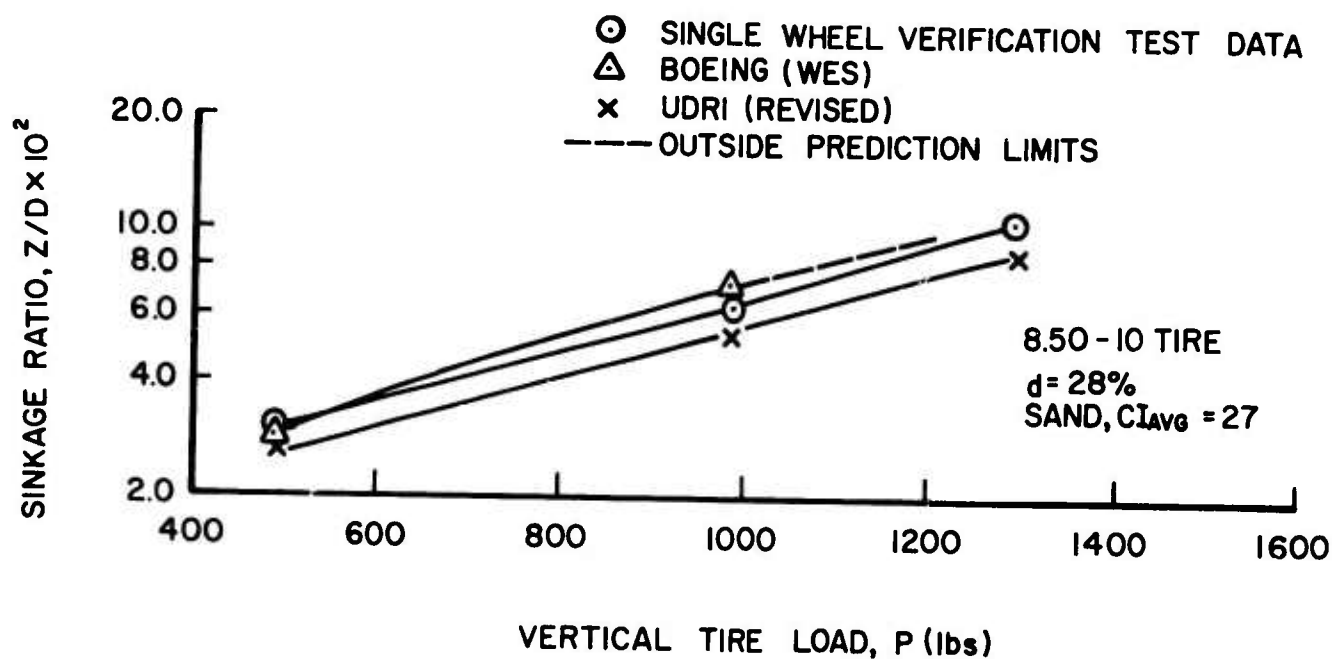


Figure 37 Sinkage Ratio vs. Vertical Tire Load, 8.50-10 Tire on Sand,  $d = 28\%$

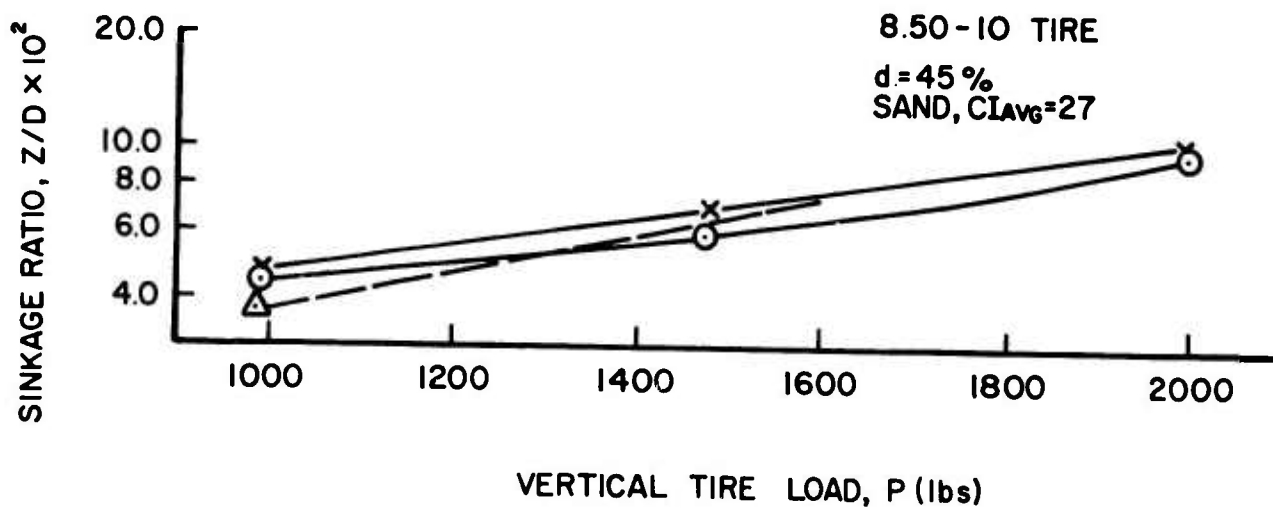


Figure 38 Sinkage Ratio vs. Vertical Tire Load, 8.50-10 Tire on Sand,  $d = 45\%$

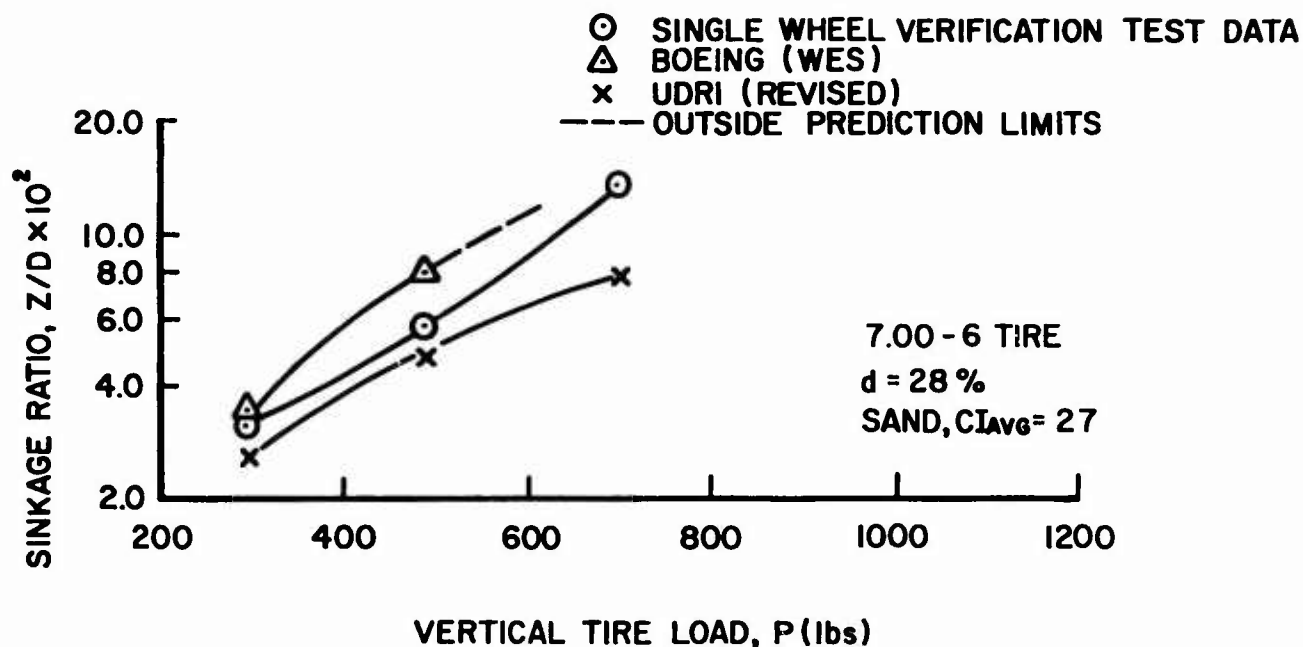


Figure 39 Sinkage Ratio vs. Vertical Tire Load, 7.00-6 Tire on Sand, d = 28%

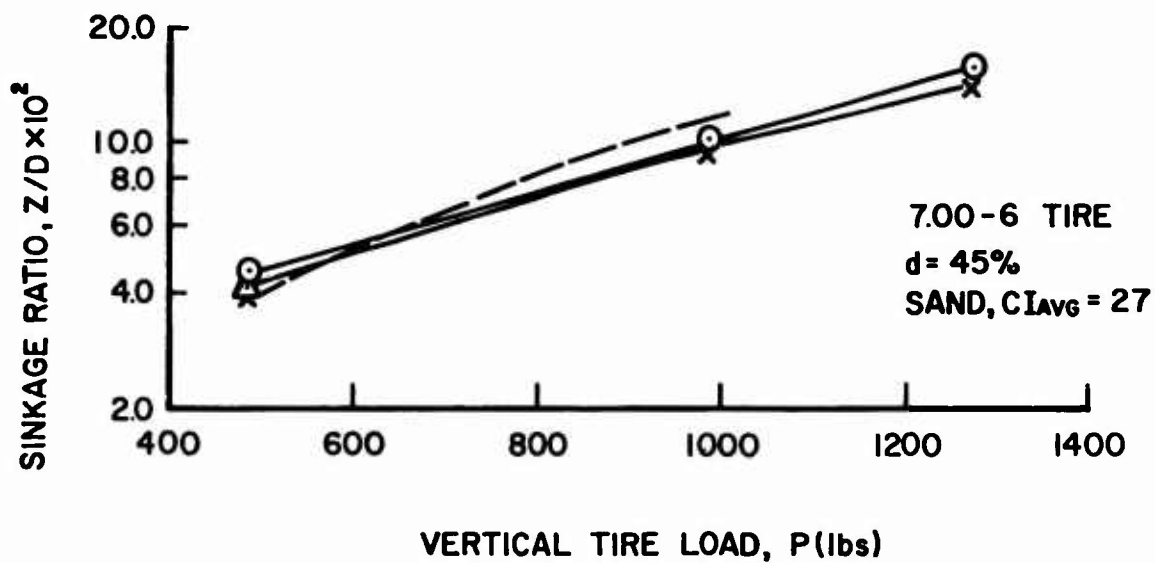


Figure 40 Sinkage Ratio vs. Vertical Tire Load, 7.00-6 Tire on Sand, d = 45%

## SECTION V

### SINGLE WHEEL RELATIVE MERIT INDEX (RMI)

#### 1. Preliminary Development

The primary variables associated with evaluating the flotation capacity of a landing gear system includes drag, sinkage, multiple wheel effects, and braking effects. Secondary variables which influence flotation capacity include turning, landing impact, and point of rotation effects. The Relative Merit Index (RMI) is a system for incorporating these primary and secondary flotation variables in a suitable manner to permit the comparative evaluation of the flotation capacity of landing gear types and configurations.

The results of the preliminary development of the basic tire-soil interaction equation (1) and empirical sinkage prediction equation (2) were used to develop the flotation criteria for rating the performance of aircraft tires operating on soil. This preliminary RMI has been developed in a separate report form and is currently under review by governmental agencies. Copies of this report are available either from AFFDL/FDFM or the University of Dayton. The preliminary drag-sinkage interaction effects were defined by

$$R/P = 0.015 + 3.09 \left( \frac{Z}{D} \right) \quad (79)$$

for the Region II velocity range, and the preliminary sinkage prediction equations which were developed for sand and clay are given by

#### Cohesive Soil

$$\frac{Z}{l} = -0.03 + 0.19 \frac{\alpha}{CI_{avg}} \quad (80)$$

$$\text{for } 0.20 \leq \frac{\alpha}{CI_{avg}} \leq 1.05$$

where  $l$  = contact footprint length (rigid surface) at the applicable tire deflection

$CI_{avg}$  = average cone index over 0" to 6" depth

$\alpha = P/A$

and

$A$  = tire contact area (rigid surface) at the applicable tire deflection

#### Cohesionless Soil

$$\frac{Z}{l} = -0.01 + 0.23 \frac{\alpha}{CI_{avg}} \quad (81)$$

$$\text{for } 0.015 \leq \frac{\alpha}{CI_{avg}} \leq 1.20$$

Combining Equations 79, 80, and 81 leads to the single wheel drag ratio relationship as given by

#### Cohesive Soil

$$R/P(\text{single wheel}) = 0.015 + (0.587 \frac{\alpha}{CI_{avg}} - 0.093) \frac{l}{D} \quad (82)$$

$$\text{for } 0.20 \leq \frac{\alpha}{CI_{avg}} \leq 1.20$$

#### Cohesionless Soil

$$R/P(\text{single wheel}) = 0.015 + (0.711 \frac{\alpha}{CI_{avg}} - 0.031) \frac{l}{D} \quad (83)$$

$$\text{for } 0.15 \leq \frac{\alpha}{CI_{avg}} \leq 1.05$$

These basic tire-soil interaction equations and sinkage prediction equations have subsequently been revised as detailed in Sections II and IV based on more recently available flotation data.

Equations 82 and 83 were combined with aircraft tire geometry variables to develop computer programs for evaluating the single wheel drag ratio relationship. These programs, which are given in Appendix III, form the basis of the preliminary rolling single wheel comparative flotation evaluation.

## 2. Comparative Flotation Evaluation

The RMI system at present has been subdivided into three basic categories to define the flotation capacity of aircraft tires when operating on soil runways. These categories are:

- a. Takeoff operations
- b. Landing operations
- c. Runway deterioration

Aircraft tires currently in use on such aircraft as C-119, C-123, C-135, C-141, C-5A and others were rated using the flotation capability computer program and the defining index for the tires operating on a high strength and a low strength cohesive and cohesionless soil.

The preliminary index system associated with each of these categories are defined as:

#### Flotation Index (FI)

The Flotation Index is designed to rate comparatively the capability of landing systems in minimizing the drag load per unit vertical load for specified operating conditions in takeoff operations. The defining FI equation is

$$FI = N[R/P(\text{single wheel})] \quad (84)$$

where N = the number of contact elements in landing gear system. The results of the Flotation Index ratings are shown in Figures 41 through 46.

#### Drag Index (DI)

The Drag Index is designed to rate comparatively the capability of landing gear systems in maximizing the drag load for specified operating conditions in landing operations. An additional variable present in the landing mode is the percent slip (S) of the braked tire. This braking condition leads to a greater drag resistance and sinkage for the aircraft tire. The two basic parameters defining braked tire-soil interaction are:

$$\frac{R_B}{P}(S) = \text{ratio of the braking drag force to the vertical load as a function of slip; and}$$

$$\frac{Z}{P}(S) = \text{ratio of instantaneous tire sinkage to the vertical load as a function of slip.}$$

Combining these two parameters gives the defining Drag Index relationship as

$$DI = \frac{\frac{R_B}{P}(S)}{\frac{Z}{P}(S)} = \frac{R_B}{Z}(S); \text{ single wheel} \quad (85)$$



SINGLE WHEEL FLOTATION INDEX (FI)  
LOW STRENGTH SOIL-CARGO TIRES

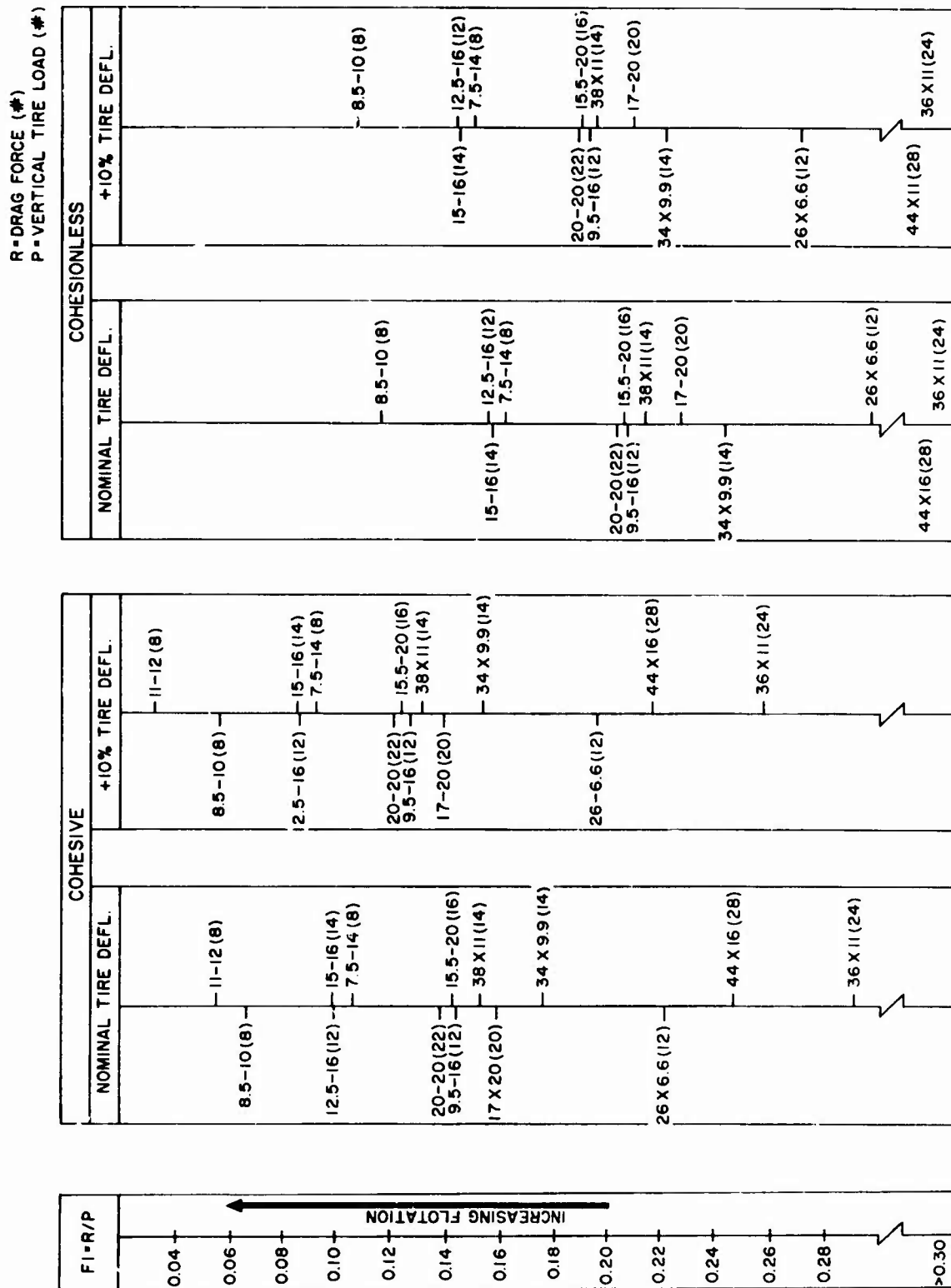
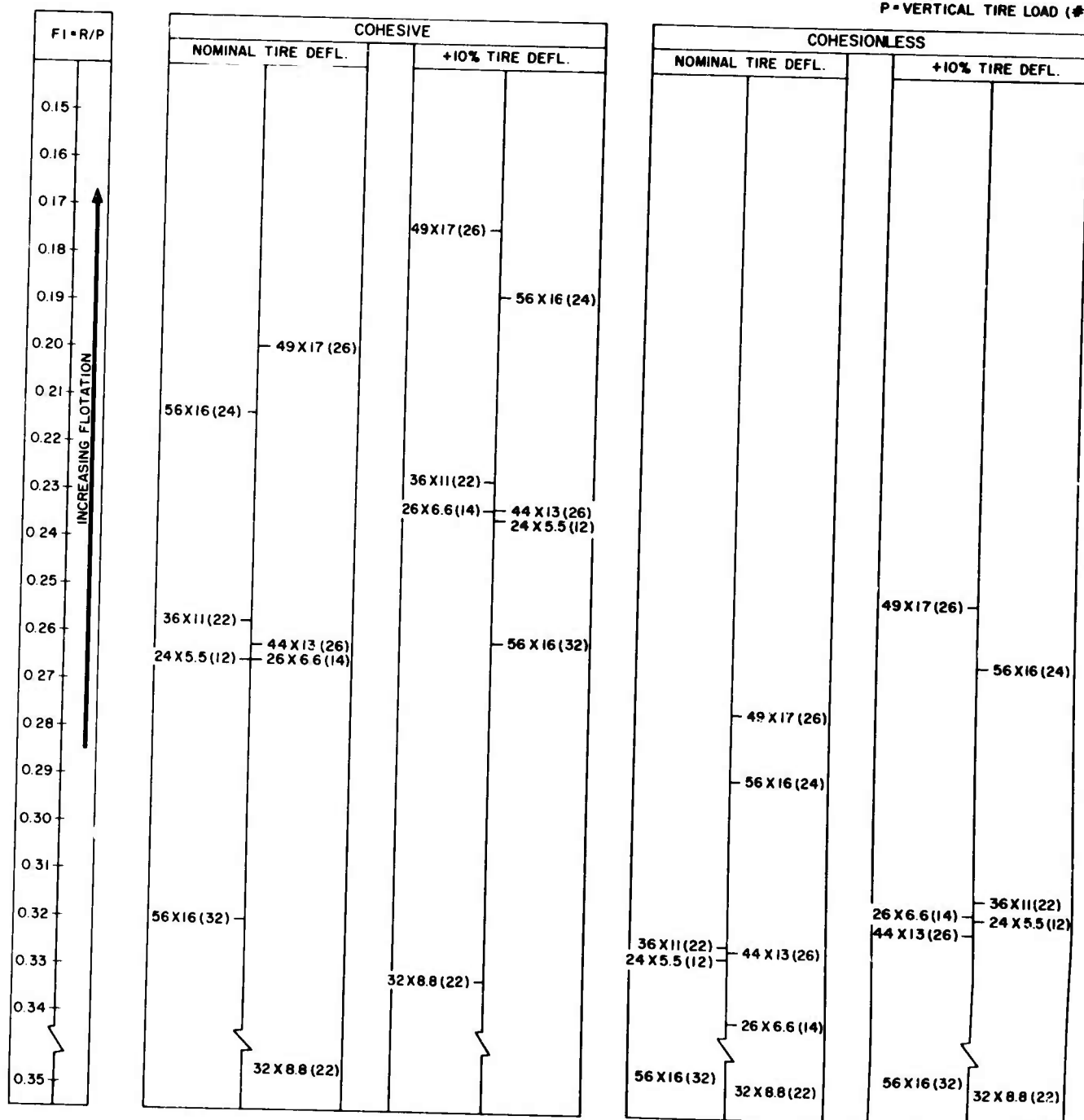


Figure 41 Flotation Index, Aircraft Cargo Tires on Low Strength Soil

R = DRAG FORCE (#)  
P = VERTICAL TIRE LOAD (#)



75

SINGLE WHEEL FLOTATION INDEX (FI)  
LOW STRENGTH SOIL-FIGHTER TIRES

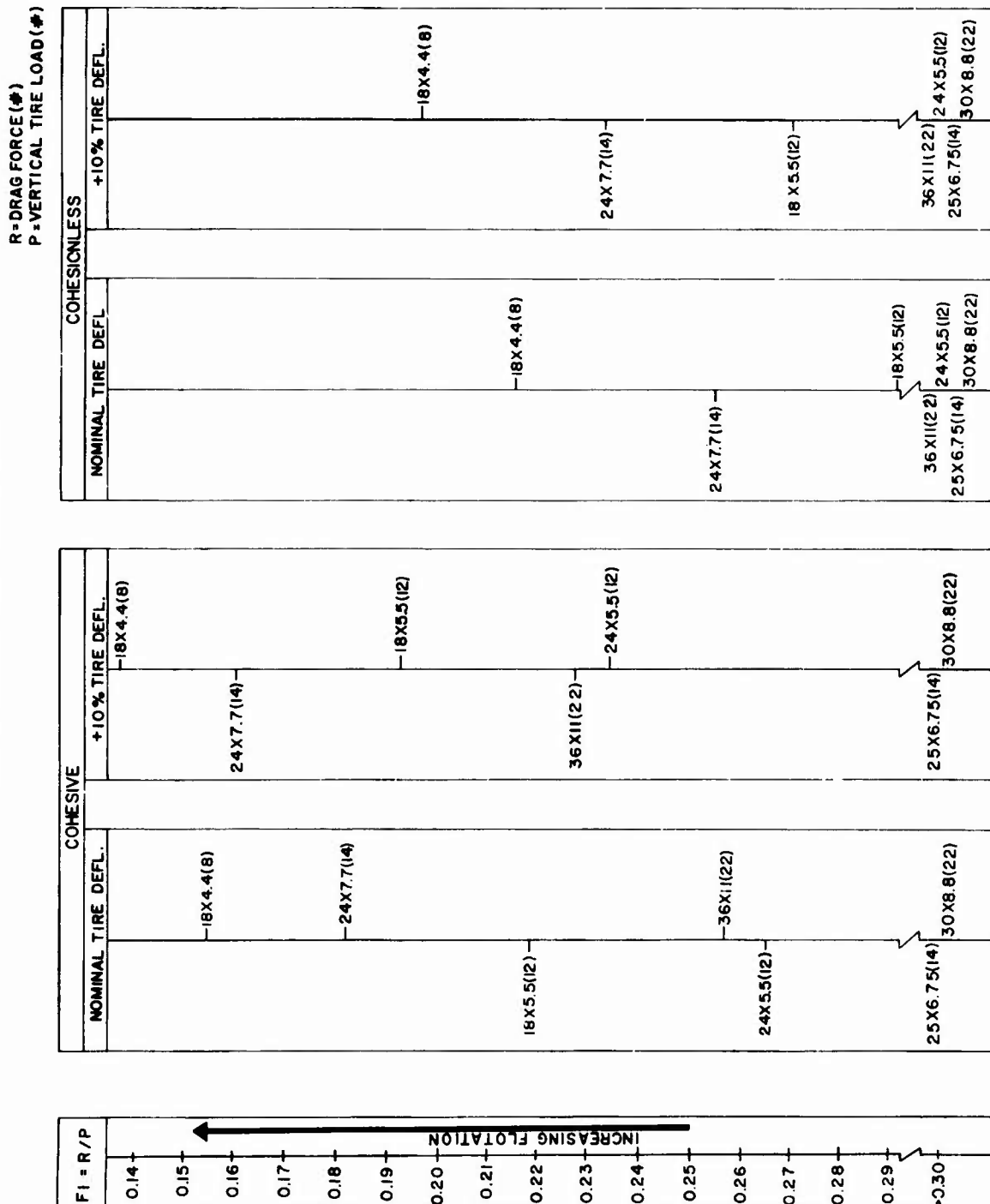


Figure 43 Flotation Index, Aircraft Fighter Tires on Low Strength Soil

SINGLE WHEEL FLOTATION INDEX (FI)  
HIGH STRENGTH SOIL-CARGO TIRES

R=DRAG FORCE (#)  
P=VERTICAL TIRE LOAD (#)

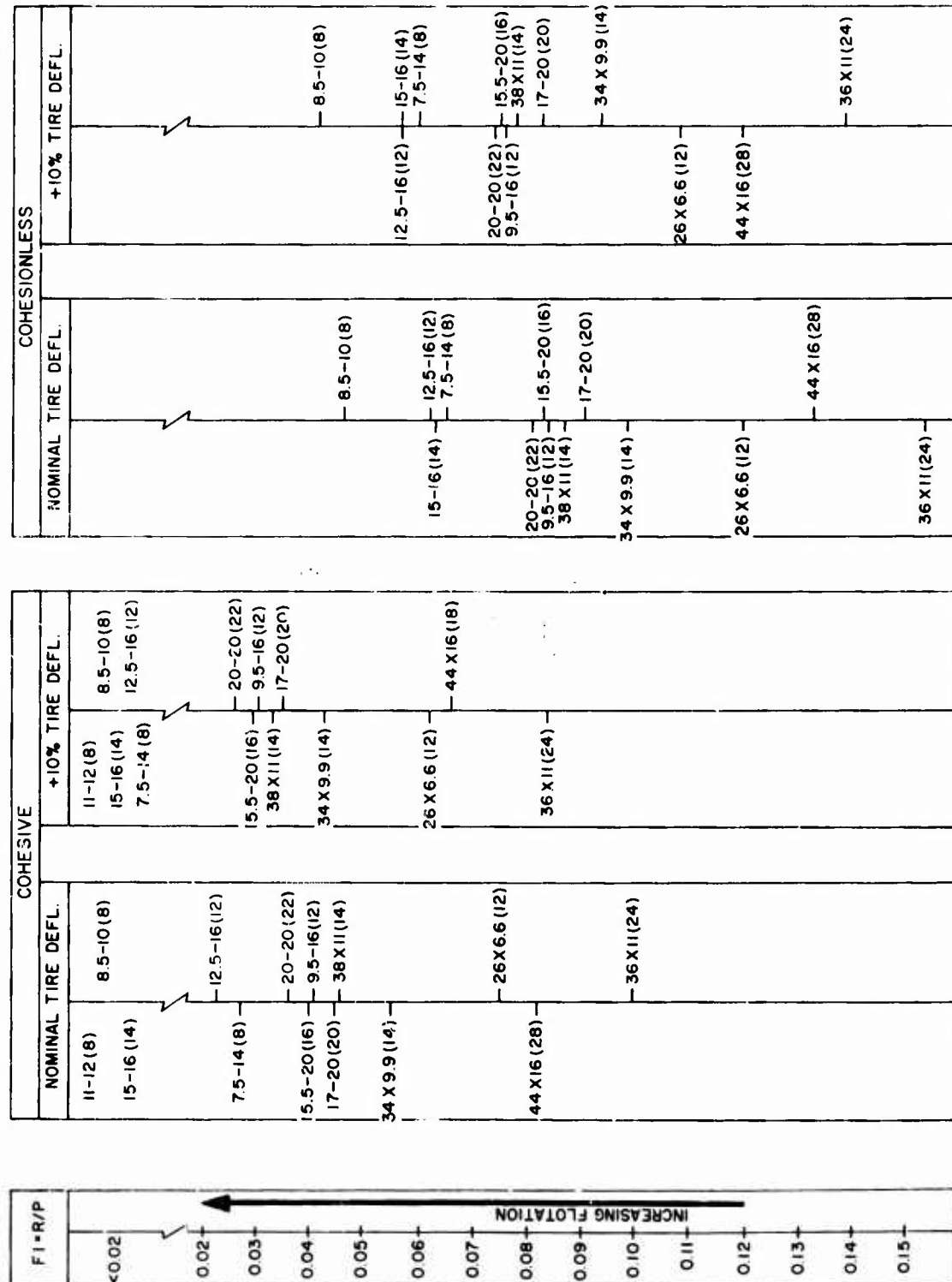


Figure 44 Flotation Index, Aircraft Cargo Tires on High Strength Soil

SINGLE WHEEL FLOTATION INDEX (FI)  
HIGH STRENGTH SOIL-BOMBER TIRES

R=DRAG FORCE (#)  
P=VERTICAL TIRE LOAD (#)

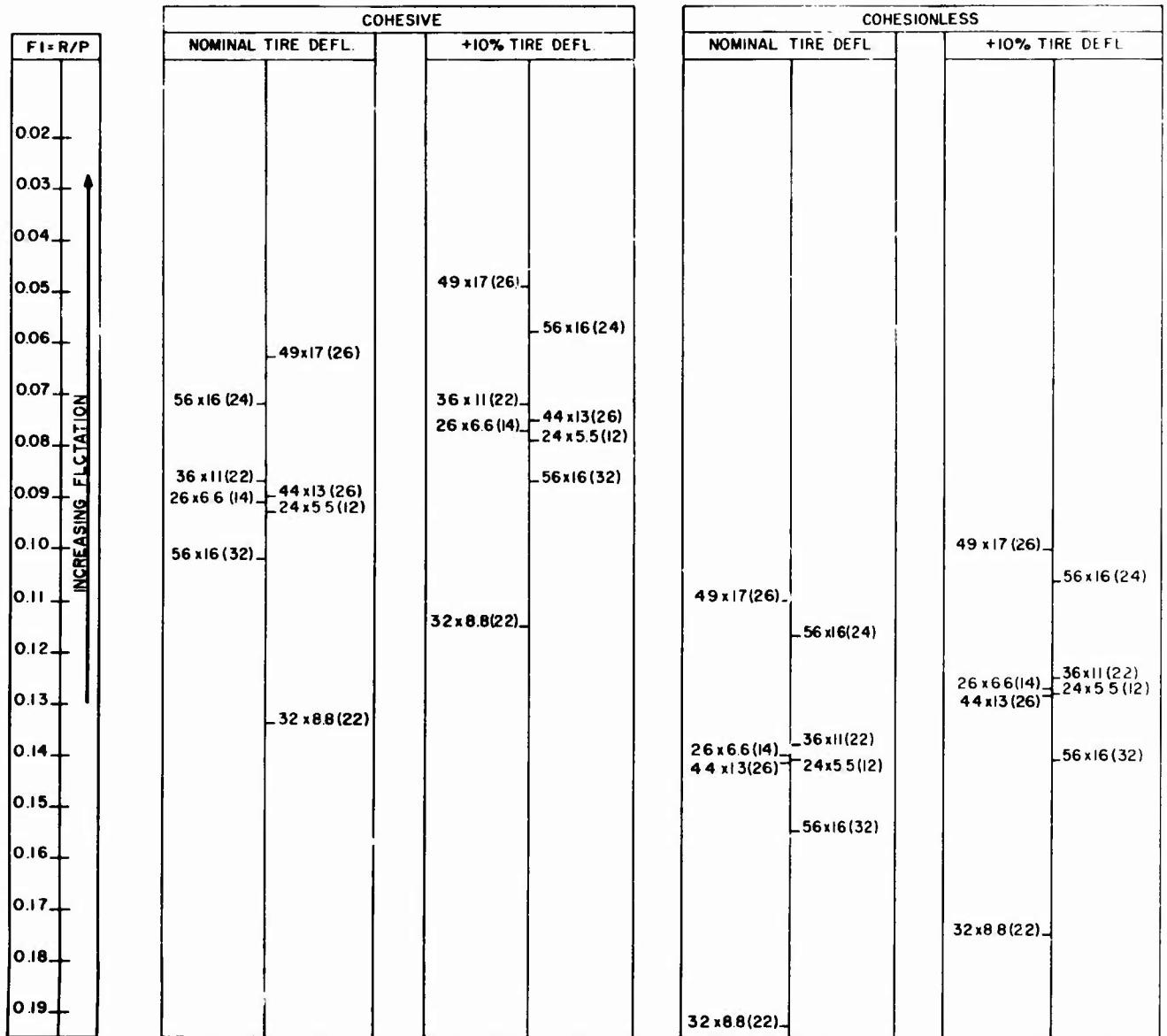


Figure 45 Flotation Index, Aircraft Bomber Tires on High Strength Soil

SINGLE WHEEL FLOTATION INDEX (FI)  
HIGH STRENGTH SOIL-FIGHTER TIRES

R=DRAG FORCE (#)  
P=VERTICAL TIRE LOAD (#)

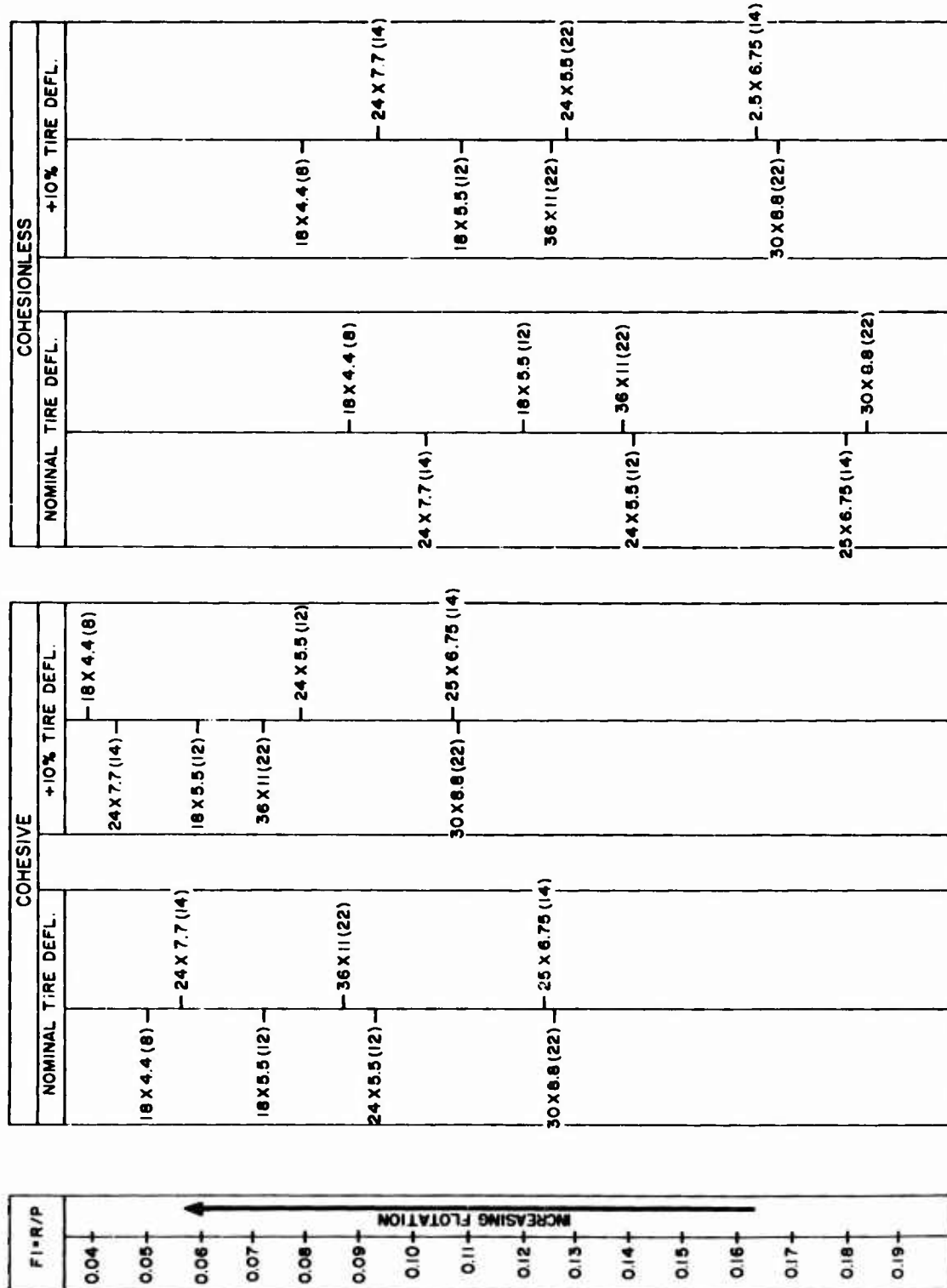


Figure 46 Flotation Index, Aircraft Fighter Tires on High Strength Soil

The Drag Index is then designed to rate comparatively the capability of landing gear systems in maximizing the braking drag force per unit instantaneous vertical sinkage for specified operating conditions in landing operations. Since an adequate braked tire-soil interaction theory substantiated by experimental verifications has not been developed at the present time, no Drag Index ratings were made on existing aircraft tires.

#### Operations Index (OI)

The Operations Index is designed to rate comparatively the destructive (deterioration) effects on soil runways of various landing gear systems as determined by the sinkage per unit vertical load for specified operating conditions in both landing and takeoff operations. The defining OI equation is

$$OI = Z/P \text{ (first pass)} \quad (86)$$

where  $Z/P$  = sinkage factor

The results of the Operations Index ratings are shown in Figures 47 through 52.

In addition to the computer program for determining flotation capacity, a nomograph was developed for evaluating the Flotation Index (FI) and Operations Index (OI). This nomograph is shown in Figure 53, and an example illustrating its use is given below. Working size copies of the nomograph are available from either AFFDL/FDFM or the University of Dayton.

#### Example of Use of Nomograph

Compare the relative flotation characteristics, as defined by the Flotation Index and the Operations Index, of the 56 x 16 (Type VII) tire to the 40 x 14 (Type VII) tire for both tires operating at a nominal tire deflection (d) of 32%.

#### Known Information

- Cohesive Soil,  $CI_{avg} = 300$  psi
- the 56 x 16 tire has a known bearing area of 340 in<sup>2</sup> at d = 40% and P (nominal) = 76,000 lbs.
- the 40 x 14 tire has a known bearing area of 97 in<sup>2</sup> at d = 20% and P (nominal) = 30,500 lbs.

# SINGLE WHEEL OPERATION INDEX (OI) LOW STRENGTH SOIL - CARGO TIRES

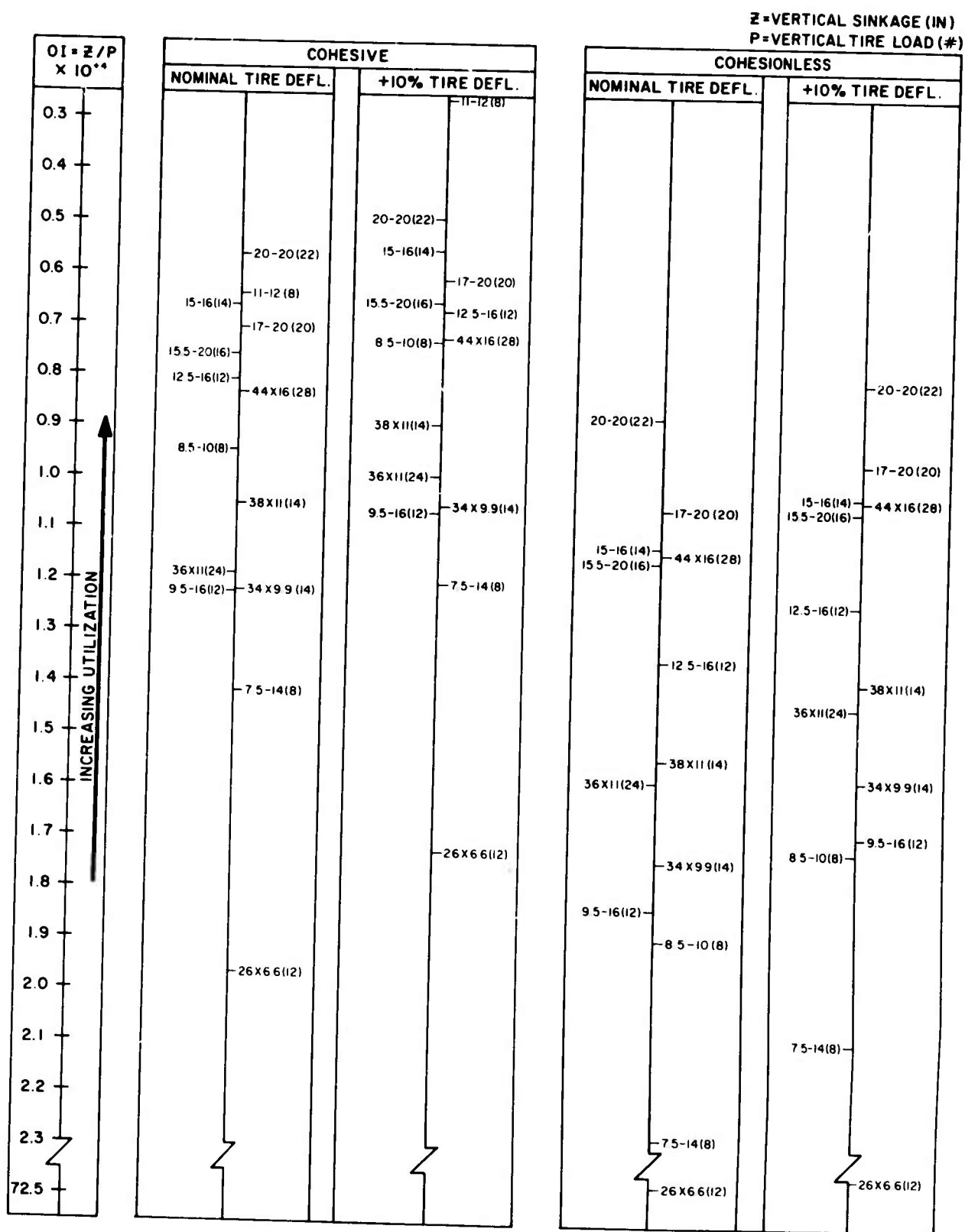


Figure 47 Operations Index, Aircraft Cargo Tires on Low Strength Soil



SINGLE WHEEL OPERATION INDEX (OI)  
LOW STRENGTH SOIL-BOMBER TIRES

Z=VERTICAL SINKAGE (IN)  
P=VERTICAL TIRE LOAD (#)

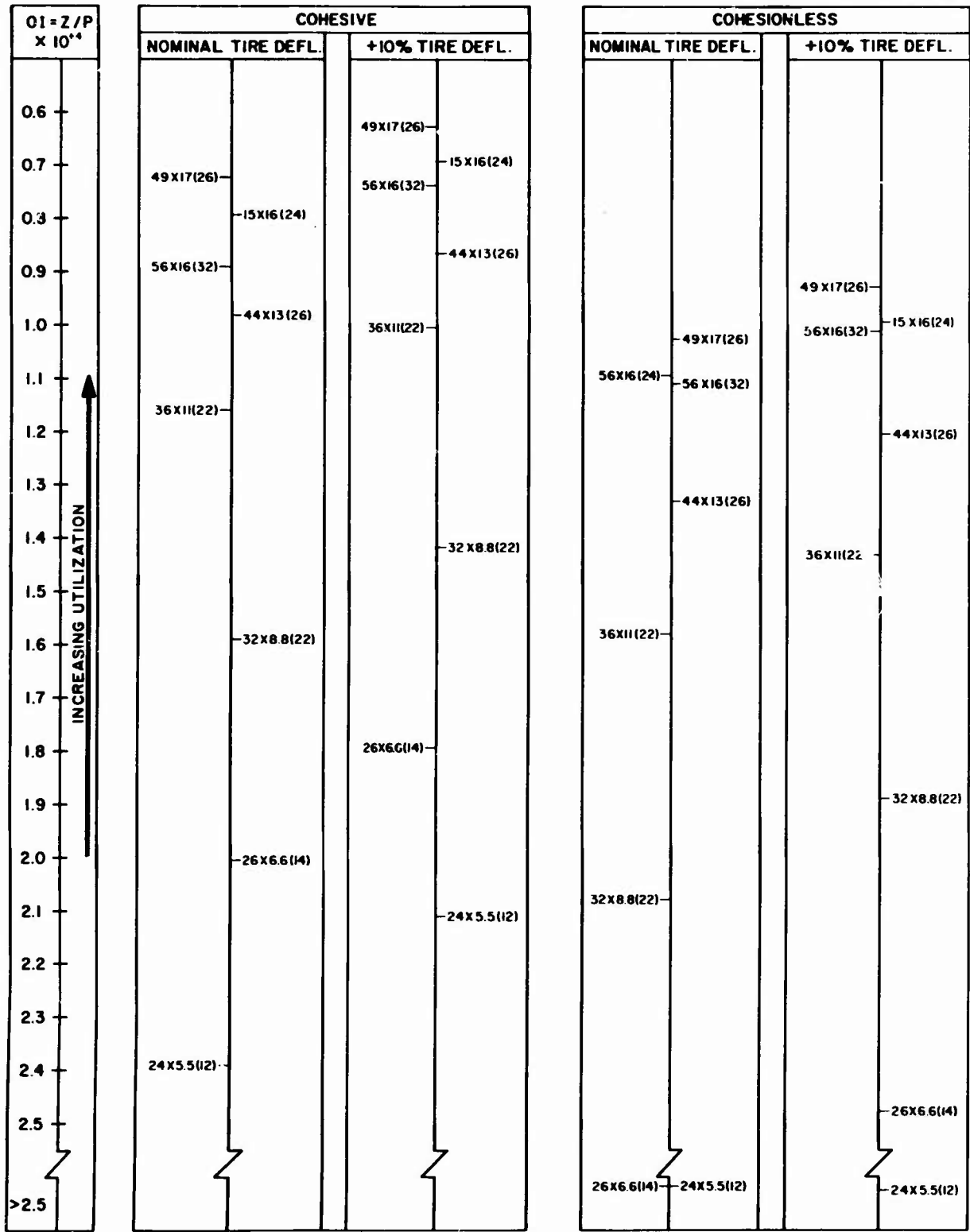


Figure 48 Operations Index, Aircraft Bomber Tires on Low Strength Soil

**SINGLE WHEEL OPERATION INDEX (OI)  
LOW STRENGTH SOIL—FIGHTER TIRES**

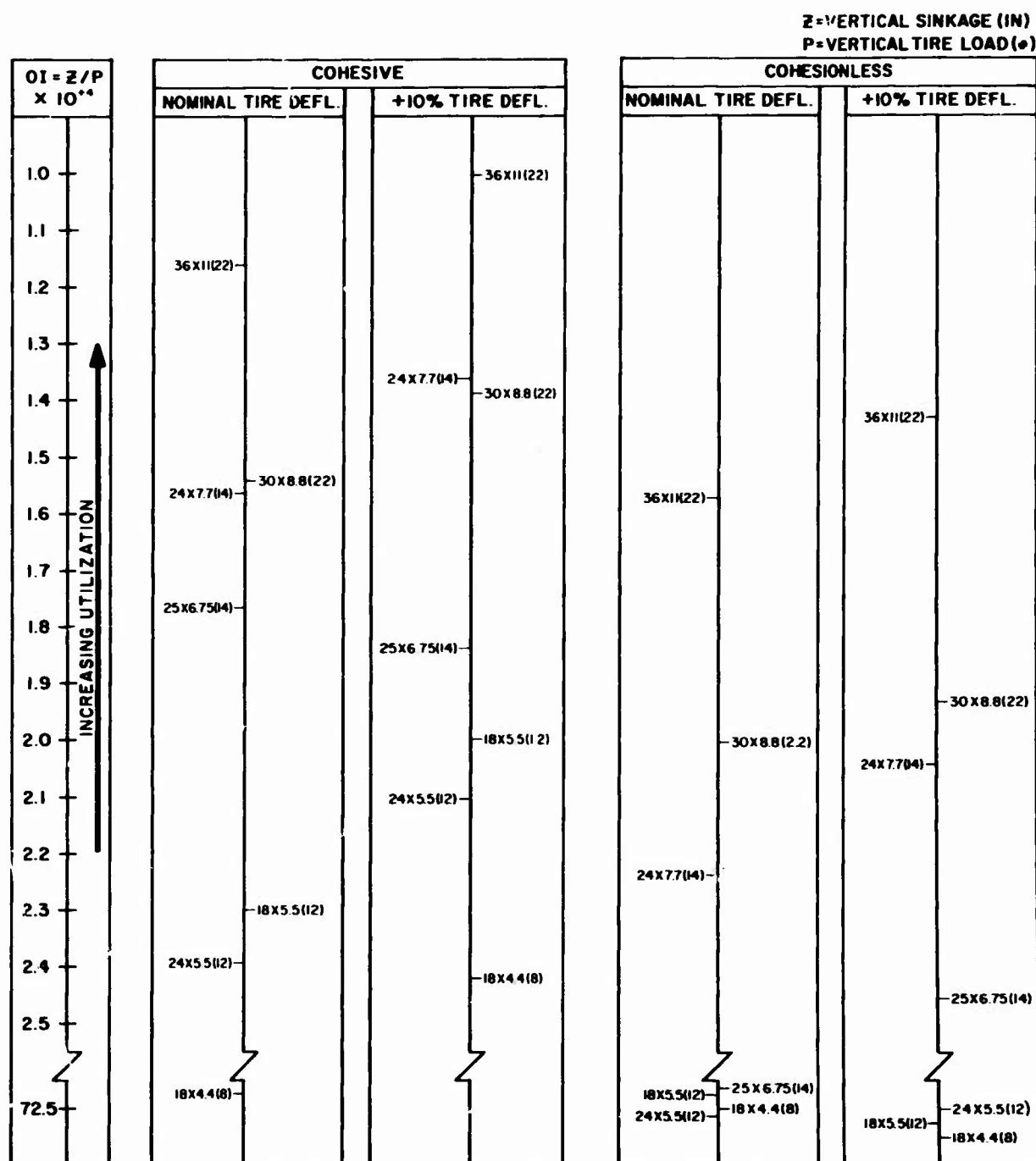


Figure 49 Operations Index, Aircraft Fighter Tires on Low Strength Soil

# SINGLE WHEEL OPERATION INDEX (OI) HIGH STRENGTH SOIL-CARGO TIRES

Z=VERTICAL SINKAGE (IN)  
P=VERTICAL TIRE LOAD (#)

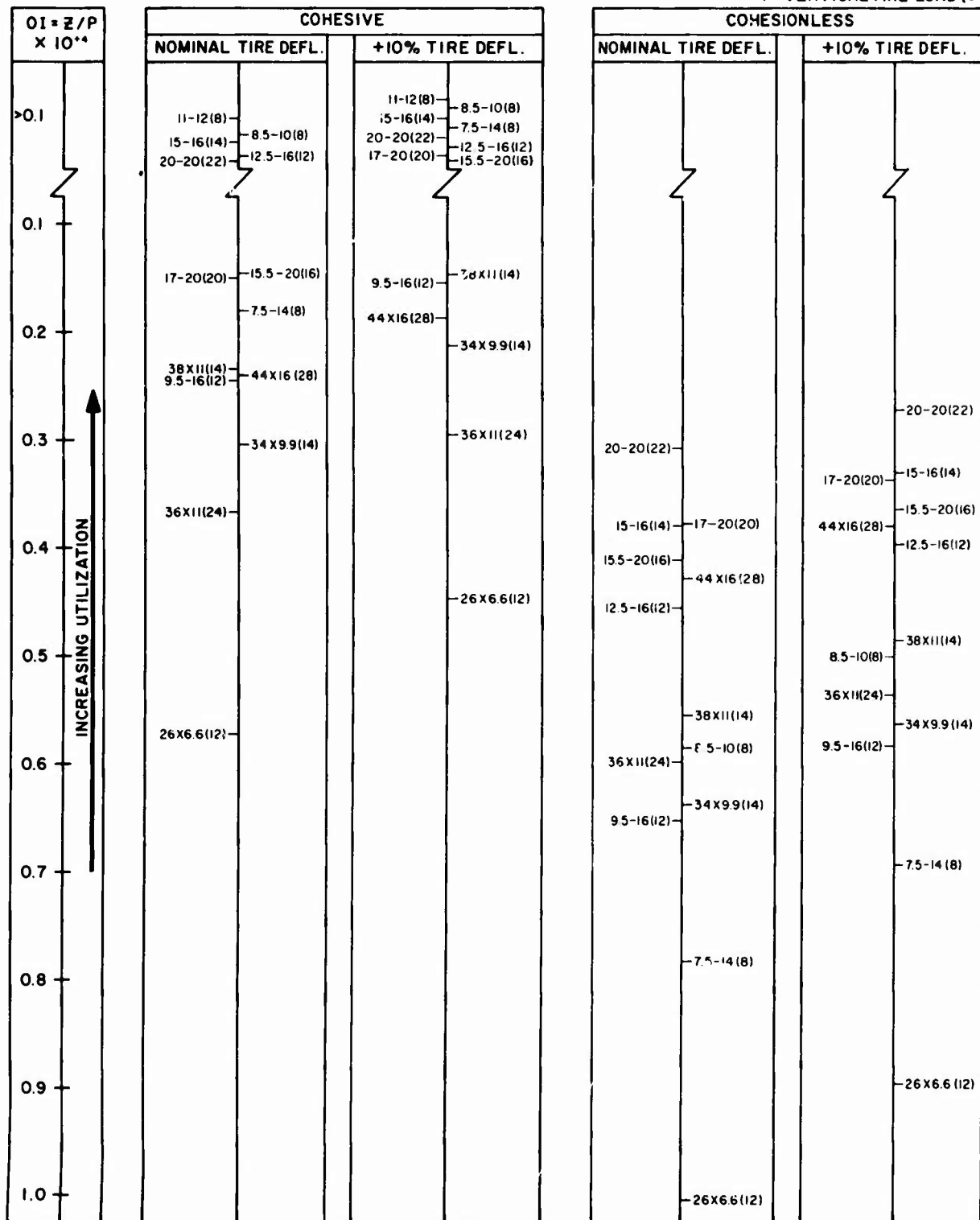


Figure 50 Operations Index, Aircraft Cargo Tires on High Strength Soil

**SINGLE WHEEL OPERATION INDEX (OI)  
HIGH STRENGTH SOIL-BOMBER TIRES**

Z=VERTICAL SINKAGE (IN)  
P=VERTICAL TIRE LOAD (#)

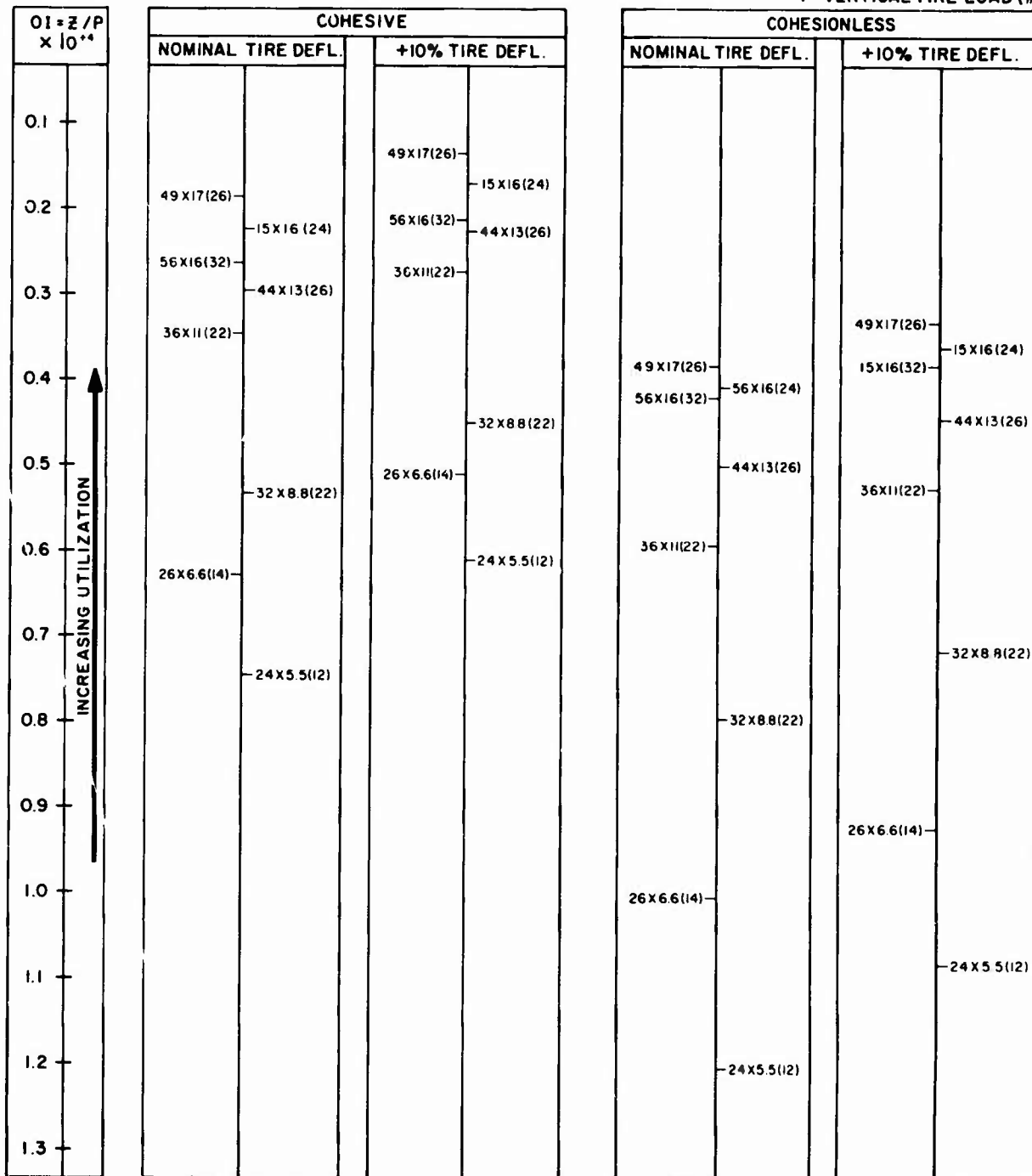


Figure 51 Operations Index, Aircraft Bomber Tires on High Strength Soil

SINGLE WHEEL OPERATION INDEX (OI)  
HIGH STRENGTH SOIL—FIGHTER TIRES

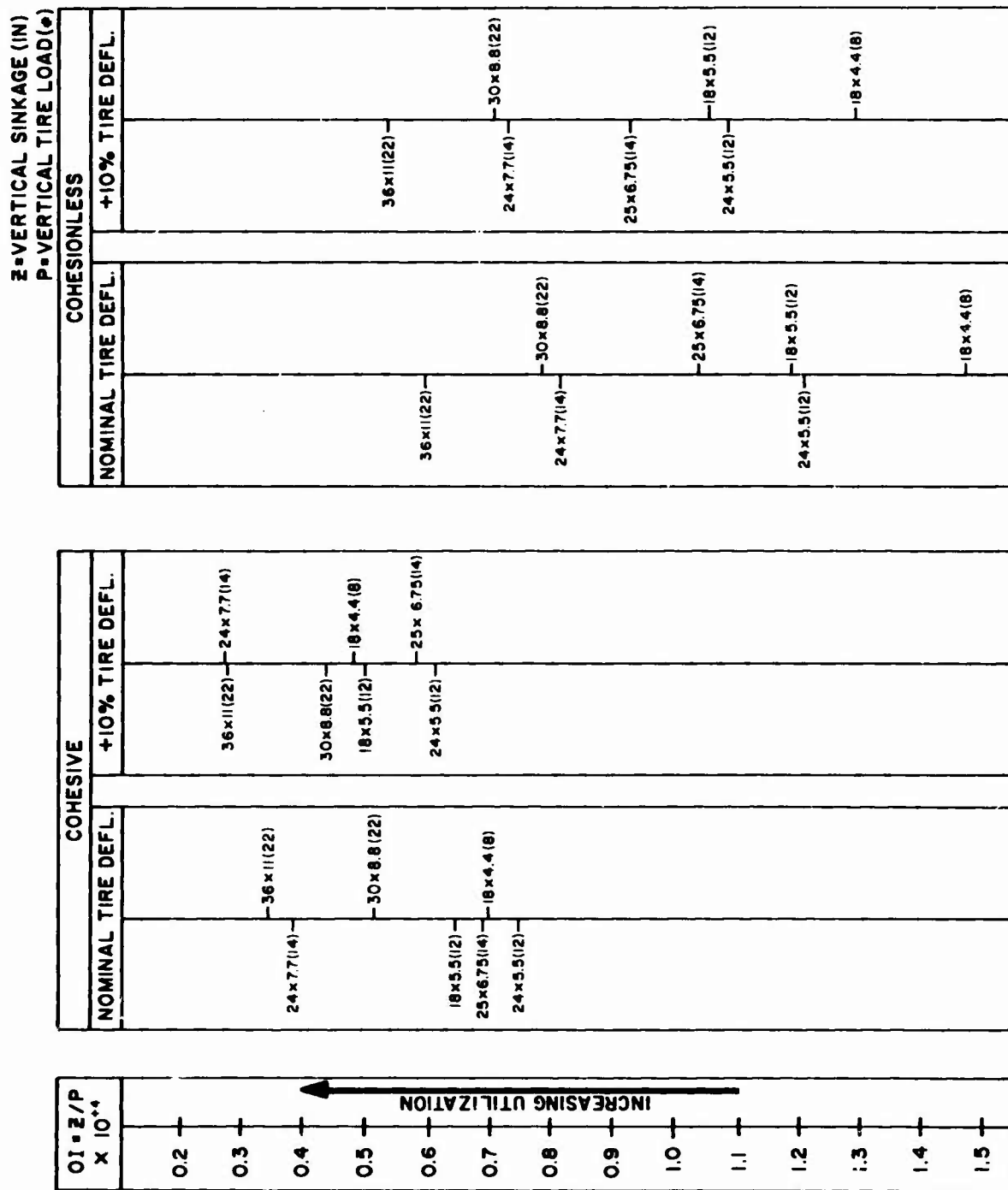


Figure 52 Operations Index, Aircraft Fighter Tires on High Strength Soil

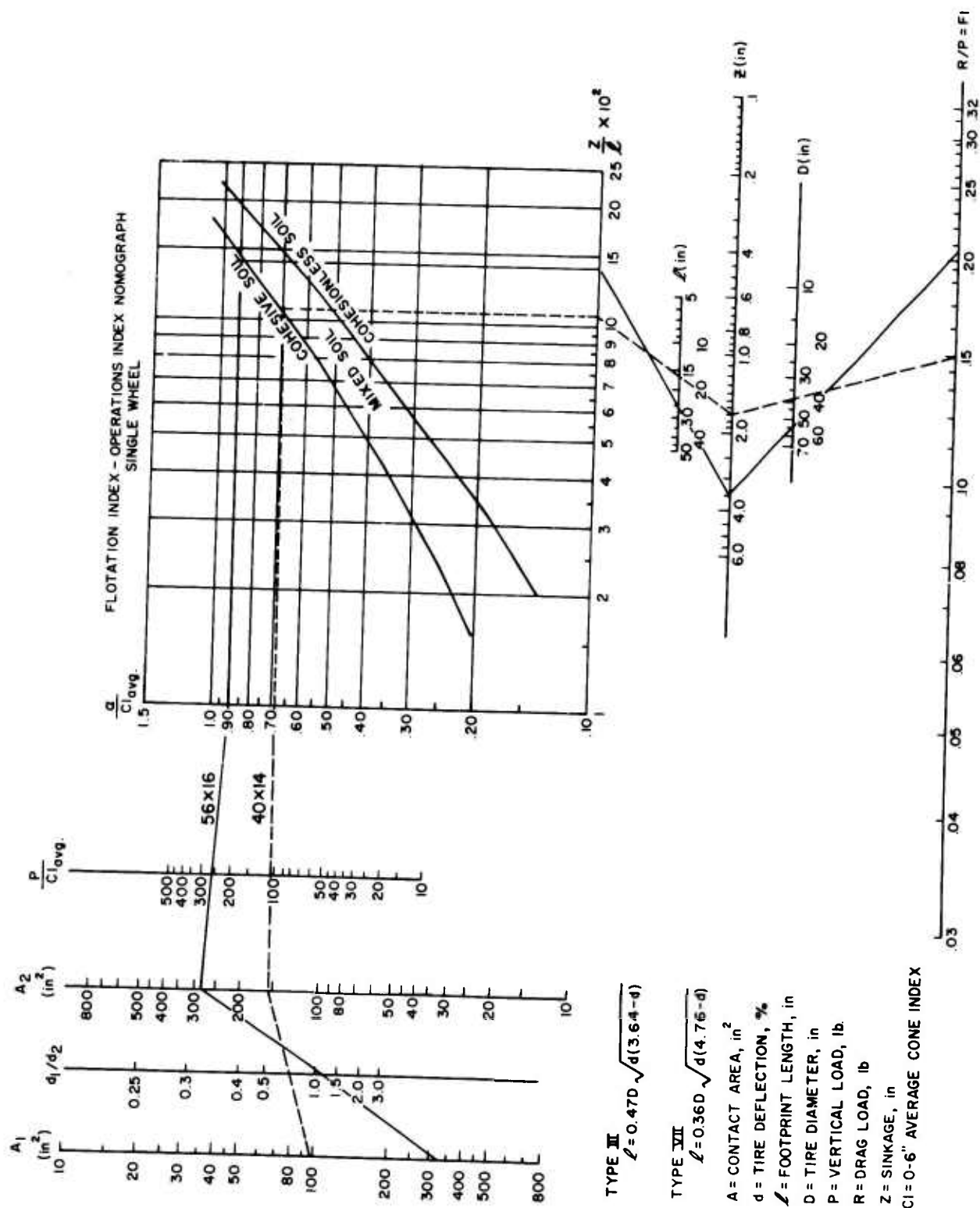


Figure 53 Flotation Index Nomograph

### Solution Nomograph

- 56 x 16 tire,  $D = 55.7''$

(1)  $d_1/d_2 = 40/32 = 1.25$

(2) Intersect  $340 \text{ in}^2 (A_1)$  with  $d_1/d_2 = 1.25$  which gives  
 $A_2 = 280 \text{ in}^2$

(3) Determine  $\frac{P}{CI_{\text{avg}}} = \frac{76,000}{300} = 253$

(4) Intersect  $280 \text{ in}^2 (A_2)$  with  $\frac{P}{CI_{\text{avg}}} = 253$

which gives  $\frac{\alpha}{CI_{\text{avg}}} = 0.90$

(5) Move horizontally to intersect the "cohesive" soil line  
and down vertically to get  $\frac{Z}{\ell} = 14.5 \times 10^{-2}$

(6) Compute  $\ell$  for Type VII by

$$\ell = 0.36D \sqrt{d(4.76-d)} = 0.36 \times 44.7 \sqrt{0.32(4.76-0.32)} = 23.8''$$

(7) Intersect  $\frac{Z}{\ell} = 14.5 \times 10^{-2}$  with  $\ell = 23.8''$  to get  $Z = 3.5''$ .

(8) Intersect  $Z = 3.5''$  with  $D = 55.7''$  which gives

$$FI_{56 \times 16} = R/P = 0.20$$

$$OI_{56 \times 16} = Z/F = \frac{3.5''}{76,000\#} = 4.6 \times 10^{-5}$$

- 40 x 14 tire,  $D = 39.3''$

(1)  $d_1/d_2 = 20/32 = 0.63$

(2) Intersect  $97 \text{ in}^2 (A_1)$  with  $d_1/d_2 = 0.63$  which gives  
 $A_2 = 155 \text{ in}^2$

(3) Determine  $\frac{P}{CI_{\text{avg}}} = \frac{30,500}{300} = 102$

(4) Intersect  $155 \text{ in}^2 (A_2)$  with  $\frac{P}{CI_{\text{avg}}} = 102$

which gives  $\frac{\alpha}{CI_{\text{avg}}} = 0.69$

(5) Move horizontally to intersect the "cohesive soil" line and down vertically to get  $\frac{Z}{\ell} = 10.5 \times 10^{-2}$

(6) Compute  $\ell$  for Type VII by

$$\ell = 0.36D\sqrt{d(4.76-d)} = 0.36 \times 39.3\sqrt{0.32(4.76-0.32)} = 16.9''$$

(7) Intersect  $\frac{Z}{\ell} = 10.5 \times 10^{-2}$  with  $\ell = 16.9''$  to get  $Z = 1.7''$

(8) Intersect  $Z = 1.7''$  with  $D = 39.3''$  which gives

$$FI_{40 \times 14} = R/P = 0.15$$

$$OI_{40 \times 14} = Z/P = \frac{1.7''}{30,500\#} = 5.6 \times 10^{-6}$$

These results indicate that the 40 x 14 tire which would encounter 25% less drag per unit vertical load than the 56 x 16 tire has a higher flotation capacity. The 56 x 16 tire would, however, cause less runway deterioration per unit vertical load than the 40 x 14 tire as shown by the OI ratings.

### 3. Summary

The results of aircraft tire-soil interaction studies have led to the development of the Single Wheel-RMI which is a system for evaluating the relative flotation capacity of aircraft tires when operating on soil runways. The RMI has been presented in both Nomographic and Rating Chart forms. The potential uses of such charts by landing gear engineers include:

- a. Design of landing systems and contact element systems for reduced sinkage and/or drag.
- b. Comparative tire flotation studies.
- c. Comparison of the performance of aircraft tires on different soil types.
- d. Determination of increased flotation with increasing tire deflection.

The preliminary single wheel criteria and index system developed to date does not include the effects of multiple tires (twin and tandem) and braking. Additionally, the influence of ground roughness and multiple passes will ultimately be included such that the RMI system can be utilized not only for comparative flotation evaluation but also as an absolute determination of the suitability of a site for aircraft operations. As current research effort provides the required information for evaluating each of these effects, the RMI will be modified to reflect these changes.



## SECTION VI

### CONCLUSIONS AND RECOMMENDATIONS FOR RESEARCH

#### 1. Conclusions

The results of the landing gear-soil interaction and flotation criteria research effort have shown that:

(1) There are at least three velocity regions for which the drag ratio exhibits distinct characteristics.

(2) In the Region II velocity range (5 knots to 40 knots), the basic tire-soil interaction as defined by the drag ratio ( $R/P$ ) and sinkage ratio ( $Z/D$ ) is given by Equation 2 for all soils although there are some differences in the performance of aircraft tires on sand and clay as shown by Equations 3 and 4.

(3) In the Region III velocity range (40 knots to approximately 70 to 90 knots), the relationship between drag ratio ( $R/P$ ) and sinkage ratio ( $Z/D$ ) has not been adequately defined; however, either Equation 5 or 6 can be used on a preliminary basis.

(4) Although considerable work remains to be done on defining multiple tire flotation performance, preliminary results indicate (a) that little reduction in the drag ratio ( $R/P$ ) per tire will occur for twin wheel configurations, and (b) that considerable reduction in drag ratio ( $R/P$ ) per tire can be expected for tandem wheel configurations where the rear tire follows in the track of the lead tire.

(5) The empirical sinkage prediction equation developed in this report can be used for estimating aircraft tire sinkages in sand and clay type soils with an approximate accuracy of  $\pm 40\%$  within the 90% confidence limits.

(6) The finite element based sinkage prediction analysis described in Section IV shows promise of providing a rational (rather than empirical) method of sinkage prediction which could ultimately provide a better insight into the tire-soil interaction phenomena and lead to more accurate sinkage analysis.

The basic tire-soil interaction equation (Equation 2), together with the sinkage prediction equations (Equations 13 through 16) were used to develop the Single Wheel Relative Merit Index (RMI) which is currently under review by cognizant government agencies. This is the first step leading to the RMI of landing gear systems.

## 2. Recommendations for Research

The main thrust of the immediate future landing gear-soil interaction and flotation criteria research effort should be directed at the following research deficient areas.

- (1) High speed (Region III) tire-soil interaction including drag and sinkage.
- (2) Multiple tire "configuration sensitivity" related to drag and flotation criteria.
- (3) Flotation evaluation of the influence of braking, turning, and impact on aircraft performance on soil.
- (4) Additional evaluation of the failure criteria for defining the capability of aircraft to operate on soil runways.

Long range flotation research effort should include studies of:

- (1) Multiple pass (operation) effects as related to runway deterioration and capability of aircraft to operate.
- (2) Influence of runway roughness on the flotation performance of aircraft on soil.

## REFERENCES

1. Kraft, David C., Analytical Landing Gear-Soils Interaction, Phase I, AFFDL-TR-68-88, Air Force Flight Dynamics Laboratory, Wright-Patterson AFB, Ohio, August 1968.
2. Kraft, David C. and Luming, Henry, Analytical Landing Gear-Soils Interaction, Phase II, Interim Report, University of Dayton Research Institute, Dayton, Ohio, January 1969.
3. Richmond, L.D., DeBord, K.G., and Fuller, J.R., Aircraft Dynamic Loads from Substandard Landing Sites, Phase I, Interim Technical Report D6-16190, The Boeing Company, Renton, Washington, November 1965.
4. Crenshaw, B.M., Lockheed Georgia Co., Marietta, Georgia, test data furnished to David C. Kraft, University of Dayton, May 1969, Subject: Aircraft Landing Gear Dynamic Loads from Operation on Clay and Sandy Soil.
5. Frietag, Dean R., Wheels on Soft Soils, an Analysis of Existing Data, Technical Report No. 3-670, U. S. Army Engineer Waterways Experiment Station, CE, Vicksburg, Miss., January 1965.
6. Nutall, C. J., Jr., A Dimensionless Consolidation of WES Data on the Performance of Sand Under Tire Loads, Technical Report No. 3-130, U. S. Army Engineer Waterways Experiment Station, CE, Vicksburg, Miss., December 1965.
7. Bekker, M.G. and Janosi, Z., Analysis of Towed Pneumatic Tires Moving on Soft Ground, Report No. RR-6, LL-62, U. S. Army Land Locomotion Laboratory, Detroit, Mich., March 1960.
8. Ladd, D. and Ulery, H., Jr., et al, Aircraft Ground Flotation Investigation, Parts II to XIX, AFFDL-TDR-66-43, Air Force Flight Dynamics Laboratory, Wright-Patterson AFB, Ohio, August 1967.
9. McCrae, J.L., Powell, C.G., and Wismer, R.D., Performance of Soils Under Tire Loads, Technical Report No. 3-666, U. S. Army Engineer Waterways Experiment Station, CE, Vicksburg, Miss., January 1965.
10. Smith, M.E. and Frietag, D.R., Deflection of Moving Tires, Technical Report No. 3-516, U. S. Army Engineer Waterways Experiment Station, CE, Vicksburg, Miss., January 1965.

11. Bekker, M. G., A Definition of Soil Trafficability, Report No. 41, Land Locomotion Laboratory, Detroit, Mich., June 1958.
12. Assur, A., "Locomotion Over Soft Soil and Snow" Paper No. 782F, Automotive Engineering Congress, SAE, Detroit, Mich., January 1964.
13. Liston, Ronald A., et al, State of the Art Report on Off-the-Road Mobility Research, Research Report No. 6, U. S. Army Land Locomotion Laboratory, Detroit, Mich., November 1966.
14. Frietag, D. R., Green, A. J., and Murphy, J. R., Jr., Normal Stresses at the Tire-Soil Interface in Yielding Soils, Highway Research Record No. 74, 1964.
15. Wismer, R. D., Performance of Soils Under Tire Loads, Technical Report No. 3-666, Report 3, U. S. Army Engineer Waterways Experiment Station, CE, Vicksburg, Miss., February 1966.
16. Aircraft Operations on Unsurfaced Soil, Soil Measurements and Analysis -- Project Rough Road Alpha, TR No. 3-624, U. S. Army Engineer Waterways Experiment Station, CE, Vicksburg, Miss., June 1963.
17. Powell, C. J. and Green, A. J., Performance of Soils Under Tire Loads, Report No. 3-666, Report 2, U. S. Army Engineer Waterways Experiment Station, CE, Vicksburg, Miss., August 1965.
18. Thompson, A. B. and Smith, M. E., Stresses Under Moving Vehicles; Wheeled Vehicles, U. S. Army Engineer Waterways Experimentation, Technical Report No. 3-545, 1960.
19. Christian, J. T., Two-Dimensional Analysis of Stress and Strain in Soils, Report No. 3, "Plane-Strain Deformation Analysis of Soil," Reports to DASA, Contract DA-22-079-eng-471, MIT, December 1966.
20. Vallabhan, C. V. G. and Reese, L. C., Finite Element Method Applied to Problems in Stresses and Deformation of Soil, NASA-Cr-66318, 1967.
21. Takagi, S., "Plane Plastic Deformation of Soils," Journal of Engineering Mechanics Division, ASCE, Vol. 88, No. EM3, 1962.
22. Drucker, D. C. and Prager, W., "Soil Mechanics and Plastic Analysis of Limit Design," Quarterly Applied Mathematics, Vol. 10, No. 2, 1952.

23. Rao, H.A.B. and Höeg, K., Two-Dimensional Analysis of Stress and Strain in Soils, Report No. 4, "Dynamic Response of Strip Footing on Elastic-Plastic Soil," Reports to DASA, Contract DA-22-079-eng-471, MIT, November 1967.
24. Jones, R.E., "A Generalization of the Direct Stiffness Method of Structural Analysis," American Institute of Aeronautics and Astronautics Journal, Vol. 2, 1964.
25. Ang, A.H.S. and Rainer, J.H., "Model for Wave Motions in Axisymmetric Solids," Journal of Engineering Mechanics Division, ASCE, Vol. 90, EM2, 1964.
26. Ang, A.H.S., "Numerical Approach for Wave Motions in Nonlinear Solid Media," Matrix Methods in Structural Mechanics, AFFDL-TR-66-80, 1965.
27. Chang, G.C. and Fair, G.S., "Finite Element Approach to Wave Motions in Elastic-Plastic Continua," AIAA Paper No. 68-145, 1968.
28. Newmark, N.M., "Methods of Computation for Structural Dynamics," Proc. ASCE, Vol. 85, 1959.
29. Sameh, A.H.M., and Ang, A.H.S., Numerical Analysis of Axisymmetric Wave Propagation in Elastic-Plastic Layered Media, Civil Engineering Studies, Structural Research Series No. 335, University of Illinois, May 1968.
30. Kraft, David C., Preliminary Single Wheel Relative Merit Index, UDRI-TR-69-16, University of Dayton Research Institute, Dayton, Ohio, May 1969.

APPENDIX I  
SINGLE WHEEL VERIFICATION TESTS

Soil Tests and Preparation

### Classification

Both of the soils selected for the test program have been used extensively by WES in previous mobility studies and the classification properties have been reported previously. For comparison purposes the grain size distribution and limits properties are given for the buckshot clay in Figure 54, and the grain size distribution for the mortar sand is shown in Figure 55.

### California Bearing Ratio

The CBR is a plate bearing test using a three-square inch piston which is penetrated continuously into the soil to a depth of one-half inch while continuously recording the load resistance with depth. Annular surcharge weights are placed around the piston prior to its penetration. The ratio of the load at 0.1 inch penetration to that load supported by a standard well graded crushed gravel multiplied by 100 is defined as the CBR of the soil.

### Cone Penetrometer Resistance

The mobility cone penetrometer is a rod device having a thirty degree cone tip and has a cross section base area of 0.5 square inch. The shaft is narrowed above the cone to minimize the friction between the side of the shaft and the hole. The cone penetrometer, which is pushed into the soil at a standard rate, measures the resistance to penetration (Cone Index) in pounds per square inch. The Cone Index is a measure of soil shear strength and its variation with depth.

### Plate Bearing Resistance

Plate bearing tests were conducted on the soil surface using three plate sizes with diameters of 1.4 inches, 2.8 inches, and 4.2 inches. The load in pounds versus plate sinkage in inches was recorded continuously with depth to a penetration depth of approximately ten inches. The results of these tests were used to determine the modulus parameters  $k_c$ ,  $k_\phi$ , and  $n$  in Bekker's sinkage equation using techniques previously detailed (11).

### Triaxial Tests

Undrained triaxial tests were run on undisturbed clay specimens taken from the test soil carts for the soil conditions of  $CI=25$  and  $CI=50$ . The triaxial specimens with zero confining pressure were approximately 1.5 inches in diameter by 3.25 inches high, while the non-zero confining pressure specimens were approximately 2.8 inches in diameter by 5.5 inches high. Each test specimen was cut and trimmed from a larger test sample. It was observed

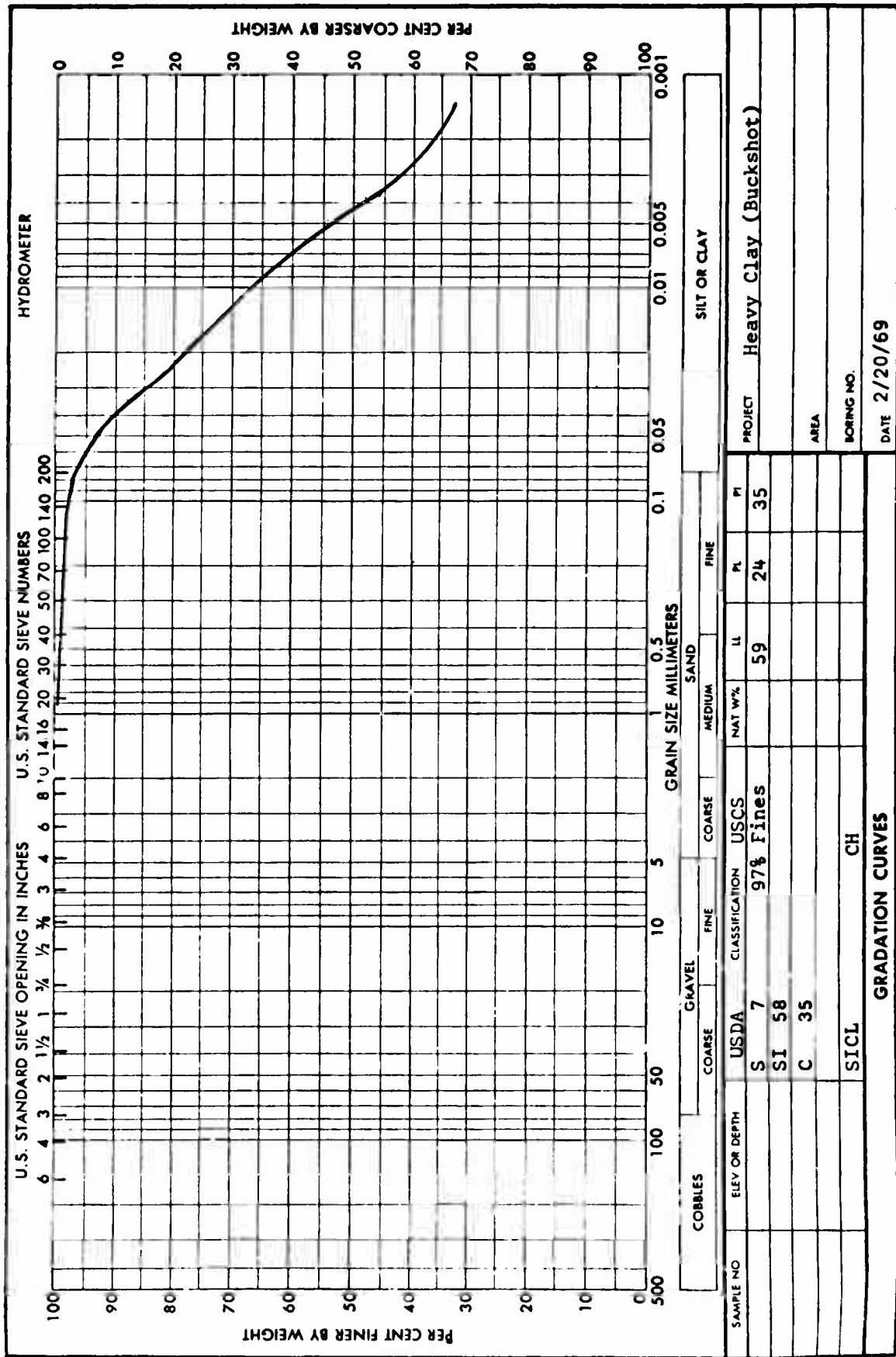
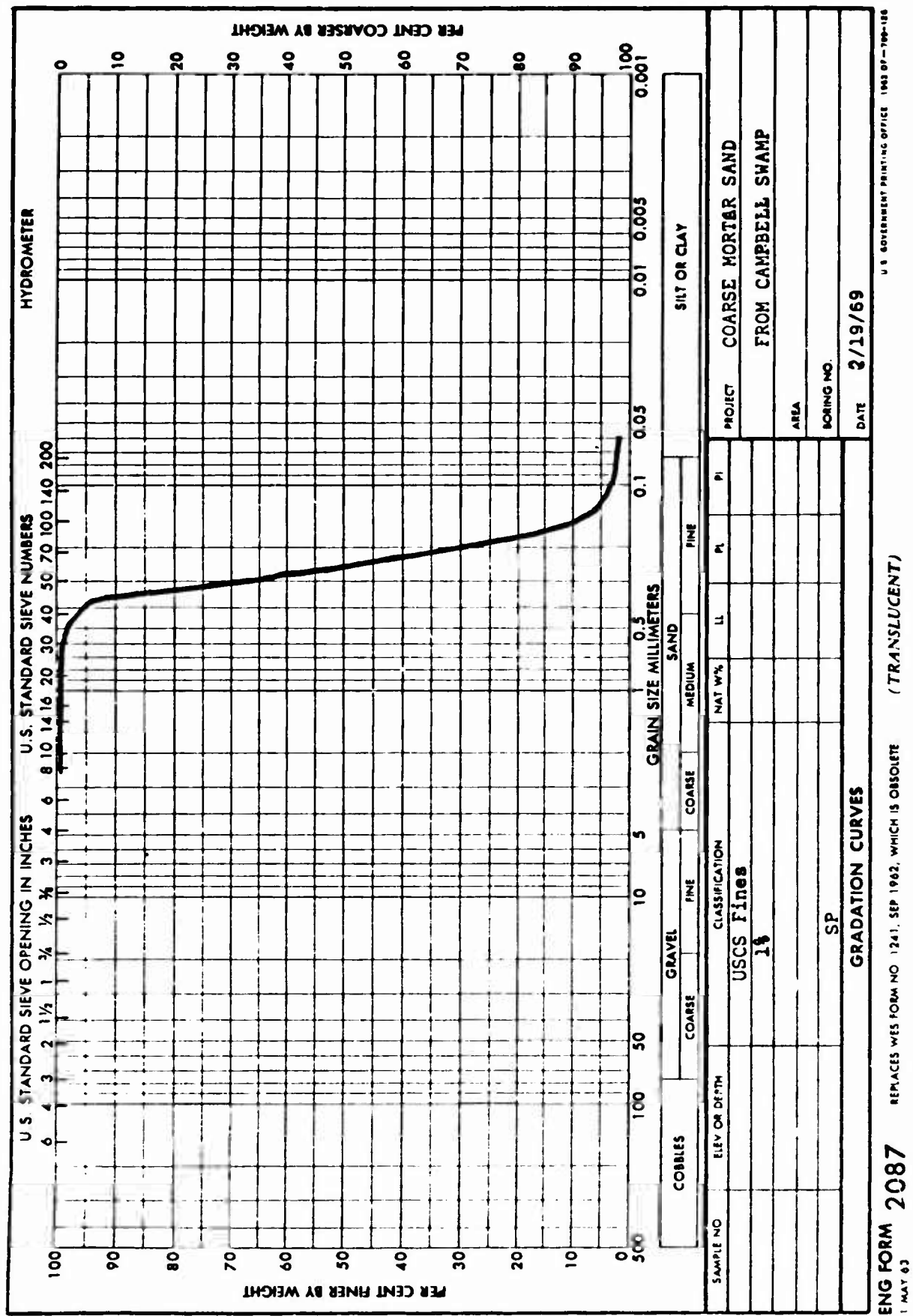


Figure 54 Grain Size Distribution, Buckshot Clay





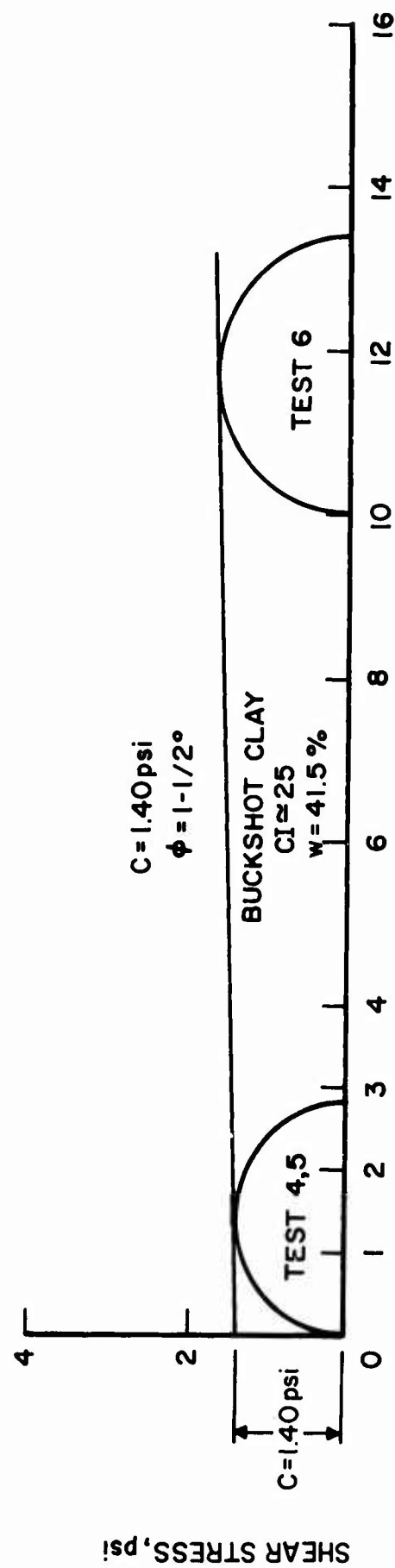
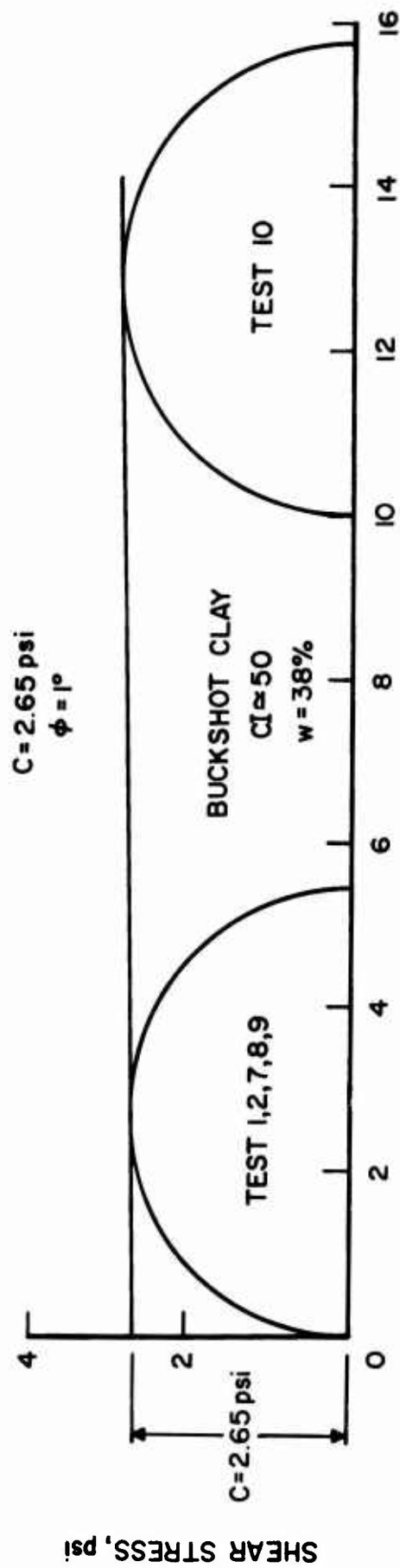
that the undisturbed samples did show some disturbance as evidenced by cracks on the outside of the soil sample. The results of the triaxial tests on clay as shown by the Mohr's circle relationship are given in Figure 56.

Triaxial tests were also conducted on air dried samples of the mortar sand. The specimen size was 2.8 inches in diameter by 6.0 inches high and the samples were prepared to a unit weight of  $99.0 \text{ pcf} \pm 1.0 \text{ pcf}$  which was the average soil unit weight in the soil carts for the CI=25 test condition. The results of the triaxial tests on the sand are shown in Figure 57.

#### Soil Preparation

The buckshot clay was processed, placed, and compacted at predetermined moistures and densities corresponding to the desired soil strength. The soil is first passed through a roller crusher and then placed in a pug mill where the soil-water mixing takes place at a selected moisture content. The soil is then placed in the soil carts in 6 inch layers with each layer compacted by pneumatic tired rollers. Previously developed empirical relationships between buckshot clay moisture content and compactive effort permitted the soil to be placed near the design soil conditions.

The mortar sand was prepared in an air dried condition. Different soil strengths were achieved by varying the density of placement of the soil. The sand was placed in uniform layers which were screened and vibrated on the surface as the filling progressed. Empirical relationships between the thickness of layer, vibratory effect, and soil density permitted the sand to be placed near the design soil conditions.



NORMAL STRESS, psi

Figure 56 Triaxial Test Results, Buckshot Clay

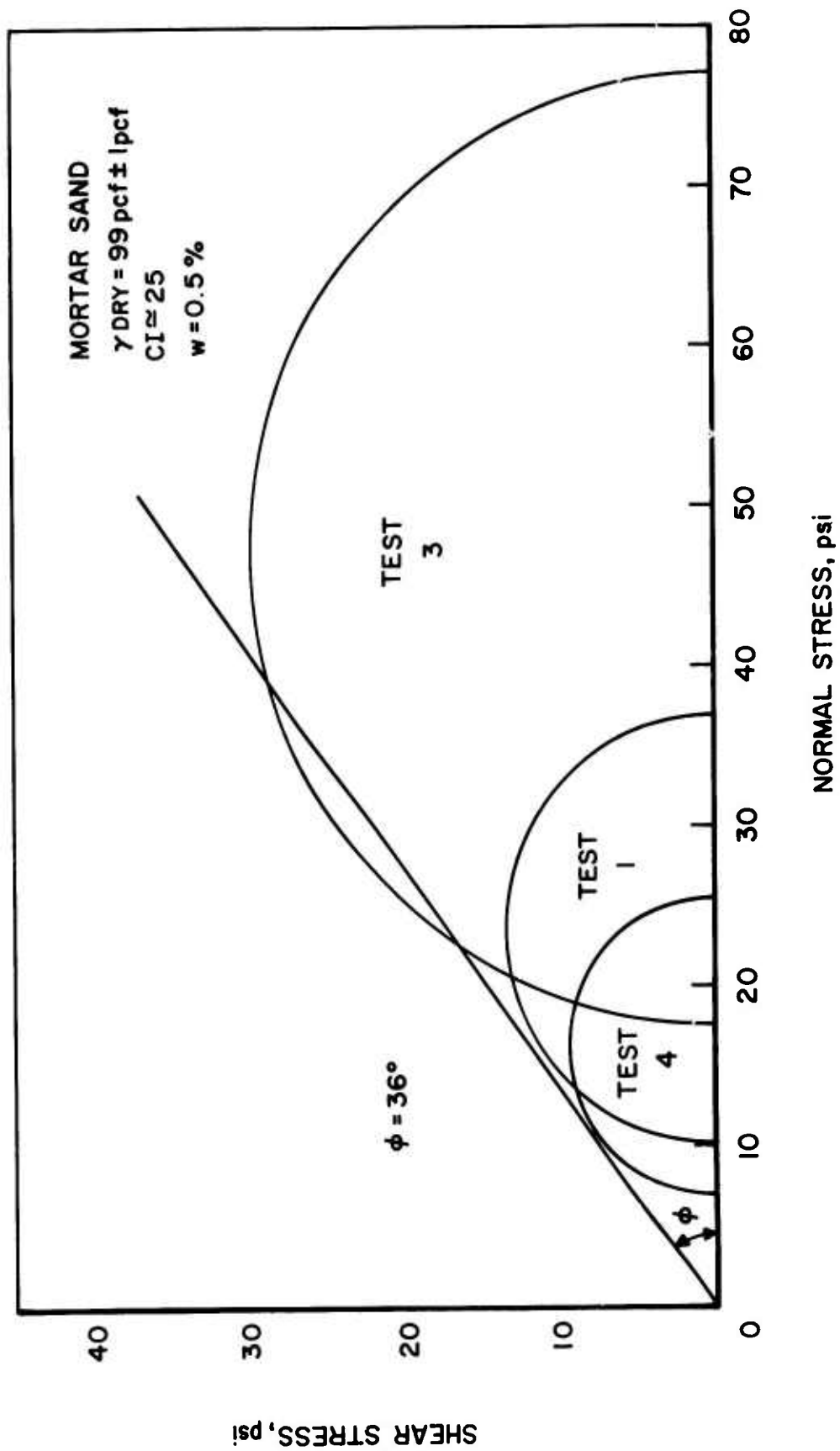


Figure 57 Triaxial Test Results, Mortar Sand

APPENDIX II

SINGLE WHEEL VERIFICATION TESTS

Soil Uniformity Measurements

Mobility cone penetration tests were conducted at two meter intervals along the soil track previous to each test run. The results of these measurements are given in Figures 58 through 70, and are identified by the Test Number which also appears in Tables 6 and 7.

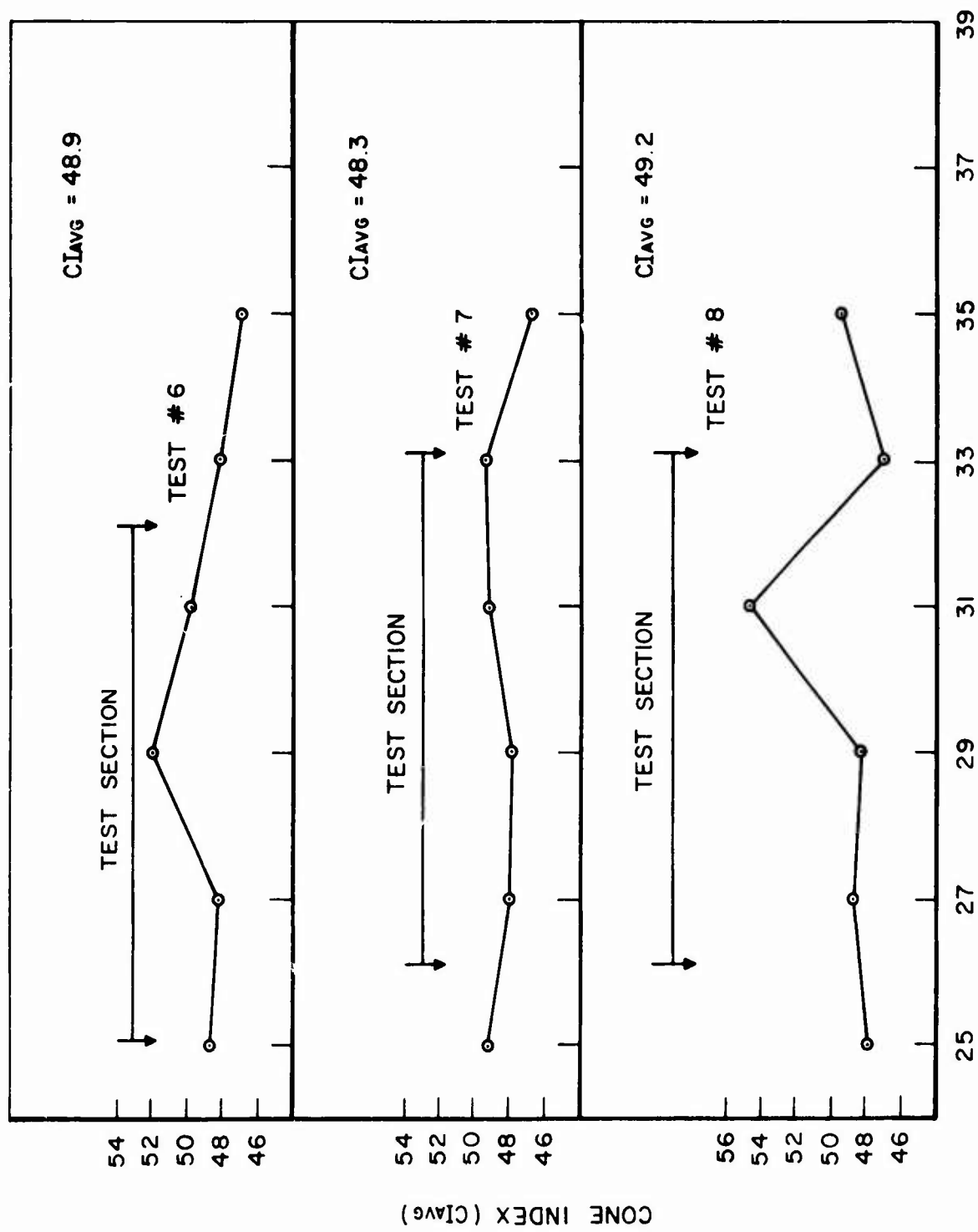


Figure 58 Soil Uniformity Measurements, Buckshot Clay, Tests 6, 7, and 8

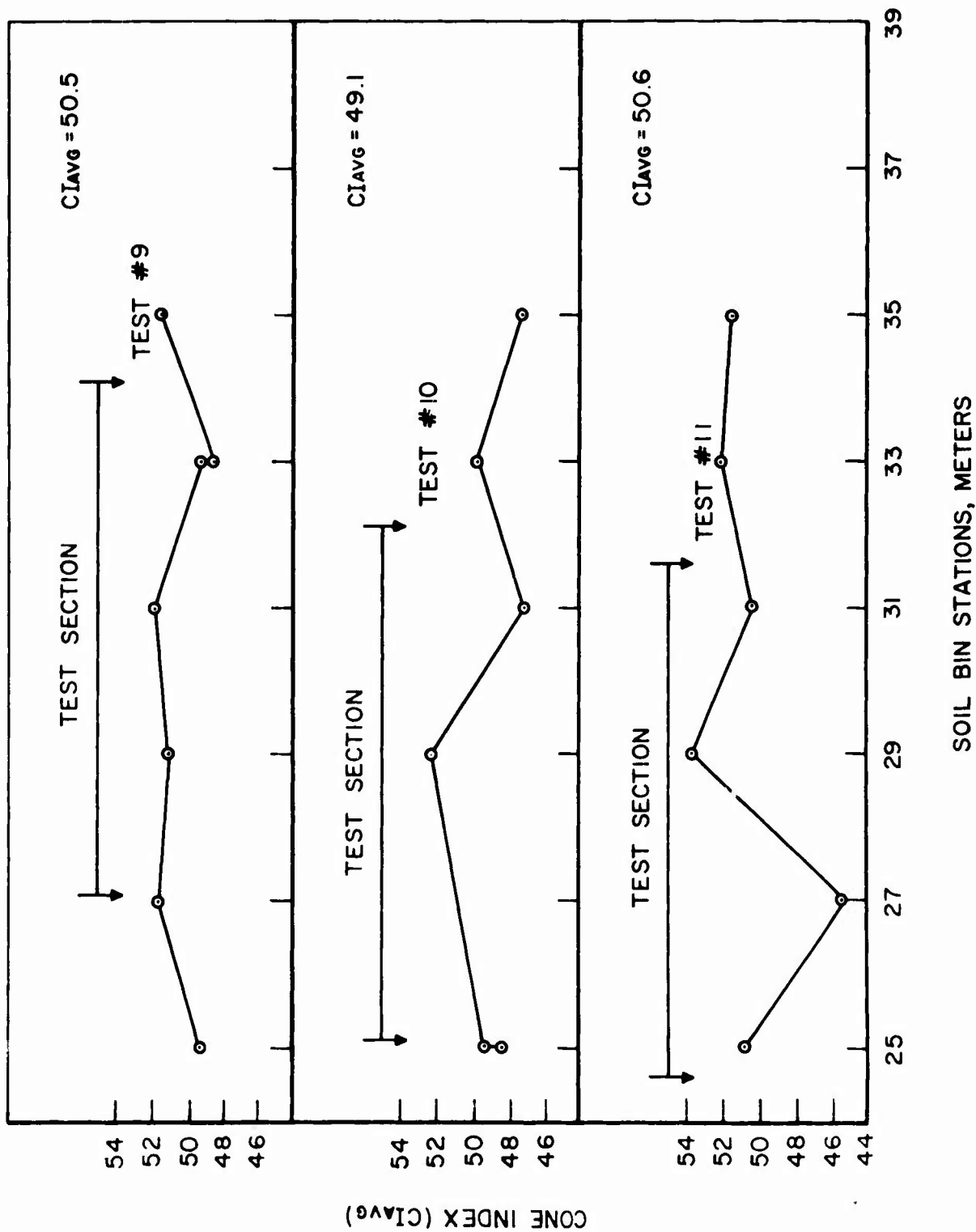
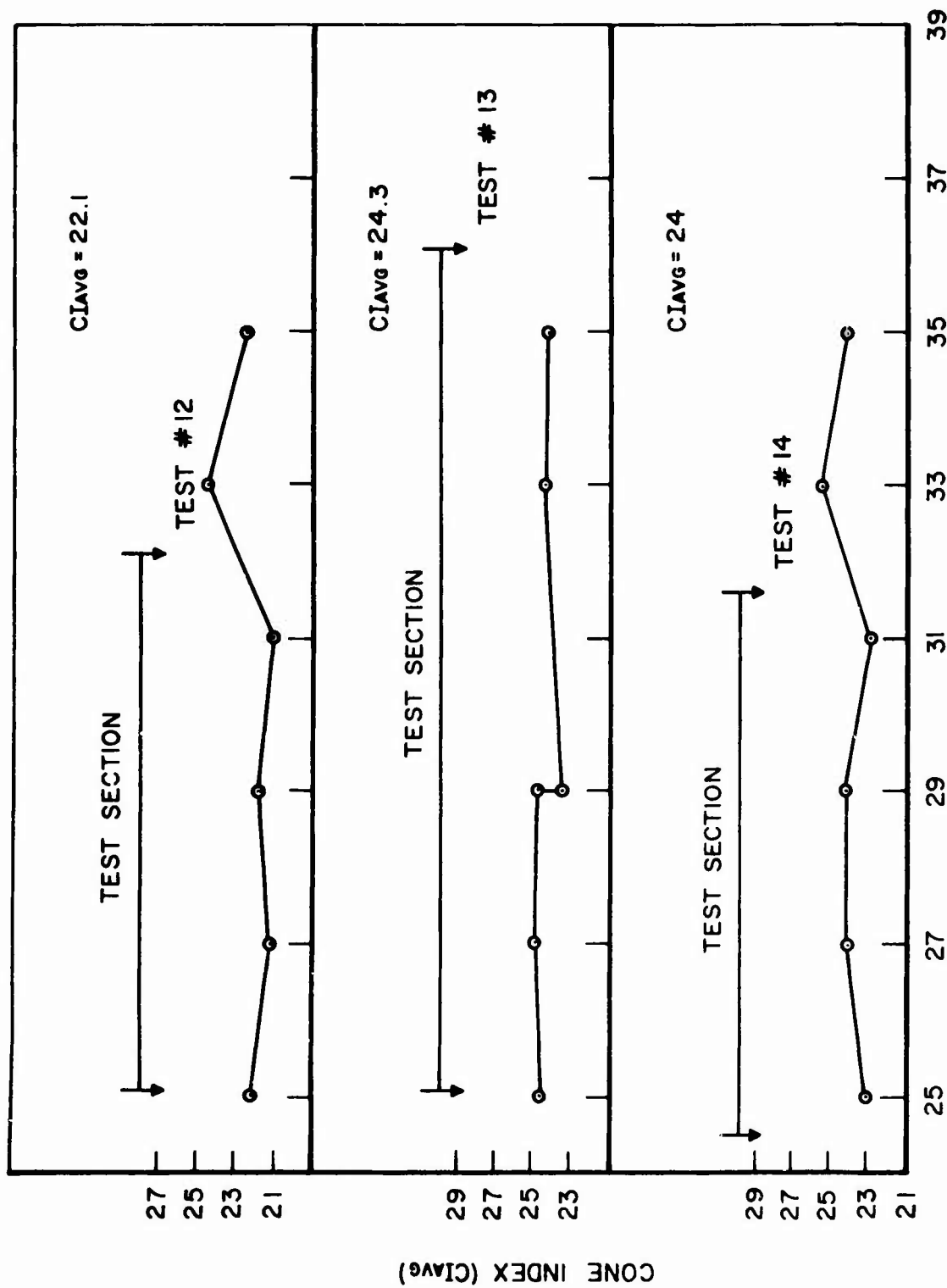


Figure 59 Soil Uniformity Measurements, Buckshot Clay, Tests 9, 10, and 11



### SOIL BIN STATIONS, METERS

Figure 60 Soil Uniformity Measurements, Buckshot Clay, Tests 12, 13, and 14



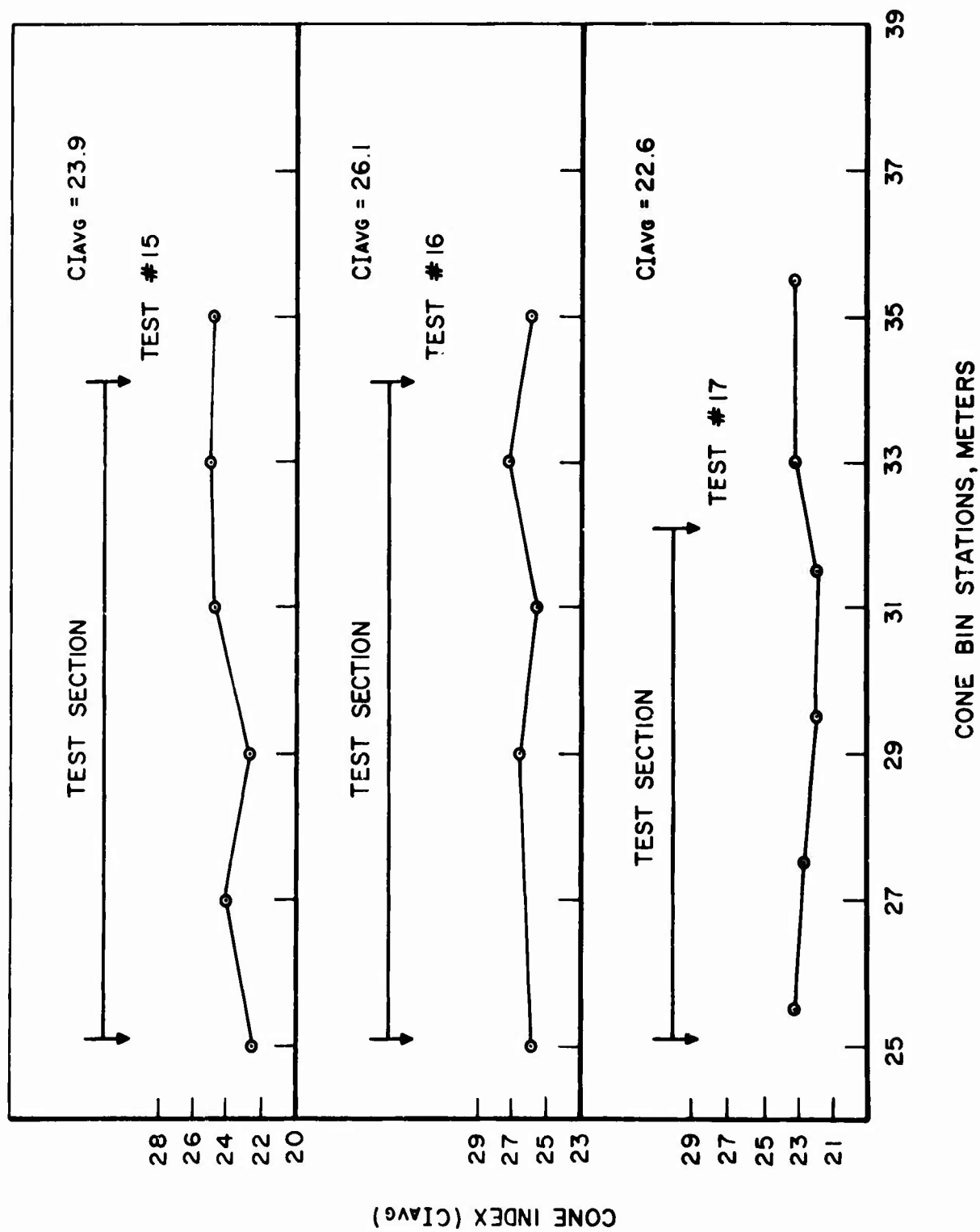


Figure 61 Soil Uniformity Measurements, Buckshot Clay, Tests 15, 16, and 17

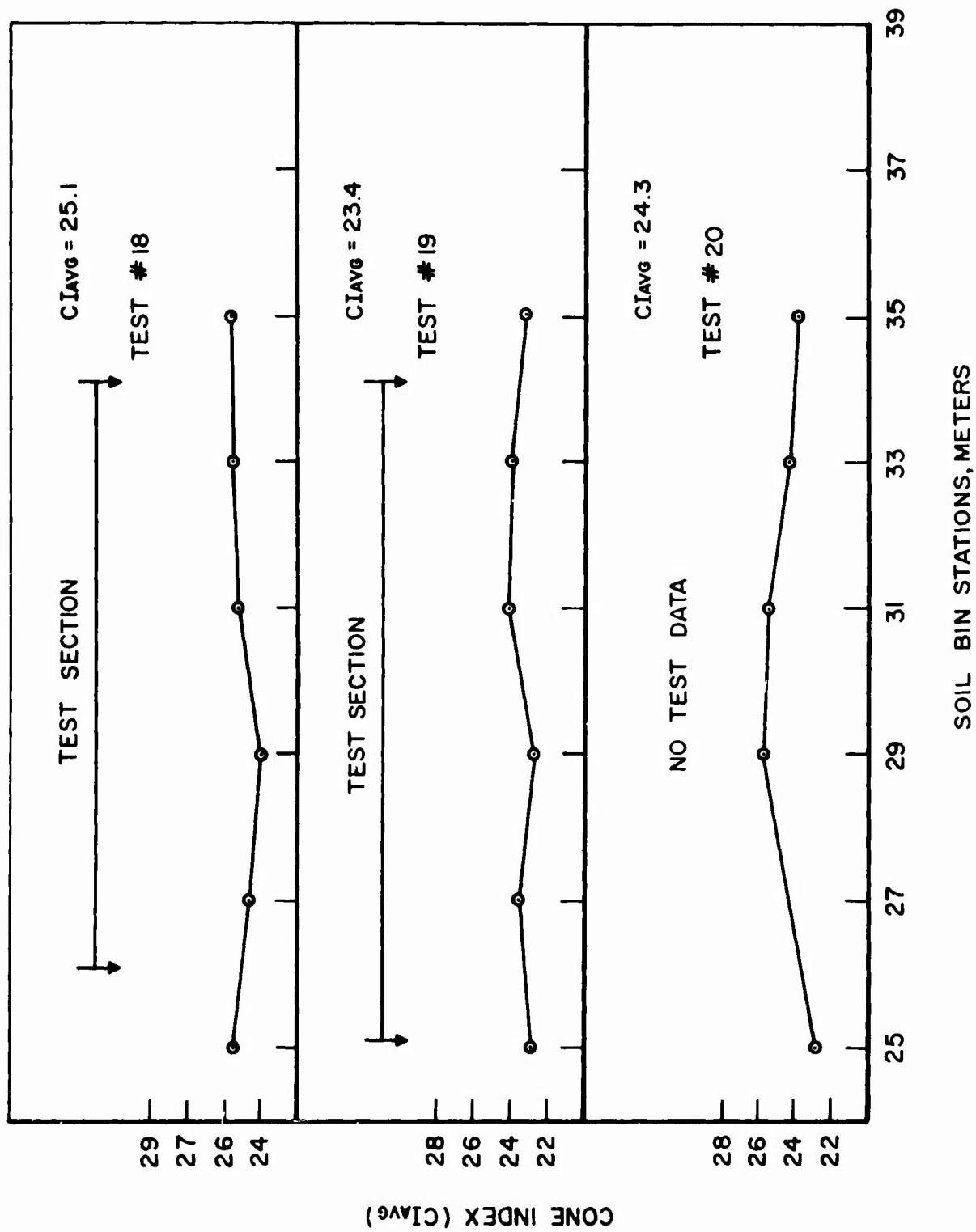


Figure 62 Soil Uniformity Measurements, Buckshot Clay, Tests 18, 19, and 20

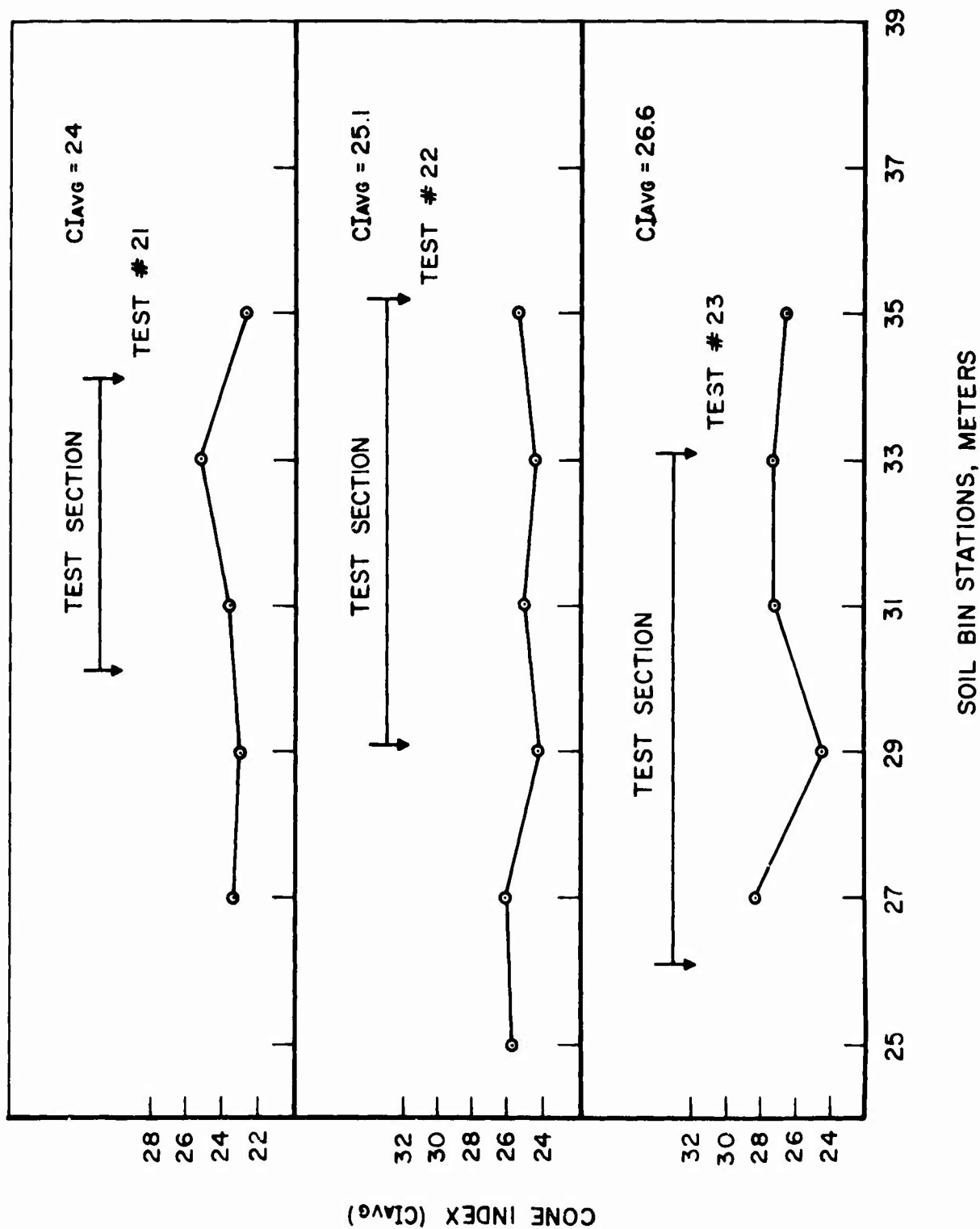


Figure 63 Soil Uniformity Measurements, Buckshot Clay, Tests 21, 22, and 23

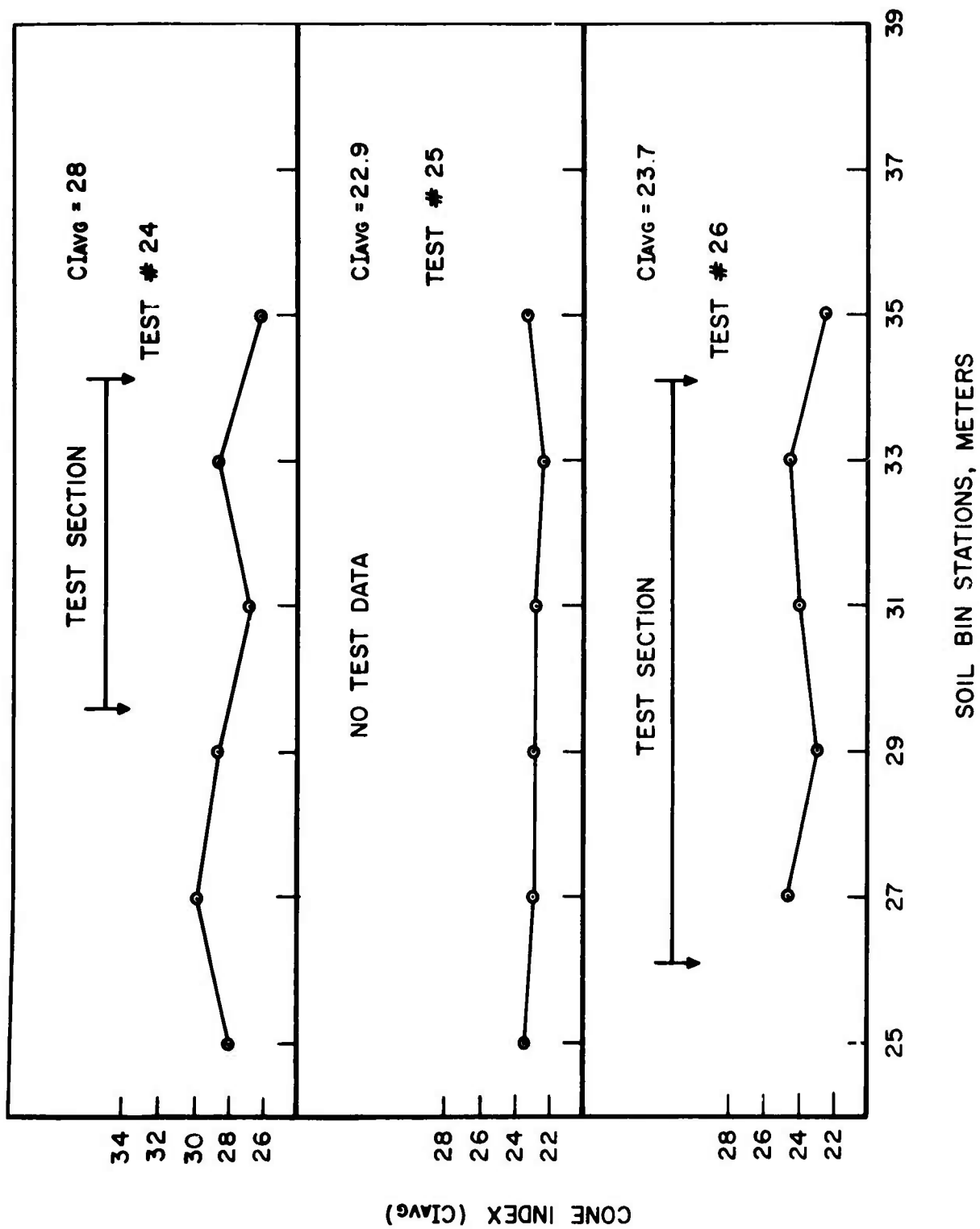


Figure 64 Soil Uniformity Measurements, Buckshot Clay, Tests 24, 25, and 26

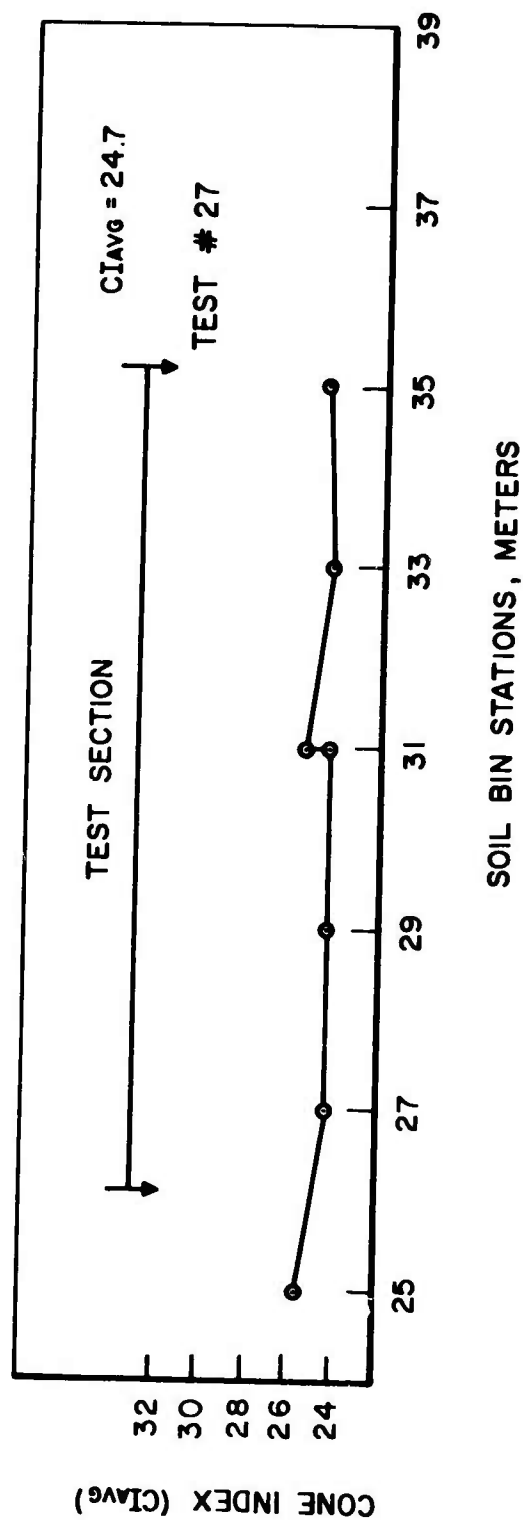


Figure 65 Soil Uniformity Measurements, Buckshot Clay, Test 27

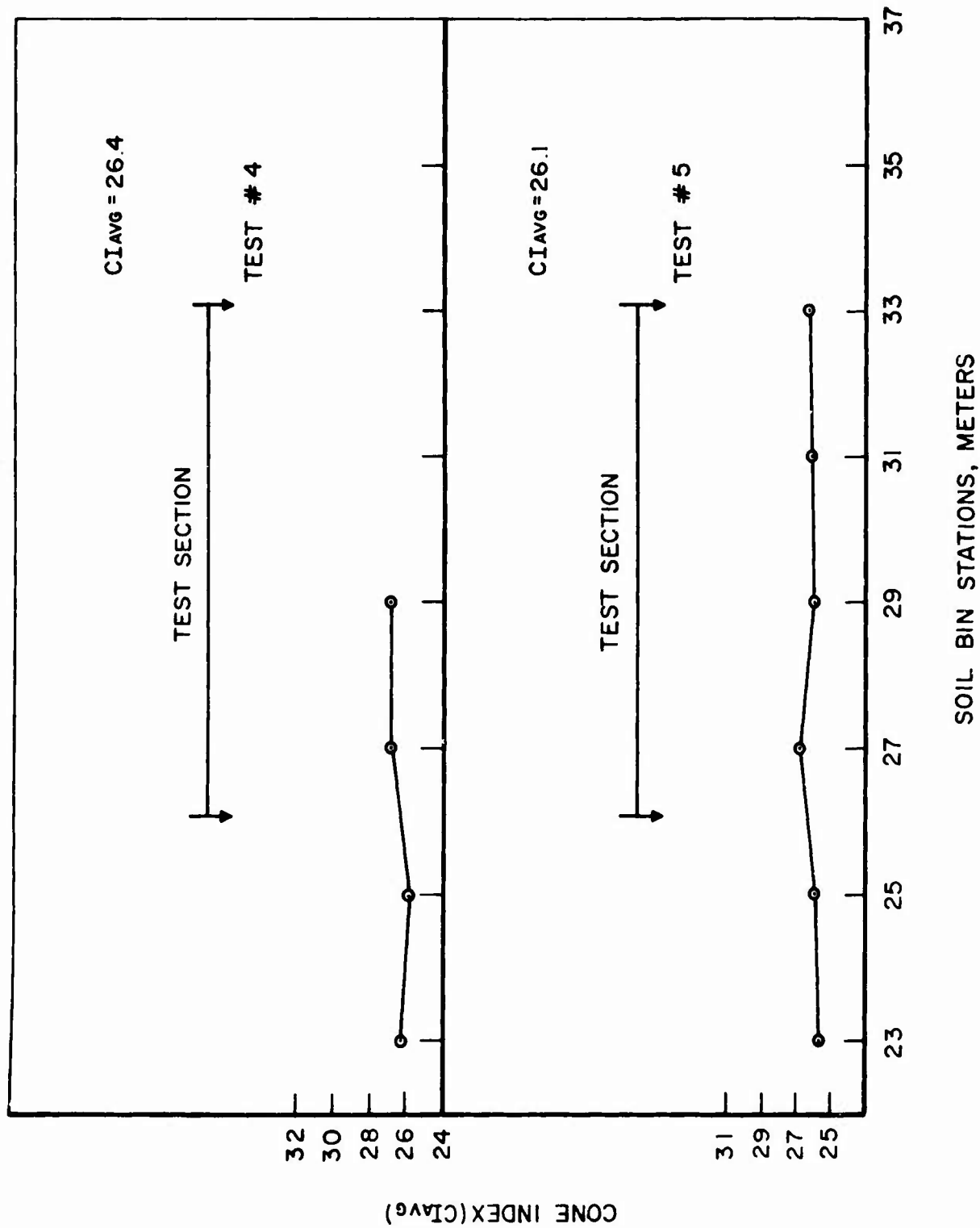


Figure 66 Soil Uniformity Measurements, Mortar Sand, Tests 4 and 5

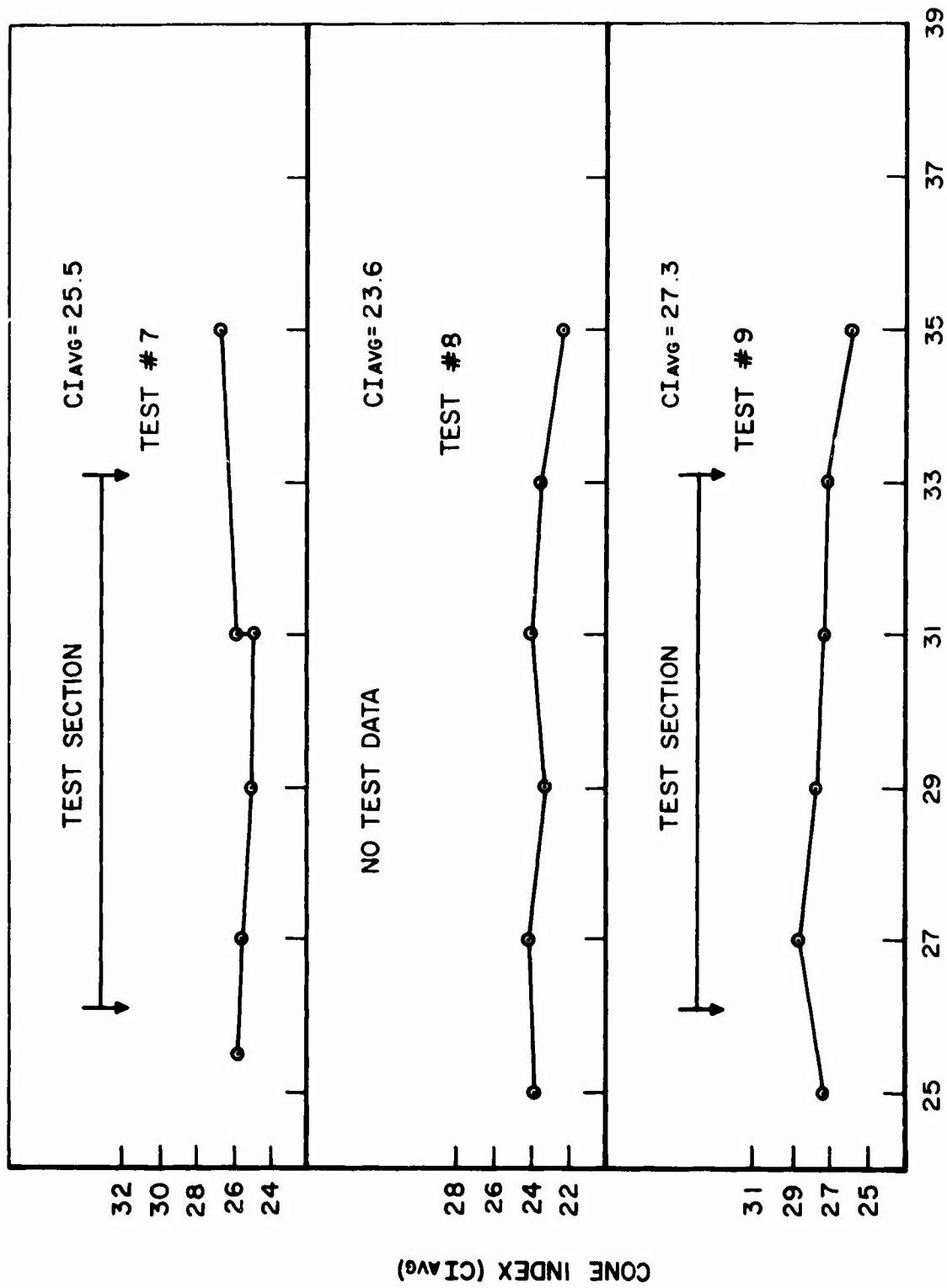


Figure 67 Soil Uniformity Measurements, Mortar Sand, Tests 7, 8, and 9

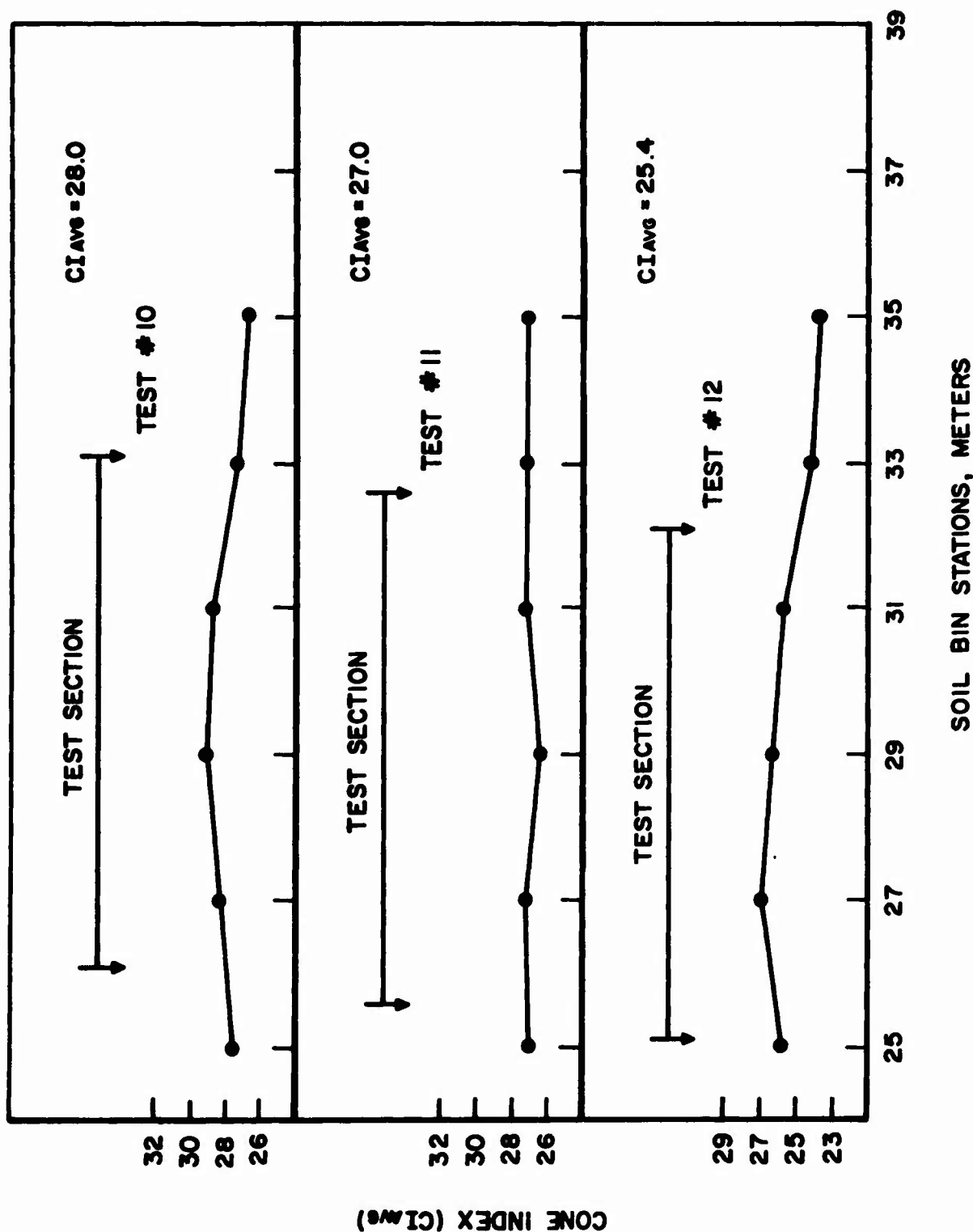


Figure 68 Soil Uniformity Measurements, Mortar Sand, Tests 10, 11, and 12



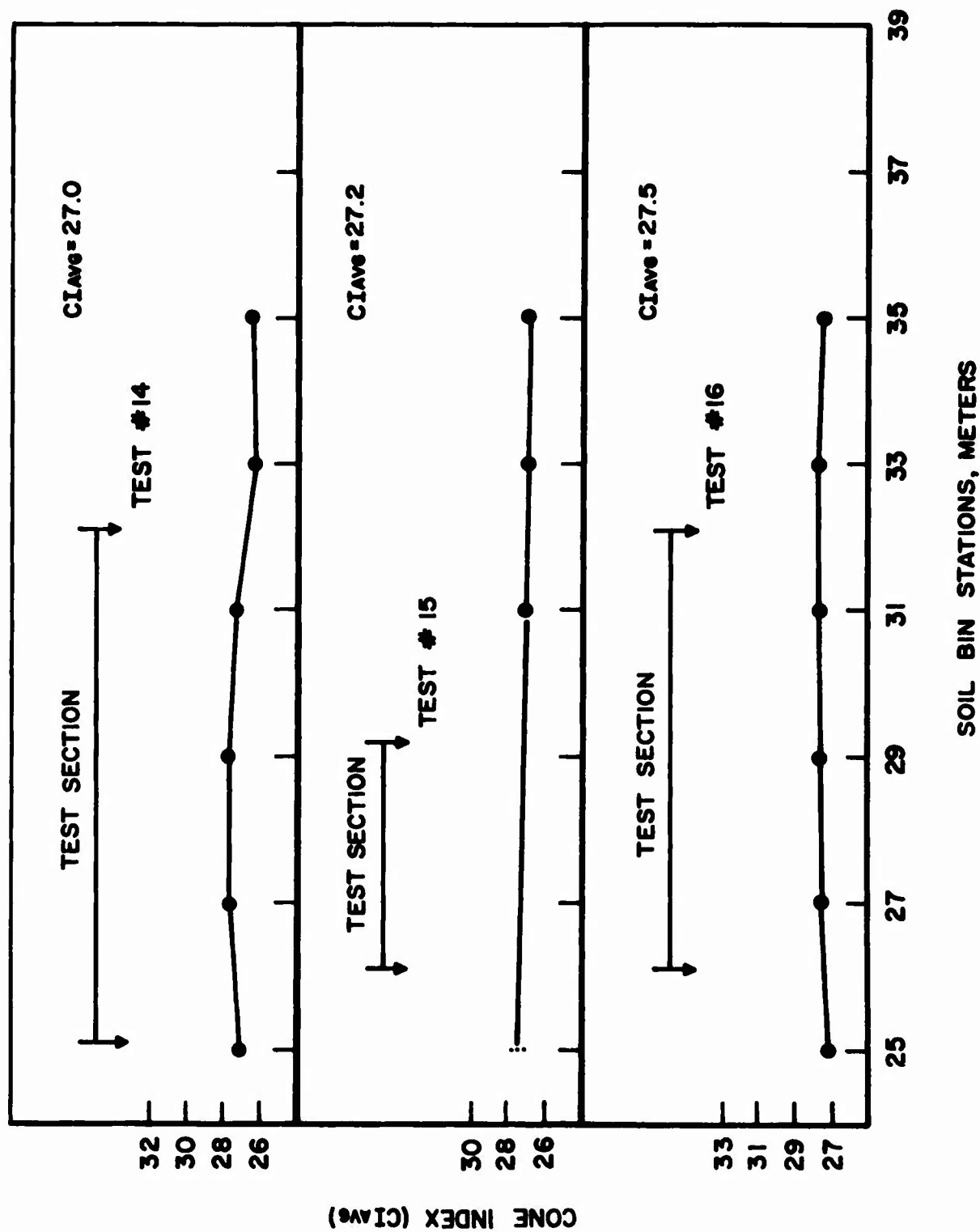


Figure 69 Soil Uniformity Measurements, Mortar Sand, Tests 14, 15, and 16

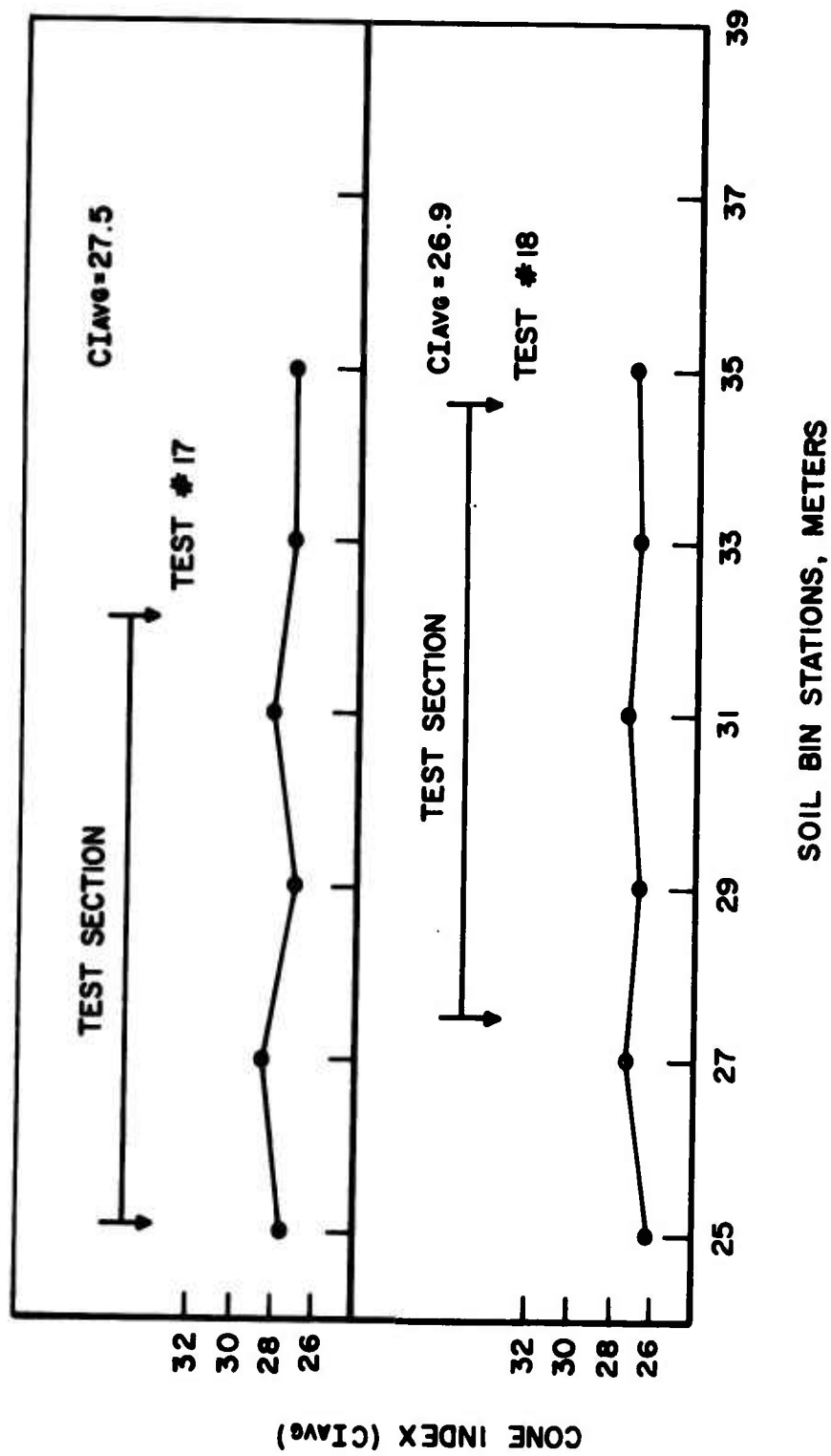


Figure 70 Soil Uniformity Measurements, Mortar Sand, Tests 17 and 18

**APPENDIX III**  
**FLOTATION INDEX-OPERATIONS INDEX**  
**COMPUTER PROGRAM**

## COMPUTER PROGRAM NOMENCLATURE

<b>A</b>	<b>Tire Contact Area (rigid surface)</b>
<b>AL</b>	<b>Major Axis of Decap</b>
<b>AS</b>	<b>Minor Axis of Decap</b>
<b>CI</b>	<b>Average Cone Index of Soil</b>
<b>D</b>	<b>Tire Outside Diameter</b>
<b>DF</b>	<b>Rim Flange Diameter</b>
<b>DLTA</b>	<b>Tire Radial Deflection</b>
<b>FH</b>	<b>Tire Free Height</b>
<b>FI</b>	<b>Flotation Index</b>
<b>FL</b>	<b>Tire Footprint Length</b>
<b>FW</b>	<b>Tire Footprint Width</b>
<b>LS</b>	<b>Load-Strength Ratio</b>
<b>OI</b>	<b>Operations Index</b>
<b>P</b>	<b>Vertical Load</b>
<b>TD</b>	<b>Tire Percent Deflection</b>
<b>TP</b>	<b>Tire Ply</b>
<b>TS1</b>	<b>Tire Size Indicator</b>
<b>TS2</b>	<b>Tire Size Indicator</b>
<b>TT</b>	<b>Tire Type</b>
<b>W</b>	<b>Tire Width</b>
<b>ZD</b>	<b>Sinkage-Tire Diameter Ratio</b>

04/23/69

```

      INTEGER TT,TP
C      FLOTATION INDEX-OPERATIONS INDEX PROGRAM-COHESIVE SOIL
      WRITE ( 6,99)
99  FORMAT(1H0,14H TT=TIRE TYPE/14H TS1=TIRE SIZE/14H TS2=TIRE SIZE,
1/13H TP=TIRE PLY/18H D=TIRE DIAMETER/15H W=TIRE WIDTH/
226HTD=TIRE DEFLECTION PERCENT/20H DF=FLANGE DIAMETER/9H P=LOAD
3/15H CI=CONE INDEX/21H OI=OPERATIONS INDEX/20H FI=FLOTATION IND
4EX////////)
      J=0
      K=2
      REAL LS
9      FORMAT (I4)
10     FORMAT (I5,2F8.3,I4)
12     FORMAT (2F8.3,F6.2,F8.3)
14     FORMAT (F12.2)
16     FORMAT (F8.2)
      I=0
19     READ (5,9) N
20     READ (5,10) TT,TS1,TS2,TP
22     READ (5,12) D,W,TD,DF
24     READ (5,14) P
26     READ (5,16) CI
      I=I+1
      FH=((D-DF)/2.)
      DLTA=((TD/100.)*FH)
      AL=(2.0)*SQRT(DLTA*(D-DLTA))
      AS=(2.0)*SQRT(DLTA*(W-DLTA))
      FL=(0.85)*(AL)
      IF (TT-3)30,30,32
20     FW=(0.93)*(AS)
      GO TO 34
32     FW=AS
34     A=(0.746)*(FL)*(FW)
36     LS=(P/(A*CI))
44     ZL=(-0.03)+(0.19)*(LS)
      OI=((ZL)*(FL)/(P))*10000.
      ZD=((OI)*(P)/(D))*0.0001
      FI=(0.015)+(3.09)*(ZD)
50  FORMAT(1H0,4HTT =,I2,10X,5HTS1 =,F6.2,10X,5HTS2 =,F6.2,10X,4HTP =,
1I3)
52  FORMAT(1H0,4H D =,F6.2,8X,3HP =,F9.2,8X,4HTD =,F6.2,10X,5HCI = ,
1F8.2)
54  FORMAT(1H0,4H A =,F7.2,6X,4HFL =,F7.2)
56  FORMAT(1H0,4HFI =,F7.3,6X,4HOI =,F7.3////////)
      WRITE (6,50) TT,TS1,TS2,TP
      WRITE (6,52) D,P,TD,CI
      WRITE (6,54) A,FL
      WRITE (6,56) FI,OI
      IF (I-K)26,60,60
60     K=K+2
      J=J+1
      IF (I-N)62,64,64
62     GO TO 20
64     STOP
      END

```

04/23/69

FLINDX - EFN SOURCE STATEMENT - IFN(S) -

```

      INTEGER TT,TP
C      FLOTATION INDEX-OPERATIONS INDEX PROGRAM-COHESIONLESS SOIL
      WRITE ( 6,99)
99  FORMAT(1H0,14H TT=TIRE TYPE/14H TS1=TIRE SIZE/14H TS2=TIRE SIZE,
1/13H TP=TIRE PLY/18H D=TIRE DIAMETER/15H W=TIRE WIDTH/
2264H TD=TIRE DEFLECTION PERCENT/20H DF=FLANGE DIAMETER/9H P=LOAD
3/15H CI=CONE INDEX/21H OI=OPERATIONS INDEX/20H FI=FLOTATION IND
45X/////////)
      J=0
      K=2
      REAL LS
9      FORMAT (I4)
10     FORMAT (I5,2F8.3,I4)
12     FORMAT (2F8.3,F6.2,F8.3)
14     FORMAT (F12.2)
16     FORMAT (F8.2)
      I=0
19     READ (5,9) N
20     READ (5,10) TT,TS1,TS2,TP
22     READ (5,12) D,W,TD,DF
24     READ (5,14) P
26     READ (5,16) CI
      I=I+1
      FH=((D-DF)/2.)
      DLTA=((TD/100.)*FH)
      AL=(2.0)*SQRT(DLTA*(D-DLTA))
      AS=(2.0)*SQRT(DLTA*(W-DLTA))
      FL=(0.85)*(AL)
      IF (TT-3)30,30,32
30     FW=(0.93)*(AS)
      GO TO 34
32     FW=AS
34     A=(0.7461)*(FL)*(FW)
36     LS=(P/(A*CI))
44     ZL=(-0.01)+(0.23)*(LS)
      OI=((ZL)*(FL)/(P))*10000.
      ZO=((OI)*(P)/(D))*0.0001
      FI=(0.015)+(3.09)*(ZO)
50  FORMAT(1H0,4HTT =,I2,10X,5HTS1 =,F6.2,10X,5HTS2 =,F6.2,10X,4HTP =,
1I3)
52  FORMAT(1H0,4H D =,F6.2,8X,3HP =,F9.2,8X,4HTD =,F6.2,10X,5HCI = ,
1F9.2)
54  FORMAT(1H0,4H A =,F7.2,6X,4HFL =,F7.2)
56  FORMAT(1H0,4HFI =,F7.3,6X,4HOI =,F7.3////////)
      WRITE (6,50) TT,TS1,TS2,TP
      WRITE (6,52) D,P,TD,CI
      WRITE (6,54) A,FL
      WRITE (6,56) FI,OI
      IF (I-K)26,60,60
60     K=K+2
      J=J+1
      IF (J-N)62,64,64
62     GO TO 20
64     STOP
      END

```

APPENDIX IV

INCREMENTAL STRAIN-DISPLACEMENT RELATIONS  
FOR STRESS POINTS NEAR THE SURFACE

Because there are no mass points above the stress points that are on the first row near the surface of the soil, the incremental strains  $\Delta\gamma_{rz}$  and  $\Delta\epsilon_z$  cannot be calculated by the usual equations. Approximate expression for these incremental strains are derived below.

#### Incremental Shear Strain

For the stress point that is on the axis of symmetry, the equation for  $\Delta\gamma_{rz}$  is the same as Equation (46), that is,

$$\Delta\gamma_{rz}^t(i, j) = 0 \quad (A-1)$$

For the stress points that do not lie on the axis of symmetry, the incremental radial displacement,  $\Delta u$ , of a point on the soil surface  $1/2h$  above the stress point (for example, Point A in Figure 24) may be approximated as the average of the incremental radial displacements of the mass points located  $\pm h$  radially from the stress point, that is,

$$(\Delta u)_A = \frac{1}{2} [\Delta u(i+1, j) + \Delta u(i-1, j)] \quad (A-2)$$

Therefore,

$$\Delta\gamma_{rz}^t(i, j) = \frac{1}{2} \left[ \frac{\Delta w^t(i+1, j) - \Delta w^t(i-1, j)}{2h} + \frac{\Delta u^t(i, j+1) - \Delta u_A^t}{\frac{3}{2}h} \right] \quad (A-3)$$

and

$$\Delta\gamma_{rz}^t(i, j) = \frac{1}{2} \left[ \frac{\Delta w^t(i+1, j) - \Delta w^t(i-1, j)}{2h} + \frac{2\Delta u^t(i, j+1) - \Delta u^t(i+1, j) - \Delta u^t(i-1, j)}{3h} \right] \quad (A-4)$$

#### Incremental Vertical Strain

The vertical stress  $\sigma_z$  at these stress points are assumed to be the average of the surrounding stress points; that is,

$$\sigma_z^t(i, j) = \frac{1}{4} [\sigma_z^t(i+1, j-1) + \sigma_z^t(i+1, j+1) + \sigma_z^t(i-1, j-1) + \sigma_z^t(i-1, j+1)] \quad (A-5)$$

and for the stress point that lies on the axis of symmetry,

$$\sigma_z^t(i, j) = \frac{1}{2} [\sigma_z^t(i+1, j-1) + \sigma_z^t(i+1, j+1)] \quad (A-6)$$



Then the incremental vertical strain is obtained from the incremental stress-strain relations by solving for  $\Delta \epsilon_z^t$  in Equation (38) or Equation (43). The results are as follows:

If the stress point is elastic or plastic unloading,

$$\Delta \epsilon_z^t(i, j) = \sigma_z^t(i, j) - \sigma_z^{t-\Delta t}(i, j) - \frac{\lambda}{\lambda + 2G} [\Delta \epsilon_r^t(i, j) + \Delta \epsilon_\theta^t(i, j)] \quad (A-7)$$

If the stress point is plastic loading,

$$\begin{aligned} \Delta \epsilon_z^t(i, j) = & \left\{ \sigma_z^t(i, j) - \sigma_z^{t-\Delta t}(i, j) - \lambda [\Delta \epsilon_r^t(i, j) + \Delta \epsilon_\theta^t(i, j)] \right. \\ & + Q \left( \frac{\sigma_z^t(i, j)}{2\sqrt{J^t}} + B \right) \left( \frac{\sigma_r^t(i, j) \Delta \epsilon_r^t(i, j) + \sigma_\theta^t(i, j) + \tau_{rz}^t(i, j) \Delta \gamma_{rz}^t(i, j)}{2\sqrt{J^t}} \right. \\ & \left. \left. + B [\Delta \epsilon_r^t(i, j) + \Delta \epsilon_\theta^t(i, j)] \right) \right\} / \left[ \lambda + 2G - Q \left( \frac{\sigma_z^t(i, j)}{2\sqrt{J^t}} + B \right)^2 \right] \quad (A-8) \end{aligned}$$

where  $\Delta \epsilon_r$ ,  $\Delta \epsilon_\theta$ ,  $\Delta \gamma_{rz}$ , and  $\sigma_z$  are obtained from Equations (36), (37), (A-4), and (A-5) respectively, and  $J$ ,  $B$ ,  $Q$  are defined by Equations (33), (63), and (64). The stresses  $\sigma_r$ ,  $\sigma_\theta$ , and  $\tau_{rz}$  are approximated by their values in the previous iteration.

APPENDIX V

DERIVATION OF THE STRESS CORRECTION EQUATIONS

When the yield function  $f$  is significantly above zero due to computational errors, the stresses are corrected such that  $f$  is again brought near to zero. The condition used for making the correction is that the correction stress vector is normal to the yield function while treating each of the components of the stress tensor, that is,  $\sigma_r$ ,  $\sigma_\theta$ ,  $\sigma_z$ ,  $\tau_{rz}$ ,  $\tau_{zr}$ , as independent variables. As defined in Equation (31),

$$\text{Yield Function} = f = \alpha I + \sqrt{J} - k$$

Defining another yield function as

$$F = J - (k - \alpha I)^2$$

where  $F$  is a function of  $\sigma_r$ ,  $\sigma_\theta$ ,  $\sigma_z$ ,  $\tau_{rz}$ , and  $\tau_{zr}$ , and is greater than zero when  $f$  is greater than zero, then the unit normal vector to the function  $F$  is given by

$$\vec{N} = \frac{\vec{\nabla} F}{|\vec{\nabla} F|} \quad (\text{A-9})$$

where  $\vec{\nabla} F$  is the gradient of  $F$ .  $\vec{\nabla} F$  has the following five components:

$$\begin{aligned} (\vec{\nabla} F)_r &= \frac{\partial F}{\partial \sigma_r} = \sigma_r - \frac{1}{3}I + 2\alpha(k - \alpha I) \\ (\vec{\nabla} F)_\theta &= \frac{\partial F}{\partial \sigma_\theta} = \sigma_\theta - \frac{1}{3}I + 2\alpha(k - \alpha I) \\ (\vec{\nabla} F)_z &= \frac{\partial F}{\partial \sigma_z} = \sigma_z - \frac{1}{3}I + 2\alpha(k - \alpha I) \\ (\vec{\nabla} F)_{rz} &= \frac{\partial F}{\partial \tau_{rz}} = \tau_{rz} \\ (\vec{\nabla} F)_{zr} &= \frac{\partial F}{\partial \tau_{zr}} = \tau_{zr} \end{aligned} \quad (\text{A-10})$$

By defining the correction vector as

$$\vec{\delta\sigma}_{i,j} \equiv (\delta\sigma_r, \delta\sigma_\theta, \delta\sigma_z, \delta\tau_{rz}, \delta\tau_{zr}) \quad (\text{A-11})$$

where each component is the correction needed for each stress component. In order to have the correction vector  $\vec{\delta\sigma}_{i,j}$  normal to the yield surface  $F$ , the following condition is required:

$$\frac{\delta\sigma_r}{(\vec{\nabla}F)_r} = \frac{\delta\sigma_\theta}{(\vec{\nabla}F)_\theta} = \frac{\delta\sigma_z}{(\vec{\nabla}F)_z} = \frac{\delta\tau_{rz}}{(\vec{\nabla}F)_{rz}} = \frac{\delta\tau_{zr}}{(\vec{\nabla}F)_{zr}} = \frac{|\vec{\delta\sigma}_{i,j}|}{|\vec{\nabla}F|} = \eta \quad (A-12)$$

From the definition of scalar product and since  $\vec{\delta\sigma}_{i,j}$  is parallel to  $\vec{\nabla}F$

$$|\vec{\delta\sigma}_{ij}| = \frac{\vec{\delta\sigma}_{ij} \cdot \vec{\nabla}F}{|\vec{\nabla}F|} \quad (A-13)$$

Therefore,

$$\eta = \frac{\vec{\delta\sigma}_{ij}}{|\vec{\nabla}F|} = \frac{\vec{\delta\sigma}_{ij} \cdot \vec{\nabla}F}{|\vec{\nabla}F|^2} \quad (A-14)$$

From Equation (A-10),

$$|\vec{\nabla}F|^2 = \left[ \sigma_r - \frac{1}{3}I + 2\alpha(k - \alpha I) \right]^2 + \left[ \sigma_\theta - \frac{1}{3}I + 2\alpha(k - \alpha I) \right]^2 + \left[ \sigma_z - \frac{1}{3}I + 2\alpha(k - \alpha I) \right]^2 + \tau_{rz}^2 + \tau_{zr}^2 \quad (A-15)$$

After expanding the squared terms and simplifying,

$$|\vec{\nabla}F|^2 = 2J + 12\alpha^2(k - \alpha I)^2 \quad (A-16)$$

From Equations (A-10) and (A-11),

$$\begin{aligned} \vec{\delta\sigma}_{ij} \cdot \vec{\nabla}F &= \delta\sigma_r \left[ \sigma_r - \frac{1}{3}I + 2\alpha(k - \alpha I) \right] + \delta\sigma_\theta \left[ \sigma_\theta - \frac{1}{3}I + 2\alpha(k - \alpha I) \right] \\ &+ \delta\sigma_z \left[ \sigma_z - \frac{1}{3}I + 2\alpha(k - \alpha I) \right] + (\delta\tau_{rz}) \tau_{rz} + (\delta\tau_{zr}) \tau_{zr} \\ &\approx \delta J - \delta \left[ (k - \alpha I)^2 \right] = \delta F \end{aligned} \quad (A-17)$$

$\delta F$  is the change of  $F$  due to the change of stresses  $\vec{\delta\sigma}_{i,j}$ , and therefore must be equal to the deviation of  $F$  from the yield surface (or from zero), that is

$$\delta F = J - (k - \alpha I)^2 \quad (A-18)$$

Substituting Equations (A-16), (A-17), (A-18) into Equation (A-14) gives

$$\eta = \frac{|\vec{\delta F}|}{|\vec{\nabla F}|} = \frac{\vec{\delta a}_{ij} \cdot \vec{\nabla F}}{|\vec{\nabla F}|^2} = \frac{J - (k - \alpha I)^2}{2J + 12\alpha^2(k - \alpha I)^2} \quad (\text{A-19})$$

From Equations (A-12) and (A-19),

$$\begin{aligned} \delta \sigma_r &= \eta (\vec{\nabla F})_r = \eta \left[ \sigma_r - \frac{1}{3} I + 2\alpha(k - \alpha I) \right] \\ \delta \sigma_\theta &= \eta (\vec{\nabla F})_\theta = \eta \left[ \sigma_\theta - \frac{1}{3} I + 2\alpha(k - \alpha I) \right] \\ \delta \sigma_z &= \eta (\vec{\nabla F})_z = \eta \left[ \sigma_z - \frac{1}{3} I + 2\alpha(k - \alpha I) \right] \\ \delta \tau_{rz} &= \eta (\vec{\nabla F})_{rz} = \eta \tau_{rz} \end{aligned} \quad (\text{A-20})$$

Therefore, the corrected stresses are:

$$\begin{aligned} \sigma'_r &= \sigma_r - \delta \sigma_r = (1 - \eta) \sigma_r + \eta \left[ (1 + 6\alpha^2) \frac{1}{3} - 2\alpha k \right] \\ \sigma'_\theta &= \sigma_\theta - \delta \sigma_\theta = (1 - \eta) \sigma_\theta + \eta \left[ (1 + 6\alpha^2) \frac{1}{3} - 2\alpha k \right] \\ \sigma'_z &= \sigma_z - \delta \sigma_z = (1 - \eta) \sigma_z + \eta \left[ (1 + 6\alpha^2) \frac{1}{3} - 2\alpha k \right] \\ \tau'_{rz} &= \tau_{rz} - \delta \tau_{rz} = (1 - \eta) \tau_{rz} \end{aligned} \quad (\text{A-21})$$

**APPENDIX VI**

**FINITE ELEMENT COMPUTER PROGRAM FOR**  
**ANALYTICAL SINKAGE ANALYSIS**

**"Lumped Parameter Iteration Method"**

### Some Preliminary Remarks About the Computer Program

a. The load curve was assumed to be symmetrical, that is, the peak is at one-half the time duration and the shape of the loading portion of the curve is the same as that of the unloading portion. Both portions were approximated by 20 equal linear segments. The "basic load curve" in the program has a peak load of 10,000 psf, as shown in Table 8, and the curve is scaled down proportionately in the program for lower peak loads.

Table 8

#### Basic Load Curve

Dimensionless Time	Applied Pressure in psf
0.0	0.0
0.025	-20.0
0.050	-110.0
0.075	-270.0
0.100	-580.0
0.125	-1050.0
0.150	-1730.0
0.175	-2630.0
0.200	-3750.0
0.225	-4890.0
0.250	-5890.0
0.275	-6770.0
0.300	-7540.0
0.325	-8190.0
0.350	-8730.0
0.375	-9170.0
0.400	-9500.0
0.425	-9740.0
0.450	-9900.0
0.475	-9980.0
0.500	-10000.0

b. One of the input data items to the program is the time increment, DT. It is calculated previous to use of the program using the stability criterion discussed in Section IV. The following procedure should be followed:

- An approximate time increment is obtained by the formula

$$(\Delta t)_{\text{approx.}} = \frac{h}{2c_1}$$

where  $h$  and  $c_1$  are the grid size and the dilatational wave velocity, respectively.

- With the above approximate time increment as a guide, a smaller time increment,  $\Delta t$ , is chosen such that the number of increments in the entire load curve,  $\frac{t_d}{\Delta t}$ , is a multiple of 40. This ensures that each linear segment of the load curve will have integral number of time increments.

c. Since the computer time required to run through a load curve is quite long, the computer program is written such that portions of the load curve can be run at separate times by using magnetic tape input and output. This can be done by specifying the starting load increment number, LB, and the ending load increment number, LEN, and setting up the appropriate tapes.

d. The computer run is monitored by printing out the vertical normal stresses, the vertical displacements, and the yield indicating table of the region under the load in a format that has the alternating pattern similar to that of the finite element model. The other stresses and displacements are not printed out because the volume of print-out would be prohibitively large. Also, not every load increment is printed out; the number of load increments that are skipped is given by the Index, ILI, which is an input data item.

e. The numerical value of each element of the yield indicating table supplies the following information:

- (i) If  $-1.0 < YIT < 0.0$ , the stress point is elastic.
- (ii) If  $-10.015 < YIT < -10.0$ , the yield function is greater than zero but has not exceeded the tolerance for yielding (which is 0.015 in this case), thus the stress point is still considered elastic.
- (iii) If  $0.0 < YIT < 10,000$ , the stress point has yielded and is loading, and no stress correction was applied. The digits to the right of the decimal point give the stress correction factor  $(1-\eta)$ , which is a number between 0.0 and 1.0.
- (iv) If  $30000.0 < YIT < 40000.0$ , the yield function has exceeded the tolerance for stress correction, and stress correction has been applied. The digits other than the ten thousand place digit gives the same information as (iii).



- (v) If  $20000.0 < YIT < 30000.0$ , the yield function is negative but has not gone below the tolerance ( $-0.015$ ) for becoming elastic again, thus the stress point is still considered plastic. The digits other than the ten thousand plate digit give the same information as (iii).
- (vi) If  $40000.0 < YIT < 70000.0$ , the stress point is plastic and unloading. The digits other than the ten thousand plate digit give the same information as (iii).

# LIST OF SYMBOLS

AL	Lame constant ( $\lambda$ ) in psf; later becomes dimensionless ( $\lambda/k$ )
AP	Soil parameter ( $\alpha$ )
BE	A variable related to the stress invariants
BE	A variable in the plastic relation related to the stress invariants (B)
C	Cohesion (c) in psf
C1	Dilatational wave velocity in fps
C2	Shear wave velocity in fps
DFW	The value of the maximum percent convergence of vertical displacement between successive iterations among all the mass points
DT	Time increment ( $\Delta t$ ) in seconds
DTT	Dimensionless time increment ( $\frac{\Delta t}{t_d}$ )
DW	Percent convergence of the vertical displacement between successive iterations
ER, ET, EZ ERZ	Strain increments ( $\Delta \epsilon_r$ , $\Delta \epsilon_\theta$ , $\Delta \epsilon_z$ , and $\Delta \gamma_{rz}$ ) at time t
FA	A constant for controlling whether the top point on the axis be a stress point (FA = -1.0) or a mass point (FA = 1.0)
FC	Yield function
FP	Load curve adjustment factor
G	Shear modulus (G) in psf; later becomes dimensionless (G/k)
H	Grid size, the distance between a mass point and a stress point (h) in inches; later becomes dimensionless (h/a)
HH	Twice the grid size (2h)
I	Index in the radial direction (i)

IC	Index for controlling the particular surrounding stress point to be calculated
ILI	The number of load increments skipped in the print out
ILP	Index for controlling which load increment is to be printed out
IT	Iteration index
J	Index in the downward direction (j)
JA	Index for controlling, during the final iteration, the entry to program for checking if the stress point has yielded
KT	Index for indicating the particular linear segment of the load curve that is being considered
LB	Starting load increment number for the particular computer run
LEN	Ending load increment number for the particular computer run
M	The number of grid points in the radial direction
MA	Index to indicate the i position of the first mass point of the row
ML	The i index for the last fictitious stress point
N	The number of grid points in the downward direction
NIN	The number of load increments in a linear segment of the load curve
P	A constant in the plastic relation (Q)
PCU	Magnitude of the applied pressure after each linear segment of the load curve
PH	Stress correction factor ( $\eta$ )
PHI	Frictional angle ( $\phi$ ) in degrees; later becomes in radians
PIN	Applied pressure increment within each linear segment
PKP	Peak load of load pulse in psf
PO	Poisson's ratio ( $\nu$ )

R	Dimensionless radius ( $r/a$ )
RAT	Stress correction factor ( $1-\eta$ )
RH	Dimensionless radius of the particular surrounding stress point considered
RHO	Weight density ( $\rho$ ) in lb/ft <sup>3</sup>
RL	Radius of the loaded area ( $a$ ) in inches; later becomes in feet
SI	The current applied surface pressure that is prescribed at the fictitious stress points
SIK	The particular applied pressure increment being considered
SJ	Second stress invariant of the stress tensor ( $J$ )
SP	Vertical normal stress ( $\sigma_z$ ) $\times 10^8$ ; use for printout purpose
SR, ST, SZ, SRZ	Radial, tangential, vertical, and shear stresses ( $\sigma_r, \sigma_\theta, \sigma_z, \tau_{rz}$ ) at time $t$
SRS, STS, SZS, SRZS	The stresses of the previous iteration at the surrounding stress point being considered
SRT, STT, SZT, SRZT	Radial, tangential, vertical, and shear stresses ( $\sigma_r, \sigma_\theta, \sigma_z, \tau_{rz}$ ) at time $t - \Delta t$
SS	First stress invariant of the stress tensor ( $I$ )
TD	Time duration of the load pulse ( $t_d$ ) in seconds
TM	Time in seconds ( $t$ )
TTD	Dimensionless time ( $t/t_d$ ) at the end of each linear segment of the load curve
U, UD, UDD	Radial displacement, velocity, and acceleration ( $u, \dot{u}, \ddot{u}$ ) at time $t$
UI	Radial displacement increment ( $\Delta u$ ) at time $t$
UPL	A variable for indicating unloading; UPL = -1.0 is not loading and UPL = 1.0 is unloading

UT, UDT, UDDT	Radial displacement, velocity, and acceleration ( $u$ , $\dot{u}$ , $\ddot{u}$ ) at time $t - \Delta t$
W, WD, WDD	Vertical displacement, velocity, and acceleration ( $w$ , $\dot{w}$ , $\ddot{w}$ ) at time $t$
WI	Vertical displacement increment ( $\Delta w$ ) at time $t$
WO	Incremental plastic work done ( $\Delta W$ )
WP	Vertical displacement ( $w$ ) $\times 10^6$ , use for printout purpose
WP	A reference plastic work done
WT, WDT, WDDT	Vertical displacement, velocity, and acceleration ( $w$ , $\dot{w}$ , $\ddot{w}$ ) at time $t - \Delta t$
YI	Yield indicating table at time $t$
YIT	Yield indicating table at time $t - \Delta t$
YS	Yield stress in shear ( $k$ ) in psf

**APPENDIX VII**  
**PROGRAM LISTING**

```

*SETUP 9      (INPUT TAPE NO.)
*SETUP 10     (OUTPUT TAPE NO.)
*IRJOS      WAP
SIB-TO SINKGE 494,XR7
C HENRY LUNING UD RESEARCH INST.
C PROGRAM FOR LOAD SINKAGE ANALYSIS
COMMON/COMMON/ U(31,33),UD(31,33),UDD(31,33),
1 W(31,33),WD(31,33),WDD(31,33),
2 UT(31,33),UDT(31,33),UDDT(31,33),
3 WT(31,33),WDT(31,33),WDDT(31,33),
4 UI(31,33),WI(31,33)
DIMENSION SP(31,33),ST(31,33),SZ(31,33),SRZ(31,33),
1 SRT(31,33),STT(31,33),SZT(31,33),SRZT(31,33),
2 YIT(31,33),YI(31,33),PCU(21),PIN(20),
3 SP(31,33),WP(31,33)
DIMENSION FMT1(4),FMT2(4)
EQUIVALENCE (U(1),SR(1)),(UD(1),ST(1)),(UDD(1),SZ(1)),
1 (WD(1),SRZ(1)),(WDD(1),YI(1)),(UT(1),SRT(1)),
2 (UDT(1),STT(1)),(UDDT(1),SZT(1)),(WT(1),SRZT(1)),
3 (WDT(1),YIT(1)),(WP(1),SP(1))
C READ IN WT. - FIRST READ CONSISTS OF SOIL PARAMETERS
C SECOND READ CONSISTS OF LOAD PARAMETERS
C THIRD READ CONSISTS OF COMPUTATIONAL PARAMETERS
C FOURTH READ CONSISTS OF LOAD CURVE
READ (5,100) RHO,PO,C2,C,PHI
READ (5,101) TD,RL,PKP
READ (5,102) H,DT,N,M
READ (5,140) (PCU(I),I=1,21)
C CALCULATE THE INDEX FOR THE LAST LOADED FICTITIOUS STRESS POINT,ML
C DETERMINE IF ML IS ODD OR EVEN
C IF ML IS EVEN, LOCATION (2,2) MUST BE A MASS POINT
C IF ML IS ODD, LOCATION (2,2) MUST BE A STRESS POINT
ML=RL/H+1.001
ML2=ML+2
AML=ML
IF (COS(AML*3.1415927).GT.0.) GO TO 160
FA=-1.
MA=2
GO TO 161
160 FA=1.
MA=2
161 M4=M-4
M2=M+2
N1=N-1
NN=N-2
C CALCULATE OTHER SOIL PARAMETERS AND PRINT THEM OUT FOR REFERENCE
C1=C2*(2.*(1.-PO)/(1.-2.*PO))*0.5
G=RHO*C2*C2/32.2
AL=2.*PO*G/(1.-2.*PO)
WRITE (6,103)
WRITE (6,104) RHO,G,PO,C2,C1
WRITE (6,105) C,PHI
PHI=PHI*3.1415927/180.
CC=(3.-SIN(PHI))*3.**0.5
AP=2.*SIN(PHI)/CC
AAD=AD*AD
YS=6.*C*COS(PHI)/CC
WRITE (6,106) AP,YS
WRITE (6,111)
WRITE (6,112) TD,RL,PKP
WRITE (6,107)

```

```

WRITE (6,108) H,DT,M,N,AL
WRITE (6,109)
WRITE (6,110) RL,TD,YS
C NON-DIMENSIONALIZING ALL PARAMETERS AND CALCULATE SOME CONSTANTS THAT
C WILL BE USED IN THE LATER LOOPS
AL=AL/YS
G=G/YS
GG=2.*G
H=H/RL
HH=2.*H
PL=RL/12.
DTT=DT/TD
CO1=YS*TD*TD**2.2/(RHO*RL*PL)
CO3= AP*(1.+PO)/(1.-2.*PO)
P=GG/(1.5+3.*CO3*AP)
DTG=DTT*GG
DTP=DTT*P
C MODIFY BASIC LOAD CURVE FOR THE SPECIFIED PEAK LOAD, CALCULATE LOAD
C INCREMENTS AND NON-DIMENSIONALIZING BOTH, CALCULATE THE NUMBER OF
C LOAD INCREMENTS IN A LINE SEGMENT. PRINT OUT ALL FOR REFERENCE
WRITE (6,115)
NIN=0.25/DTT+0.001
FMIN=NIN
TTD=0.
FP=PKP/10000.
PC=PCU(1)
DO 163 J=1,20
TTD=TTD+0.025
JJ=J+1
PI=(PCU(JJ)-PC)*FP/FMIN
PC=PCU(JJ)
PCM=PC*FP
PIN(J)=PI/YS
PCU(JJ)=PCM/YS
163 WRITE (6,116) J,TTD,PC,PCM,PI,PCU(JJ),PIN(J)
C READ IN THE FORMAT FOR PRINT OUT AND CALCULATE THE INDICES FOR
C CONTROLLING THE PRINT OUT PATTERN.
IF (FA.GT.0.) GO TO 167
READ (5,127) FMT1
READ (5,127) FMT2
GO TO 165
167 READ (5,127) FMT2
READ (5,127) FMT1
165 J1=MA
J2=5-MA
L1=12+MA
L2=17-MA
C READ IN STARTING LOAD INCREMENT NUMBER AND ENDING LOAD INCREMENT
C NUMBER, CALCULATE PRINT CONTROL INDEX, TIME OF THE PULSE, AND INITIAL
C APPLIED PRESSURE SI, AND PRINT OUT FOR REFERENCE.
READ (5,141) LB,LEN,ILI
ILP=LB+ILI-1
IE=LEN
SL=LB-1
TM=SL*DT
TR=TM/TD/0.025+1.
KT=TR+0.001
TK=KT
LS=KT*NIN
KU=1
IF (KT.LE.20) GO TO 165

```



```

KT=42-KT
KU=-1
SIK=-PIN(KT-1)
GO TO 166
165 SIK=PIN(KT)
166 KTU=KT+KU
SI=(TB-TK)*(PCU(KTU)-PCU(KT))+PCU(KT)+SIK
WRITE (6,117)
WRITE (6,118) LB,LEN,SI,SIK,TA
IF (LB.NE.1) GO TO 164
C IF THIS IS THE VERY FIRST RUN, ALL STRESSES AND DISPLACEMENTS ARE
C FIRST SET EQUAL TO ZERO, AND THE YIELD INDICATING MATRIX IS SET TO BE
C ELASTIC
F=-FA
DO 7 J=1,N
F=-1.*F
MM=1.5001-F*0.5
ME=N2-MM
DO 7 I=1,M,2
UT(I,J)=0.
VT(I,J)=0.
U(I,J)=0.
V(I,J)=0.
UD(I,J)=0.
VD(I,J)=0.
UDD(I,J)=0.
VDD(I,J)=0.
UT(I,J)=0.
VT(I,J)=0.
UDT(I,J)=0.
VDT(I,J)=0.
UDDT(I,J)=0.
VDDT(I,J)=0.
IF (I.EQ.(M+1)) GO TO 7
L=I+1
SR(L,J)=0.
ST(L,J)=0.
SZ(L,J)=0.
SRZ(L,J)=0.
YIT(L,J)=-1.
7 CONTINUE
MD=1./C
GO TO 162
C 164 IF THIS IS A CONTINUATION RUN, THE STRESSES, DISPLACEMENTS, AND
C YIELD INDICATING TABLE OF THE PRECEDING RUN ARE READ IN FROM TAPE,
C STORED AS QUANTITIES AT TIME T-DT, THEY ARE ALSO EQUATED AS
C QUANTITIES AT TIME T FOR THE FIRST ITERATION
164 READ (9) UT,VT,UDT,VDI,DDDT,DDDT,UI,M1
F=-FA
DO 8 J=2,N1
F=-1.*F
MM=1.5001+F*0.5
ME=N2-MM
2 DO 2 I=1,M,2
U(I,J)=UT(I,J)
V(I,J)=VT(I,J)
UD(I,J)=UDT(I,J)
VD(I,J)=VDI(I,J)
IF (I.EQ.(M+1)) GO TO 8
L=I+1

```

```

      SP(L,J)=SPT(L,J)
      ST(L,J)=STT(L,J)
      SZ(L,J)=SZT(L,J)
      SRZ(L,J)=SRZT(L,J)
      R CONTINUE
      WR=SRT(1,1)
C STARTING POINT OF MOST OUTER LOOP, FOR CALCULATION OF EACH LOAD
C INCREMENT. THE STARTING APPLIED SURFACE PRESSURE ARE STORED IN AT THE
C FICTITIOUS STRESS POINTS, ROW J=1.
      169 DO 97 ILL=LB,LEN
          TM=TM+DT
          DO 5 I=MA,ML,2
              5 SZ(I,1)=SI
          DO 4 I=ML2,31,2
              4 SZ(I,1)=0.
C STARTING POINT OF THE ITERATION LOOP.
          JA=1
          IT=0
          6 IT=IT+1
          DFW=0.
          F=FA
C STARTING POINT FOR THE LOOP INCREMENTING EACH ROW GOING DOWNWARD
          DO 80 J=2,NM
              F=-1.*F
              MM=2.5001+F*0.5
              ME=M4+MM
C STARTING POINT OF THE LOOP FOR CALCULATING EACH ROW STARTING WITH THE
C LEFT MASS POINT
              DO 70 I=MM,ME,2
                  IP=I+1
                  IV=I-1
                  R=I-2
                  R=R*H
C CALCULATE, AT EACH MASS POINT, THE ACCELERATIONS FROM THE DYNAMIC
C EQUATIONS OF MOTION. THE PARTICULAR EQUATION TO USE DEPENDS ON THE
C LOCATION OF THE MASS POINT.
                  UDS=UD(I,J)
                  WDS=WD(I,J)
                  US=U(I,J)
                  WS=W(I,J)
                  IF(I.GT.2) GO TO 12
                  UDD(2,J)=0.
                  WDD(2,J)=CO1*(SZ(2,J+1)-SZ(2,J-1)+4.*SRZ(3,J))/MM
                  GO TO 16
                  12 IF (J.GT.2.OR.I.GT.ML) GO TO 13
                  UDD(I,2)=0.
                  GO TO 14
                  13 UDD(I,J)=CO1*((SR(IP,J)-SR(IM,J)+SRZ(I,J+1)-SRZ(I,J-1))/MM
                      1+(SR(IP,J)+SR(IM,J)-ST(IP,J)-ST(IM,J))/2./R)
                  14 WDD(I,J)=CO1*((SZ(I,J+1)-SZ(I,J-1)+SRZ(IP,J)-SRZ(IM,J))/MM
                      1+(SRZ(IP,J)+SRZ(IM,J))/2./R)
C CALCULATE THE DISPLACEMENTS AND VELOCITIES AT TIME T FROM THE
C QUADRATURE EQUATIONS.
                  16 U(I,J)=UT(I,J)+DTT*UDT(I,J)+DTT*DTT*(UDDT(I,J)/3.+UDD(I,J)/6.)
                  W(I,J)=WT(I,J)+DTT*WDT(I,J)+DTT*DTT*(WDDT(I,J)/3.+WDD(I,J)/6.)
                  UD(I,J)=UDT(I,J)+DTT*(UDDT(I,J)+UDD(I,J))/2.
                  WD(I,J)=WDT(I,J)+DTT*(WDDT(I,J)+WDD(I,J))/2.
                  IF (IT.EQ.1) GO TO 10
C AVERAGE WITH THE DISPLACEMENTS FROM THE PRECEDING ITERATION.
                  U(I,J)=(U(I,J)+US)/2.
                  W(I,J)=(W(I,J)+WS)/2.

```

```

      UD(I,J)=(UD(I,J)+UDS)/2.
      VD(I,J)=(VD(I,J)+VDS)/2.
C 10 CALCULATE THE DISPLACEMENT INCREMENTS
      UI(I,J)=L(I,J)-UI(I,J)
      VI(I,J)=W(I,J)-VI(I,J)
C DETERMINE THE DISPLACEMENTS OF THE SECOND TO THE LAST ROW BY AVERAGING
      IF (J.LT.MN) GO TO 19
      IF (I-2) 9,11,15
      11 WI(2,N1)=VI(3,J)/2.
      UI(2,N1)=0.
      GO TO 9
      15 WI(I-1,N1)=(WI(I-2,J)+WI(I,J))/4.
      UI(I-1,N1)=(UI(I-2,J)+UI(I,J))/4.
      IF (I.EQ.(M-1)) GO TO 19
      9 WI(I+1,N1)=(WI(I+2,J)+WI(I,J))/4.
      UI(I+1,N1)=(UI(I+2,J)+UI(I,J))/4.
      19 CONTINUE
      IF (IT.LL.2) GO TO 17
C CALCULATE THE PERCENT CONVERGENCE OF THE VERTICAL DISPLACEMENT
C BETWEEN THIS AND THE PRECEDING ITERATION. LOCATE THE LARGEST PERCENT
C AND SAVE IT FOR LATER REFERENCE.
      DW=ABS(1.-WS/W(I,J))
      IF (DW.LE.DFM) GO TO 17
      DFM=DW
      ILD=ILL
      ITD=IT
      ID=I
      JD=J
C CALCULATE THE STRESSES AT THE SURROUNDING STRESS POINTS. IC CONTROLS
C WHICH STRESS POINT IS BEING CONSIDERED
C IC=1 IS FOR THE ONE IMMEDIATELY BELOW
C IC=2 IS FOR THE ONE IMMEDIATELY TO THE LEFT
C IC=3 IS FOR THE ONE IMMEDIATELY TO THE RIGHT.
      17 IC=0
      K=I
      L=J+1
      RH=R
C STARTING POINT OF PROGRAM FOR CALCULATING STRESSES OF EACH SURROUNDING
C STRESS POINT.
      18 IC=IC+1
      IF (K.EQ.1) GO TO 64
C SAVE THE STRESSES OF THE PRECEDING ITERATION, AND CHECK YIELD INDICAT-
C ING MATRIX TO DETERMINE WHICH STRESS STRAIN RELATION TO USE.
      SRS=SR(K,L)
      STS=ST(K,L)
      SZS=SZ(K,L)
      SRZS=SRZ(K,L)
      IF (YIT(K,L)) 20,35,35
C 20 STRESS POINT IS ELASTIC.
C CALCULATE THE STRAIN INCREMENTS FROM THE DISPLACEMENT INCREMENTS.
C WHICH EQUATION TO USE DEPENDS ON THE LOCATION OF THE STRESS POINT.
      20 IF (L.GT.2) GO TO 22
      IF (K.GT.2) GO TO 21
      SZ(2,2)=(SZ(3,2)+S1)/2.
      ET=0.
      FRZ=0.
      GO TO 26
      21 IF (K.GT.ML.OP.IC.LT.3) GO TO 32
      SZ(K,2)=(S1+SZ(K-1,3))/2.
      GO TO 25
      31 SZ(K,2)=(SZ(K+1,1)+SZ(K-1,1)+SZ(K+1,3)+SZ(K-1,3))

```

```

1      -SZ(K-2,2)-SZ(K+2,2))/2.
GO TO 25
32 IF (K.EQ.(ML+1)) GO TO 31
23 SZ(K,2)=(SZ(K+1,1)+SZ(K-1,1)+SZ(K+1,3)+SZ(K-1,3))/4.
25 ET=(UI(K+1,2)+UI(K-1,2))/2./RH
ERZ=(WI(K+1,2)-WI(K-1,2))/HH+(UI(K,3)-UI(K-1,2)/2.-UI(K+1,2)/2.)*4
1./3./HH
26 FR=(UI(K+1,2)-UI(K-1,2))/HH
F7=(SZ(K,2)-SZT(K,2)-AL*(ER+ET))/(AL+GG)
FF=AL*(ER+ET+FZ)
GO TO 30
22 IF(K.GT.2) GO TO 24
FR=2.*UI(3,L)/HH
ET=ER
ERZ=0.
GO TO 29
24 ET=(UI(K-1,L)+UI(K+1,L))/2./RH
FR=(UI(K+1,L)-UI(K-1,L))/HH
IF (IT.GT.1.OR.K.GT.NL.OR.IC.LT.3) GO TO 28
IF (ABS(W(K+1,L)).GT.0.1E-33) GO TO 28
FRZ=(UI(K,L+1)-UI(K,L-1))/HH
GO TO 29
28 ERZ=(WI(K+1,L)-WI(K-1,L)+UI(K,L+1)-UI(K,L-1))/HH
29 EZ=(#I(K,L+1)-#I(K,L-1))/HH
C CALCULATE THE STRESSES FROM THE ELASTIC RELATIONS.
EE=AL*(ER+ET+FZ)
30 SR(K,L)=SRT(K,L)+EE+GG*ER
ST(K,L)=STT(K,L)+EE+GG*ET
SZ(K,L)=SZT(K,L)+EE+GG*EZ
SRZ(K,L)=SRZT(K,L)+G*ERZ
GO TO 59
C 35 STRESS POINT IS PLASTIC.
C CALCULATE THE STRAIN INCREMENTS FROM THE DISPLACEMENT INCREMENTS.
C WHICH EQUATION TO USE DEPENDS ON THE LOCATION OF THE STRESS POINT.
35 UPL=-1.
IF (L.GT.2) GO TO 47
IF (K.GT.2) GO TO 37
SZ(2,2)=(SZ(3,3)+S1)/2.
ET=0.
ERZ=0.
GO TO 43
37 IF (K.GT.NL.OR.IC.LT.3) GO TO 40
SZ(K,2)=(SZ(K-1,3)+S1)/2.
GO TO 41
38 SZ(K,2)=(SZ(K+1,1)+SZ(K-1,1)+SZ(K+1,3)+SZ(K-1,3)
1      -SZ(K-2,2)-SZ(K+2,2))/2.
GO TO 41
40 IF (K.EQ.(NL+1)) GO TO 38
39 SZ(K,2)=(SZ(K+1,1)+SZ(K-1,1)+SZ(K+1,3)+SZ(K-1,3))/4.
41 ET=(UI(K+1,2)+UI(K-1,2))/2./RH
ERZ=(WI(K+1,2)-WI(K-1,2))/HH+(UI(K,3)-UI(K-1,2)/2.-UI(K+1,2)/2.)*4
1./3./HH
43 FR=(UI(K+1,2)-UI(K-1,2))/HH
C THE NEXT STATEMENT CHECKS THE YIELD INDICATING MATRIX TO DETERMINE IF
C THE STRESS POINT IS UNLOADING. IT IS UNLOADING IF YIT IS GREATER THAN
C 40000.
IF (YIT(K,L).GT.40000.) GO TO 46
SJ=SQRT(((SRS-ST5)**2+(STS-SZ(K,2))**2+(SZ(K,2)-SR5)**2+6.*S5ZS*
1SRZS)/6.)
SS=SRS+STS+SZ(K,2)
BE=C03-SS/SJ/6.

```

```

      SJ2=2.*SJ
      C73=SZ(K,2)/SJ2+BE
      EPT=ER+ET
      FZ=(SZ(K,2)-SZT(K,2)-AL*ERT+P*SZB*((SRK*EK+STS*ET+SRZS*ERZ
1/2.)/SJ2+BE*ERT))/(GG+AL-P*SZB*SZB)
      GO TO 51
46 FZ=(SZ(K,2)-SZT(K,2)-AL*(ER+ET))/(AL+GG)
      GO TO 51
47 IF(K.GT.2) GO TO 49
      ER=2.*UI(3,L)/HH
      ET=ER
      ERZ=0.
      GO TO 50
49 ET=(UI(K-1,L)+UI(K+1,L))/2./RH
      EP=(UI(K+1,L)-UI(K-1,L))/HH
      ERZ=(WI(K+1,L)-WI(K-1,L)+UI(K,L+1)-UI(K,L-1))/HH
50 FZ=(WI(K,L+1)-WI(K,L-1))/HH
51 FE=ER+ET+EZ
      AE=AL*FE
C THE NEXT STATEMENT CHECKS UNLOADING AGAIN. IF UNLOADING, GO TO
C UNLOADING RELATION.
      IF (YIT(K,L).GT.40000.) GO TO 53
C CALCULATE THE STRESSES FROM THE PLASTIC RELATIONS.
      W0=SRB*ER+STS*ET+SRZS*ERZ/2.+SZ(K,L)*EZ
      IF (L.EQ.2) GO TO 54
      SS=SRB+STS+SZS
      SJ=SQRT(((SRB-STB)**2+(STS-SZS)**2+(SZS-SRB)**2+6.*SRZS*SRZS)/6.)
      BE=C03-SS/SJ/6.
      SJ2=2.*SJ
      SZ(K,L)=SZT(K,L)+GG*EZ+AE-(SZS/SJ2+BE)*(W0/SJ2+BE*FE)*P
54 WE=(W0/SJ2+BE*FE)*P
      SR(K,L)=SRT(K,L)+GG*ER+AE-(SRB/SJ2+BE)*WE
      ST(K,L)=STT(K,L)+GG*ET+AE-(STS/SJ2+BE)*WE
      SRZ(K,L)=SRZT(K,L)+G*ERZ-SRZS*AE/SJ2
      GO TO 59
C 53 STRESS POINT IS UNLOADING. UNLOADING RELATION IS USED.
53 IF (L.EQ.2) GO TO 50
      SZ(K,L)=SZT(K,L)+AE+GG*EZ
58 SR(K,L)=SRT(K,L)+AE+GG*ER
      ST(K,L)=STT(K,L)+AE+GG*ET
      SRZ(K,L)=SRZT(K,L)+G*ERZ
C 59 CHECK IF THE STRESS POINT HAS YIELDED. THIS IS DONE ONLY FOR THE
C FINAL ITERATION. JA INDEX CONTROLS THE ENTRY.
59 IF (JA.LT.2) GO TO 64
C CALCULATE THE YIELD FUNCTION
      SS=SR(K,L)+ST(K,L)+SZ(K,L)
      SSW=(SR(K,L)-ST(K,L))**2+(ST(K,L)-SZ(K,L))**2+(SZ(K,L)-SR(K,L))**2
      SRW=(SRZ(K,L))**2
      SJS=SSJ/6.+SRW
      SJ=SQRT(SJS)
      FC=AP*SS+SJ-1.
C CHECK IF THE YIELD FUNCTION IS GREATER THAN THE TOLERANCE ABOVE ZERO.
C AND MAKE THE APPROPRIATE CHANGE IN THE YIELD INDICATING TABLE
      IF (FC.GT.0.015) GO TO 63
      IF (YIT(K,L).LT.0.) GO TO 60
      IF (FC.GT.-0.015) GO TO 63
60 GO TO (64,61,64),IC
61 YI(K,L)=FC
      IF (FC.GT.0.) YI(K,L)=-10.-FC
      GO TO 64
C 63 STRESS POINT HAS YIELDED. CHECK IF IT IS UNLOADING.

```

```

63 WO=SR(K,L)*ER+ST(K,L)*ET+SZ(K,L)*EZ+SRZ(K,L)*ERZ/2.
   IF (WO.GT.WR) WR=WO
   IF (WO.LT.-0.05*WK.AND.IC.EQ.2) UPL=1.
C CALCULATE THE STRESS CORRECTION FACTOR.
   SSP=(1.-AP*SS)**2
   PH=(SJS-SSP)/(2.*SJS+12.*AAP*SSP)
   PAK=PH*((1.+6.*AAP)*SS/3.-2.*AP)
   RAT=1.-PH
   FCJ=AIN(10000.*FC)
   IF (FC.LT.0.) FCJ=20000.-FCJ
   YI(K,L)=FCJ+RAT
   IF (UPL.GT.0.) YI(K,L)=YI(K,L)+40000.
C STRESS CORRECTION IS MADE BY THE FOLLOWING STATEMENTS ONLY IF THE
C YIELD FUNCTION IS GREATER THAN A TOLERANCE.
   IF (FC.LT.0.020) GO TO 64
   YI(K,L)=YI(K,L)+30000.
   SRKL=SR(K,L)
   STKL=ST(K,L)
   SZKL=SZ(K,L)
   SR(K,L)=SRKL*RAT+PAK
   ST(K,L)=STKL*RAT+PAK
   SZ(K,L)=SZKL*RAT+PAK
   SRZ(K,L)=RAT*SRZ(K,L)
C STATEMENT 64 CONTROLS THE SWITCHING TO CALCULATE THE STRESSES AT THE
C THREE SURROUNDING STRESS POINTS.
64 GO TO (65,68,70), IC
65 K=I-1
   L=J
   RH=R-H
   GO TO 18
68 K=I+1
   L=J
   RH=R+H
   GO TO 18
70 CONTINUE
80 CONTINUE
   IF (IT.LE.2) GO TO 6
   WRITE (6,143) DFW,ILD,ITD,ID,JD
   IF (JA.EQ.2) GO TO 81
C CHECK IF THE CONVERGENCE IS GOOD ENOUGH. RETURN TO CALCULATE ANOTHER
C ITERATION IF NOT ACCURATE ENOUGH.
   IF (DFW.GT.0.002.AND.IT.LT.7) GO TO 6
C IF ACCURATE ENOUGH, ADJUST JA INDEX AND CALCULATE FINAL ITERATION.
   JA=2
   GO TO 6
81 CONTINUE
C THE FOLLOWING LOOP SAVES ALL THE DISPLACEMENTS AND STRESSES FOR THE
C CALCULATION OF THE NEXT TIME INCREMENT.
   F=-FA
   DO 95 J=2,N1
   F=-1.*F
   MM=1.5001+F*0.5
   ME=M2-MM
   DO 95 I=MM,ME,2
   IF (I.EQ.(M+1)) GO TO 94
   L=I+1
   YIT(L,J)=YI(L,J)
   SRT(L,J)=SR(L,J)
   STT(L,J)=ST(L,J)
   SZT(L,J)=SZ(L,J)
   SRZT(L,J)=SRZ(L,J)

```

```

      SP(L,J)=SZ(L,J)*100.
94  UT(I,J)=U(I,J)
      WT(I,J)=W(I,J)
      WP(I,J)=W(I,J)*1.0E 06
      UDT(I,J)=UD(I,J)
      WDT(I,J)=WD(I,J)
      UDDT(I,J)=UDD(I,J)
95  WDDT(I,J)=WDD(I,J)
      SRT(1,1)=WR
      DO 180 II=MA,31,2
180  SP(II,1)=SZ(II,1)*100.
C IF THE END OF A LINEAR SEGMENT OF THE LOAD CURVE IS REACHED, SIK IS
C CHANGED TO THE APPLIED PRESSURE INCREMENT OF THE NEXT LINEAR SEGMENT.
      IF (ILL.LT.LS) GO TO 96
      LS=LS+NIN
      KT=KT+KII
      SI=PCU(KT)
      SIK=PIN(KT)
96  CONTINUE
C PRINT OUT THE VERTICAL STRESSES AND DISPLACEMENTS IN THE REGION UNDER
C THE LOADED AREA FOR MONITORING THE COMPUTER RUN.
      IF (ILL.LT.ILP) GO TO 97
181  WRITE (6,125) ILL,IT,TM
      DO 183 J=1,NN,2
      JJ=J+1
      WRITE (6,FMT1) J,(SP(I,J),I=J1,13,2)
183  WRITE (6,FMT2) JJ,(SP(I,JJ),I=J2,13,2)
182  WRITE (6,126) ILL
      DO 184 J=2,N1,2
      JJ=J+1
      WRITE (6,FMT1) J,(WP(I,J),I=J1,13,2)
184  WRITE (6,FMT2) JJ,(WP(I,JJ),I=J2,13,2)
      WRITE (6,136) ILL,IT
      DO 186 J=1,NN,2
      JJ=J+1
      WRITE (6,FMT1) J,(YIT(I,J),I=J1,13,2)
186  WRITE (6,FMT2) JJ,(YIT(I,JJ),I=J2,13,2)
      ILP=ILP+ILI
      WRITE (6,130) WR
207  IF (ILL.EQ.IE) GO TO 201
      GO TO 97
201  WRITE (6,125) ILL,IT,TM
      DO 203 J=1,NN,2
      JJ=J+1
      WRITE (6,FMT1) J,(SP(I,J),I=L1,25,2)
203  WRITE (6,FMT2) JJ,(SP(I,JJ),I=L2,25,2)
202  WRITE (6,126) ILL
      DO 204 J=2,N1,2
      JJ=J+1
      WRITE (6,FMT1) J,(WP(I,J),I=L1,25,2)
204  WRITE (6,FMT2) JJ,(WP(I,JJ),I=L2,25,2)
      WRITE (6,136) ILL,IT
      DO 206 J=1,NN,2
      JJ=J+1
      WRITE (6,FMT1) J,(YIT(I,J),I=L1,25,2)
206  WRITE (6,FMT2) JJ,(YIT(I,JJ),I=L2,25,2)
      IE=IE+50
97  SI=SI+SIK
C SAVE ON TAPE ALL THE STRESSES, DISPLACEMENTS, VELOCITIES, AND ACCELER-
C ATIONS FOR SUBSEQUENT COMPUTER RUNS.
      WRITE (6,130) WR

```

```

98 WRITE (10) UT,UDT,UDDT,UT,UDT,UDDT,UI,UI
   WRITE (6,120) XT,LS,LP,SI,SIK
99 STOP
100 FORMAT(F8.1,F6.2,5F8.1)
101 FORMAT (2F10.3,F10.2)
102 FORMAT (F8.3,F12.8,2I5)
103 FORMAT(1H1,19X,15H SOIL PROPERTIES)
104 FORMAT(23X,7HDENSITY,17X,5H $\gamma$  =,F10.1,10H LBS/CU-FT/23X,15HSHEAR
   1 MODULUS,13X,3H $G$  =,F10.1,10H LBS/SQ-FT/23X,14HPOISSON'S RATIO,11X,4H
   2  $\nu$  =,F10.2/23X,29HSHEAR WAVE VELOCITY C2 =,F10.1,7H FT/SEC/
   2 23X,29HDILATATIONAL WAVE VEL. C1 =,F10.1,7H FT/SEC//)
105 FORMAT(23X,8HCOHESION,18X,5H $c$  =,F10.1,10H LBS/SQ-FT/23X,14HFRICITION
   1 IN ANGLE,10X,5H $\phi$  =,F10.1,4H DEG//)
106 FORMAT(23X,29HFOR YIELD CRITERIA  $\alpha$  =,F16.6/49X,5H $\beta$  =,F16.6,
   110H LBS/SQ-FT//)
107 FORMAT(1H0,19X,24HCOMPUTATIONAL PARAMETERS)
108 FORMAT(23X,10HSPACE MESH,
   116X,5H $\Delta x$  =,F10.4,3H IN/23X,29HBASIC TIME INCREMENT  $\Delta t$  =,
   2F10.7,4H SEC//23X,11HNUMBER OF I,10X,5H $N_I$  =,14/23X,11HNUMBER OF J,
   315X,5H $N_J$  =,14/23X,10HLOADED-FREE BORDER,7X,4H $N_{LF}$  =,14//)
109 FORMAT(1H0,19X,50HCHARACTERISTIC PARAMETERS FOR NON-DIMENSIONALIZI
   1 NG)
110 FORMAT(23X,14HLENGTH =  $R_L$  =,F10.2,3H IN/23X,14HTIME =  $T_D$  =,F10
   1.2,4H SEC/23X,14HSTRESS =  $\sigma$  =,F10.2,10H LBS/SQ-FT//)
111 FORMAT (1H0,19X,15HLOAD PARAMETERS)
113 FORMAT (23X,29HTIME DURATION OF PULSE  $T_D$  =,F10.5,4H SEC/
   1 23X,29HRADIUS OF LOADED AREA  $R_L$  =,F10.5,3H IN/
   2 23X,29HPEAK PRESSURE OF PULSE  $P_{KP}$  =,F10.1,10H LBS/SQ-FT//)
112 FORMAT (1H//)
115 FORMAT (6X,99H AT DIMENSIONLESS BASIC LOAD DIMENSIONED
   1 DIMENSIONED DIMENSIONLESS DIMENSIONLESS/100H J TIME
   2 T/TD CURVE LOAD CURVE LOAD INCREMENT LOAD
   3 CURVE LOAD INCREMENT//)
116 FORMAT (1X,I3,F14.3,F18.1,F16.3,F15.5,1PE10.7,2E18.7)
117 FORMAT (1H1,18X,34HPARAMETERS FOR THIS PARTICULAR RUN)
118 FORMAT (23X,27HSTARTING LOAD INCREMENT NUMBER  $L_0$  =,I6/23X,57HEND
   1 ING LOAD INCREMENT NUMBER  $L_{EN}$  =,I6/23X,57HSTARTING SURFACE PRES
   2 SURE  $S_0$  =,1PE17.7,16H (DIMENSIONLESS)/23X,57HPRESSURE (OR L
   3 CAD) INCREMENT  $S_{IK}$  =,1PE17.7,16H (DIMENSIONLESS)/23X,10HSTARTIN
   4 G TIME,20X,4HTM =,F12.7,4H SEC//)
119 FORMAT (3X,23HSTRESS POINT IS PLASTIC//)
120 FORMAT (3X,3I5,5E17.8)
125 FORMAT (49HVERTICAL STRESS DISTRIBUTION (SZ*100.) AT  $L_L$  =,I5,
   16H,  $T$  =,I3,8H, TIME =,F10.6,5H SEC//)
126 FORMAT (58HVERTICAL DISPLACEMENT DISTRIBUTION (W*10.0E 06) AT  $L_L$ 
   1  $L$  =,I5,6H,  $T$  =,I3,8H, TIME =,F10.6,5H SEC//)
129 FORMAT (4A6)
130 FORMAT (2X,F14.8//)
134 FORMAT (1X,I2,2X,I1F11.5)
136 FORMAT (40HLYIELD INDICATING TABLE (YIT) AT  $L_L$  =,I5,0H,  $T$  =,
   1 I3//)
140 FORMAT (5F11.2)
141 FORMAT (3I5)
142 FORMAT (F8.1,F12.8)
143 FORMAT (2X,2(E17.8,4I8))
END

```

```

*IRMAP SINKIN
   ENTRY .UN00.
.UN00. PZF UNIT09
UNIT09 FILE .5(2),READY,INPUT,=IN,=LK=342
END

```



```

*IB MP SINKOU
ENTRY .UN10.
.UN10. PZF UNIT10
UNIT10 FILE .S(2),READY,INOUT,SIN,SLK=342
END

```

\*DATA

```

      0.000      0.0      10000.0
0.500  0.00002500  33  30
      0.0      -20.0      -110.0      -270.0      -300.0
-1050.0      -1750.0      -2650.0      -3750.0      -4090.0
-5890.0      -6770.0      -7540.0      -8190.0      -8750.0
-5170.0      -5200.0      -5740.0      -5900.0      -5900.0
-10000.0
(1X,I2,2X,5F21.6)
(1X,I2,F16.6,5F21.6)
      1      30
$EOF

```

Unclassified  
Security Classification

DOCUMENT CONTROL DATA - R&D		
(Security classification of title, body of abstract and indexing annotation must be entered when the overall report is classified)		
1. ORIGINATING ACTIVITY (Corporate author) University of Dayton Research Institute 300 College Park Dayton, Ohio 45409		2a. REPORT SECURITY CLASSIFICATION UNCLASSIFIED
		2b. GROUP
3. REPORT TITLE  Aircraft Landing Gear-Soils Interaction and Flotation Criteria, Phase II		
4. DESCRIPTIVE NOTES (Type of report and inclusive dates) Final Report, 15 May 1968 to 15 June 1969		
5. AUTHOR(S) (Last name, first name, initial) Kraft, David C. Luming, Henry Hoppenjans, J. Richard		
6. REPORT DATE August 1969	7a. TOTAL NO. OF PAGES 147	7b. NO. OF REFS 30
8a. CONTRACT OR GRANT NO. AF 33(615)-3199; F33615-69-C-1439	8b. ORIGINATOR'S REPORT NUMBER(S)  AFFDL-TR-69-76	
a. PROJECT NO. n/a		
c.	9b. OTHER REPORT NO(S) (Any other numbers that may be assigned this report)	
d.	none	
10. AVAILABILITY/LIMITATION NOTICES This document is subject to special export controls and each transmittal to foreign governments or foreign nationals may be made only with prior approval of the Air Force Flight Dynamics (FDFM), Wright-Patterson AFB, Ohio, 45433		
11. SUPPLEMENTARY NOTES	12. SPONSORING MILITARY ACTIVITY Vehicle Equipment Division AF Flight Dynamics Laboratory Wright-Patterson AFB, Ohio 45433	
13. ABSTRACT The determination of aircraft flotation performance and operations capability on semi- and unprepared soil runways is a critical factor in developing forward area airfields in limited warfare situations. This investigation, which is a part of a continuing effort, was directed at defining landing gear-soil interaction and developing the flotation criteria to permit comparative evaluation of the relative merits of various landing gear configurations. A basic aircraft tire-soil interaction equation relating the drag ratio (R/P) to sinkage ratio (Z/D) was developed for the Region II velocity range (15 knots to 40 knots). The influence of high velocity and multiple wheel configurations on flotation performance was determined on a preliminary basis. Empirical sinkage prediction equations were developed for predicting the sinkage of aircraft type tires on cohesive and cohesionless soils with an estimated accuracy of $\pm 40\%$ . The results of the Single Wheel Verification Tests are reported and used to verify the developed flotation analysis equations. An analytical approach to sinkage prediction using finite element techniques was developed to give a more rational approach to sinkage analysis. The soil was assumed to be an elastic-perfectly plastic medium. The results of this analytical approach as given by the computer program and the results of a test case evaluation are described in detail. A preliminary Single Wheel Relative Merit Index (RMI) was developed for permitting a comparative evaluation of the flotation characteristics of aircraft tires on soil. The results of the use of this RMI to rate the flotation capacity of aircraft tires currently used on cargo, bomber, and fighter aircraft are presented in graphical form.		

DD FORM 1 JAN 64 1473

UNCLASSIFIED  
Security Classification

14. KEY WORDS	LINK A		LINK B		LINK C	
	ROLE	WT	ROLE	WT	ROLE	WT
Aircraft Flotation; Aircraft Ground surface Drag; Aircraft Tire Sinkage; Aircraft Tire; Soil Mechanics, Dynamic Loading of Soil; Relative Merit Index of Aircraft Tire Flotation Capability (R.M.I.); Finite Element Method; Lumped Parameter Iteration Method; Computer Program, Aircraft Flotation Tests, Runway Deterioration						

INSTRUCTIONS

1. **ORIGINATING ACTIVITY:** Enter the name and address of the contractor, subcontractor, grantee, Department of Defense activity or other organization (*corporate author*) issuing the report.

2a. **REPORT SECURITY CLASSIFICATION:** Enter the overall security classification of the report. Indicate whether "Restricted Data" is included. Marking is to be in accordance with appropriate security regulations.

2b. **GROUP:** Automatic downgrading is specified in DoD Directive 5200.10 and Armed Forces Industrial Manual. Enter the group number. Also, when applicable, show that optional markings have been used for Group 3 and Group 4 as authorized.

3. **REPORT TITLE:** Enter the complete report title in all capital letters. Titles in all cases should be unclassified. If a meaningful title cannot be selected without classification, show title classification in all capitals in parenthesis immediately following the title.

4. **DESCRIPTIVE NOTES:** If appropriate, enter the type of report, e.g., interim, progress, summary, annual, or final. Give the inclusive dates when a specific reporting period is covered.

5. **AUTHOR(S):** Enter the name(s) of author(s) as shown on or in the report. Enter last name, first name, middle initial. If military, show rank and branch of service. The name of the principal author is an absolute minimum requirement.

6. **REPORT DATE:** Enter the date of the report as day, month, year, or month, year. If more than one date appears on the report, use date of publication.

7a. **TOTAL NUMBER OF PAGES:** The total page count should follow normal pagination procedures, i.e., enter the number of pages containing information.

7b. **NUMBER OF REFERENCES:** Enter the total number of references cited in the report.

8a. **CONTRACT OR GRANT NUMBER:** If appropriate, enter the applicable number of the contract or grant under which the report was written.

8b, 8c, & 8d. **PROJECT NUMBER:** Enter the appropriate military department identification, such as project number, subproject number, system numbers, task number, etc.

9a. **ORIGINATOR'S REPORT NUMBER(S):** Enter the official report number by which the document will be identified and controlled by the originating activity. This number must be unique to this report.

9b. **OTHER REPORT NUMBER(S):** If the report has been assigned any other report numbers (*either by the originator or by the sponsor*), also enter this number(s).

10. **AVAILABILITY/LIMITATION NOTICES:** Enter any limitations on further dissemination of the report, other than those

imposed by security classification, using standard statements such as:

- (1) "Qualified requesters may obtain copies of this report from DDC."
- (2) "Foreign announcement and dissemination of this report by DDC is not authorized."
- (3) "U. S. Government agencies may obtain copies of this report directly from DDC. Other qualified DDC users shall request through \_\_\_\_\_."
- (4) "U. S. military agencies may obtain copies of this report directly from DDC. Other qualified users shall request through \_\_\_\_\_."
- (5) "All distribution of this report is controlled. Qualified DDC users shall request through \_\_\_\_\_."

If the report has been furnished to the Office of Technical Services, Department of Commerce, for sale to the public, indicate this fact and enter the price, if known.

11. **SUPPLEMENTARY NOTES:** Use for additional explanatory notes.

12. **SPONSORING MILITARY ACTIVITY:** Enter the name of the departmental project office or laboratory sponsoring (*paying for*) the research and development. Include address.

13. **ABSTRACT:** Enter an abstract giving a brief and factual summary of the document indicative of the report, even though it may also appear elsewhere in the body of the technical report. If additional space is required, a continuation sheet shall be attached.

It is highly desirable that the abstract of classified reports be unclassified. Each paragraph of the abstract shall end with an indication of the military security classification of the information in the paragraph, represented as (TS), (S), (C), or (U).

There is no limitation on the length of the abstract. However, the suggested length is from 150 to 225 words.

14. **KEY WORDS:** Key words are technically meaningful terms or short phrases that characterize a report and may be used as index entries for cataloging the report. Key words must be selected so that no security classification is required. Identifiers, such as equipment model designation, trade name, military project code name, geographic location, may be used as key words but will be followed by an indication of technical context. The assignment of links, rules, and weights is optional.